Early Prevention Method for Power Systems Instability

Dmitrova, Evgenia; Nielsen, Arne Hejde; Jóhannsson, Hjörtur; Johansen, Knud

Publication date:
2013

Document Version
Publisher's PDF, also known as Version of record

Evgenia Dmitrova

Early Prevention Method for Power Systems Instability

Center for Electric Power and Energy

PhD Thesis, May 2013

Early Prevention Method for Power Systems Instability, Center for Electric Power and Energy

Author(s):
Evgenia Dmitrova

Supervisor(s):
Arne Hejde Nielsen, Associate Professor at DTU Elektro
Hjörtur Jóhannsson, Assistant Professor at DTU Elektro
Knud Johansen, Senior Engineer at Energinet.dk

Department of Electrical Engineering
Centre for Electric Power and Energy (CEE)
Technical University of Denmark
Elektrovej 325
DK-2800 Kgs. Lyngby
Denmark

http://www.cee.dtu.dk

Tel: (+45) 45 25 35 00
Fax: (+45) 45 88 61 11
E-mail: cee@elektro.dtu.dk

Release date: 31st of May 2013

Class: 1 (offentlig)

Edition: 1. udgave

Comments: This report is a part of the requirements to achieve PhD in Electrical Engineering at Technical University of Denmark.

ABSTRACT

In the scope of this work, a method capable of fast identification of the proper countermeasure, that prevents emerging instability, has been developed. The focus is placed on the prevention of aperiodic small signal angular instability by means of manipulations applied to load nodes (nodes containing no voltage sources).

The main functionality of the early prevention method is to deliver control solution allowing escape from instability on the basis of data obtained by PMU measurements. The developed algorithm performs identification of the optimal node for countermeasure application and defines which amount of countermeasure would be sufficient to bring a critical generator to the stable operation.

The early prevention method is addressing the possibility of near real time analysis, utilizing computationally efficient algorithms. The method is providing efficient countermeasure matching a given operational conditions and predicts the resulting stability margins for the new steady state, while avoiding time consuming time domain simulations. The method has been validated on the Western Danish power system model, containing 464 buses.

The case study of aperiodic small signal angular instability was created. Utilizing synthetic PMU data, the early prevention method proposed a location and an amount of the countermeasure which will prevent instability; the prediction of the resulting stability margins corresponding to application of the suggested countermeasure was carried out. The predicted effect of the suggested countermeasure application is in a good agreement with the results obtained by RMS dynamic simulation.

Developed method enables adaptive preventive control for near real-time stability maintenance. The achieved results are opening promising perspective for power system's evolution to self-curing systems, for which the human factor involved in control, will keep diminishing.

RESUMÉ

Dette projekt har resulteret i udviklingen af en ny metode der kan identificere passende kontrol handlinger der kan afvige forekomsten af stabilitets problem i elforsyningssystemer. Det primære fokus er at undgå forekomsten af aperiodisk småsignal rotorvinkelstabilitet ved at manipulere belastningen i belastningsknudepunkter (knudepunkter som ikke er forbundet til en spændingskilde).

Hovedfunktionen af den udviklede metode er at levere en kontrolløsning, der på baggrund af data opsamlet fra PMU'er, kan bringe systemet tilbage til stabil driftstilstand. Den udviklede algoritme identificerer det optimale knudepunkt at foretage ændringerne i og definerer størrelsen af det indgreb som er passende for at få den kritiske generator tilbage til stabil drift.

Den udviklede metode åbner op for muligheden for en nær realtids analyse ved at gøre brug af optimerede beregningseffektive algoritmer. Metoden bidrager med en effektiv kontrol handling der matcher en given driftstilstand og forudser de resulterende stabilitetsmarginer som kan opnås når kontrol handlingerne er blevet udført, uden at anvende tidskrævende simuleringer i tidsdomænet.
Metoden blev valideret på en model for elforsyningssystemet i Vestdanmark (DK1), hvilket indeholder 464 busser.

Yderligere studier af aperiodisk småsignal rotorvinkelstabilitet er blevet udført. Ved at gøre brug af syntetiske PMU målinger, foreslår den udviklede metode hvor i systemet kontrolhandlingen skal udføres og omfanget af det indgreb der vil forhindre ustabilitet. Derudover estimerer metoden også hvad burde at blive den resulterende stabilitetsmargin når kontrolhandlingen er blevet udført.
Den estimerede margin er i god overensstemmelse med de opnåede resultater gennem dynamisk RMS simulation.

Den udviklede metode tillader adaptiv forebyggende kontrol i nær realtid for at bibeholde stabiliteten i system.

De opnåede resultater baner vejen for fremtidens selv-helende elforsyningssystemer, hvori graden af den menneskelige afhængighed fortsat vil aftage.

TABLE OF CONTENT

LIST OF PUBLICATIONS

The listed papers have been written as part of this PhD project and contain the main theoretical conclusions and results of the project; they are included in the following appendixes.

[B] Evgenia Dmitrova, Hjörtur Jóhannsson and Arne Hejde Nielsen, “Fast Assessment of the Effect of Preventive Wide Area Emergency Control”, 4th European Innovative Smart Grid Technologies (ISGT) Conference, October 2013, Copenhagen

[C] Evgenia Dmitrova, Hjörtur Jóhannsson and Arne Hejde Nielsen, “Early Prevention of Instability-Use of Self Propagating Graph for the Fast Search for Optimal Grid Nodes to Apply Countermeasures”, PowerTech, June 2013, Grenoble

[D] Evgenia Dmitrova, Hjörtur Jóhannsson and Arne Hejde Nielsen, “Assessment of the impact that individual voltage source has on a generator’s stability”, The 10th International Power and Energy Conference IPEC, December 2012, Ho Chi Minh

[E] Evgenia Dmitrova, Hjörtur Jóhannsson and Arne Hejde Nielsen, “Early prevention of instability - search for optimal grid nodes for applying countermeasures”, International Conference on Environment and Electrical Engineering EEEIC, May, 2012, Venice

ABBREVIATIONS

The following abbreviations have been used in this thesis:

AGC	Automatic Generation Control
ASSAI	Aperiodic Small Signal Angular Instability
ASSAS	Aperiodic Small Signal Angular Stability
CEF	Control efficiency factor
EEAC	Extended equal area criteria
FIFO	First In First Out
GTC	Grid Transformation Coefficient
IPS	Instability Prevention System
LTC	Load Tap Changer
LU	Low-Up (decomposition)
OEL	Over excitation limiter
PLSS	Programmable Load Shedding System
PMU	Phasor Measurement Unit
RLSS	Remote Load Shedding System
RMS	Root Mean Square
SA	Sensitivity Analysis
TEF	Transient Energy Function

THESIS ORGANISATION

The topics addressed in this thesis are discussed in the articles written during the project period. Articles are attached in the appendixes. The thesis is organized as described below; the interrelation between thesis chapters and corresponding articles is mentioned as well.

Chapter 1: Contains the motivation description and addresses the main goals of the project.

Chapter 2: Contains overview of theoretical background, as well as revision of latest developments in the field of real time stability assessment methods.

Chapter 3: Provides the conceptual description of the early prevention method. Including ideological motivation, application scope and structure skeleton.

Chapter 4: Describes a method for identification of the optimal location for countermeasure application based on the sensitivity analysis.
Appendix [B] contains the article covering the topics addressed in this chapter.

Chapter 5: Addresses the problem of minimization of the number of nodes to be processed through sensitivity analysis by means of utilization of self-propagating graph algorithm.
The description of the self-propagating graph algorithm and its validation is reflected in the article attached in the Appendix [C]

Chapter 6: Concerns the definition of the size of countermeasure which would be sufficient for instability prevention, the assessment of the new steady state along with prediction of the resulting active power stability margin is carried out.
The methods described in this chapter are presented in two papers; the first addresses the problem of pre-assessment of the equivalent Thevenin voltage variation when a certain change to admittance matrix is provided. Article can be found in appendix [D], the fast assessment of the reachability of the new steady state and corresponding stability margin prediction is adressed in the paper attached in appendix [E].

Chapter 7: The developed method is tested on the Western Danish Power System.

Chapter 8: Contains conclusion and projections for the further research.

1 INTRODUCTION

Over the last decade the development of power systems has taken a new direction due to pressure of environmental concerns and market influence accompanied by outstanding innovation in monitoring and control techniques. All these factors are acting side by side resulting in emerging of new environmentally friendly smart grid solutions for efficient power systems operation. This development led to targeting new strategy for power systems evolution focused on reduction of fossil fuel based production by moving towards extended integration of renewable energy. Those ideas are changing common principles of power system control and operation considerably.

1.1 Motivation

Large scale integration of such renewable energy sources as wind and photovoltaic results in uncertainty in generation. Furthermore, additional complexity is appearing in the grid topology as energy source is allocated at a place where it naturally appears (wind sights, and excessively sunny regions), meaning that placement of generation is not anymore defined by proximity to the large consumers, and in many cases might be distant from the actual load centers. Another change in power systems structure is introduction of distributed generation; power production is not anymore mainly falling at several central stations, which was it was typical for conventional fossil fuels based generation. Additionally, development of energy markets is pushing power systems towards the most economically efficient functioning, resulting in operation closer to stability limits, by this causing contradiction between efficiency and reliability. In order to resolve this conflict of interests advanced flexibility and new control solutions need to be introduced in power systems.

In modern power systems uncertainty is introduced on both sides of the energy balance: production and consumption, which increase the challenge for the system operator. In order to ensure the oprerator awareness regarding the actual system state technologies allowing real-time monitoring should be utilized. Complete observability of the power system at any moment would give the opportunity for integration of adaptive control, which would adjust to the current operational conditions, hence providing better efficiency and reliability. The development of phasor measurement technology opens new

horizons for real time monitoring and control. Being inspired by new perspectives, new methods allowing real-time stability assessment already started to emerge.

The next natural step is utilization of the information obtained from the real-time monitoring for the prevention of critical operation conditions. Metaphorically saying, listening to the pulse of power system, which is wide area measurements, allows diagnosing of the diseases currently presented in the system, including stability problems, and enables proper treatment prescription on the early stage of the emerging critical operation. Fast identification of the proper countermeasures aimed on prevention of upcoming undesirable operational conditions is the main motivation for this thesis. The focus is placed on the development of early prevention methods for power systems instability, in particular aperiodic small signal angular instability.

1.2 Goal of the project

Conventionally, the stability assessmen is presently carried out basing on off-line computer simulations. The obvious disadvantage of this approach is potential mismatch of actual operational conditions and ones considered in the model, as actual loading might vary considerably from the predefined in the model, additional challenge is representation of renewable energy as it has considerable level of uncertainty. This approach is quite time consuming and doesn't provide stability boundary corresponding to actual operational conditions, instead expected stability boundary (on the basis of expected loading and generation) might be defined. As the difference between predefined and actual stability boundary is uncertain, nowadays large stability margins with respect to predefined stability limit are traditionally used to ensure secure operation. Integration of wide area measurements enables identification of stability boundaries for the current operational conditions, which allow increase power systems efficiency. On the other hand, operating system close to the stability limits raises the challenge of ensuring required safety and reliability. Effective algorithms for prevention of instability should be developed in order to provide fast automated control reaction opposing the worsening of operational conditions, by this enabling the concept of self-healing systems.

The goal of the project is the development of the approach capable of identification of the proper control measures, aimed on prevention of aperiodic small signal angular instability. There are three main problems to be considered during research activity. The first one can be formulated as: search of the optimal nodes in the grid for the countermeasure application. Being able to define which of the nodes in the grid are having higher potential of affecting the stability of a given generator gains better targetting for control. Thus the positive effect on the stability of a troubled generator can be achieved with smaller "effort". The second task is definition of the minimum countermeasure needed for successful instability prevention. After the optimal node for the control ap-

plication is found, it should be defined which control action directed to this node would be sufficient for satisfactory improvement of stability. Finally.the last task to be solved is to provide algorithm which would allow speeding up the search of the optimal node for countermeasure application, as for the large systems this procedure would be time consuming if each node in the grid is supposed to be considered as potential candidate for the control action. The main purpose of this task is to achieve execution of early prevention algorithm within short time frame providing functionality of emergency control.

Solution of these three tasks is giving a solid basis for creation of automated early prevention system for near real-time stability management. Early prevention algorithm may serve both as an advisory supportive tool for the control room and as automated decision making tool for self-healing system when not favorable stability conditions occur. Furthermore, reduction of the human factor while stressed situations might be achieved, as proposed algorithm would shield a dispatcher with complete awareness about the problematic units in the grid and the ways to improve their stability at the early stages of critical operation.

2
STABILITY OF POWER SYSTEMS: REAL-TIME METHODS FOR MONITORING AND CONTROL.

Power system failures triggered by instability cause considerable shortage of power supply over large areas. Major blackouts may affect millions of consumers for several hours [1]. The recovery of normal operational conditions is a complicated process which requires a lot of time and efforts from control room personnel. The number of failures causing stability problems is not large comparing to the overall number of disturbances. However these incidents are characterized by the large shortages in power and correspondingly severe economic consequences. For this reason, special attention is paid to providing sufficient stability of power systems both on the stage of network planning and on the daily operational level. This section considers which stability problems modern power systems face to and what methods for stability monitoring and control are currently available.

2.1 Safe Operation of modern Power Systems: new concepts and challenges

The key requirement for the power system is reliability. One of the essential factors for reliable operation is stability of power system. There are multiple factors defining how stable the power system is. In order to quantify the level of system stability the term stability margin was introduced. Stability margin for steady state operation is defined as the margin between the maximum possible power flow and a given power flow expressed in percent of maximum power flow [2]. Historically the minimum stability margin was mainly defined by requirements for safe and uninterruptible power supply to the customers. Respectively, to ensure survival of the system after being exposed to severe disturbance large steady state stability margin (typically 20 %) during normal operational conditions was maintained [3]. However, with the introduction of energy markets, the tendency to operate power systems closer to stability boundaries is stimulated by economic reasons, demanding utilization of the available power system capabilities with the highest efficiency. To meet the requirement of efficient exploitation of the system capabilities the extent of possible added loading still allowing stable operation should be defined. Thus, identification of the actual stability boundaries for given operational conditions became popular topic for the research over the last decades. At

the same time the uncertainty level in analysis of power system has increased due to integration of renewable energy. Traditionally, load was the most unpredictable factor as besides normal fluctuations it is dependent on weather. For this reason generally several models reflecting different season loading are considered for stability assessment. Integration of considerable amount of renewables to power systems resulted in inducing uncertainty in generation as well. Such renewables as wind and photovoltaic generation are very dependent on weather. Alteration of wind and sun is very volatile, entailing vagueness to long term forecast. This means that stability boundary obtained for the pre-modeled operational conditions have a risk of being irrelevant to the actual system operational conditions. Modern power systems deal with power balance where all the components of the equation are volatile.

$$P_{gen}=P_{load} + P_{losses} \quad \textbf{(2.1)}$$

Electrical load is a fluctuating component by its nature. At any moment of operation power system experiences a number of switching operations of electricity consuming objects. Individual load variation has an arbitrary stochastic pattern; however, considering system in general, the typical profile with low and peak hours of loading can be formed. There are multiple methods for load forecasting, mainly based on various statistical approaches [4], [5]. The problem of load variation is classical for power systems; respectively large methodological skeleton for dealing with this concern has been developed over decades [6]. Nevertheless the new aspect of load controllability emerged with the development of communication infrastructure and control technologies. Controllable load may become one of the powerful tools for optimizing normal operation, power system balancing and withstanding contingences [7]. From this perspective electrical load becomes more manipulative asset rather than volatile.

The adequate assessment of the power system losses under condition of massive renewable integration to the grid is another great challenge for modern power systems. Volatile power injections from wind turbines and photovoltaic are altering power flow thus modifying power losses. The impact on losses of the different distributed generation technologies is analyzed in [8].

To balance electrical load and power losses adequate generation should be provided at any moment of operation. Generally, generation plan was made based on load forecast and pre-estimated loss level. Respectively the unit commitment was scheduled and executed. In other words, the required power production from the given generation unit was assured in advance with large certainty. The situation has completely changed for power systems containing considerable amount of variable generation. In order to adjust power balance maintenance to the volatile uncertain generation more flexibility in generation capacity is required [9], [10]. One of the opportunities to provide required flexibility is energy storage utilization. There are different technologies for the energy storages under development currently, e.g. fuel cells, super capacitors, flywheels, batteries and storage

systems based on compressed air [11]. It is supposed that energy storages will be able to smooth variation in generation allowing reliability of power supply.
Due to two main driving forces: economic and environmental, the concepts of power system operation are moving away from the conventional in order to meet new challenges and provide better performance.

2.2 PMU and their application for real-time monitoring and control

Development of the phasor measurement technology [12], and further intensive implementation of phasor measurement units (PMU) to the real power systems [13], accompanied with development of computational facilities, offers new opportunities for wide area monitoring and control in real time. The real-time system state assessment getting promising perspectives due to the ability of new measurement technologies to provide direct measurements of voltage and current phasors synchronized in time. Synchronization is realized by slicing the sinusoidal waveforms of voltages and currents over the system using signals from the Global Positioning System Satellite (GPS) for timing (Figure 2-1). PMU technology allows getting snap-shots of the system on the rate of up to 60 samples per cycle [14], which gives a great gain in rapidity of power system analysis, comparing to traditional numerical iterative methods. Considering computational efficiency advantage, further implementation of the wide area measurement technology based on the usage of PMU is accepted as a nearest-years strategy by TSOs all over Europe [15].

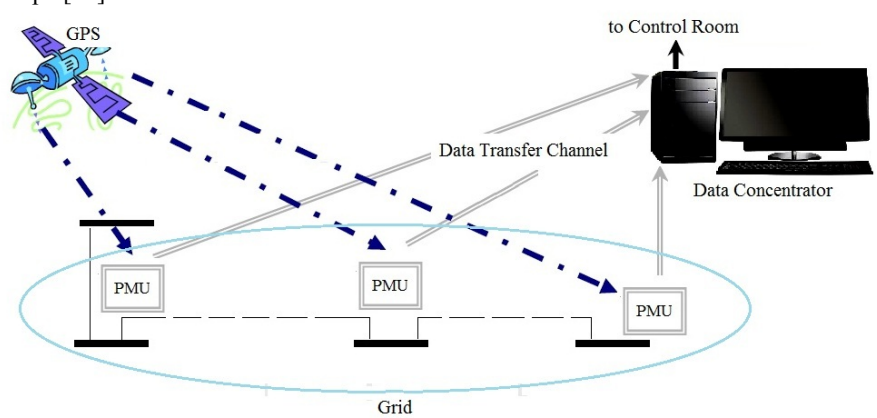

Figure 2-1: WAMS architecture

Wide area measurement systems (WAMS) bring new opportunities to the field of monitoring and control of power systems. Examples of perspective areas of PMU based technologies application are as follows:

- Visualization of power system in real-time
- Basis for the development of the efficient critical operation warning systems
- Validation of the system models
- Dynamic stability assessment
- Real-time control
- Monitoring systems parameters
- Improvement of the oscillations damping
- Creation of the adaptive protection systems
- Post-prosection of the blackouts event-lines and system response to the disturbances

As a technology, PMUs are comparatively new invention. It was introduced in the year 1983 [16], and got practical realization being implemented into real power systems over the last decade. For the moment, proper operation of PMU under the normal operational conditions is proved, however adequacy of their measurement provided over the transients is questionable. The reason for this is that phasor representation of the sinusoidal wave doesn't contain frequency (stationary sinusoidal waveform representation). Respectively the necessary condition for fair interpretation of PMU data is invariability of the frequency for all measured points in the system. That assumption is fair for steady state operation as variation of frequency in different grid areas is negligible. However, that cannot be taken for the system under the transient conditions, as frequency of different system areas might vary. The problem of PMU data interpretation and their response standardization under transient conditions is the topic of ongoing discussion [17]. Even though for the moment WAMS technology has problems performing under transients, there is expectation that system operation will more and more rely on the monitoring and control solutions based on PMU technology [14].

2.3 Classification of instability mechanisms in power systems

In order to clarify what is meant under the term "power system stability" the definition given in [18] is brought:

"Power system stability is the ability of an electric power system, for a given initial operating condition, to regain a state of operating equilibrium after being subjected to a physical disturbance, with most system variables bounded so that practically the entire system remains intact".

The term "disturbance" in this case is refer both to large disturbances, such as short circuits, protection malfunction, equipment failures , physical destruction caused by non-technical factors (e.g. natural disasters, human factor etc.) ; and small disturbances, e.g. load fluctuation, variation of renewable generation, etc.

With respect to the different physical phenomena staying behind, the instability mechanisms are classified in [18] as in Figure.2-2:

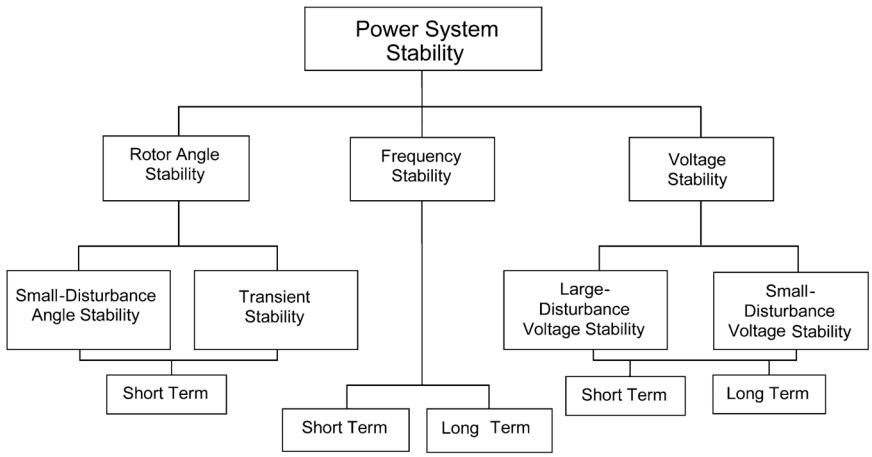

Figure 2-2: Power System Stability Classification [18]

2.3.1 Rotor angle stability

Rotor angle stability refers to the ability of synchronous machines remain in synchronism when being exposed to the disturbance. The stability of rotor angle is defined by existence of equilibrium between opposing mechanical and electrical torques applied to the shaft of generator. To provide constant rotational speed, rotating mechanical torque conditioned by the amount of the supplied fuel should be compensated by breaking electromechanical torque conditioned by system load. Imbalance of the torques leads to acceleration or deceleration of rotor which might lead to rotor angle instability.
Rotor angle stability can be classified with respect to two criteria:

1) The scope of triggering disturbance:
    a) small signal stability
    b) transient stability

Considering small disturbances linearization of rotor motion equation might be applied for the analysis of system behavior while for analysis of transient stability nonlinearity of the dependency between torque imbalance and rotor angle should be taken into account. The time frame for small signal angular stability is in order up to tens of seconds, depending on the disturbance and system configuration. For the transient period time frame of interest comprise up to 20 seconds [19].

2) The mode of the rotor angle variation:
    a) aperiodic

b) oscillatory

The change in electrical torque of the synchronous machine can be presented as a combination of two components as follows [20]:

$$\Delta T_E = T_S \Delta\delta + T_D \Delta\omega \qquad \textbf{(2.2)}$$

$T_s\Delta\delta$-is the synchronizing torque component, where T_s is the synchronizing torque coefficient;
$T_D\Delta\omega$-is the damping torque component, where T_D is the damping torque coefficient;

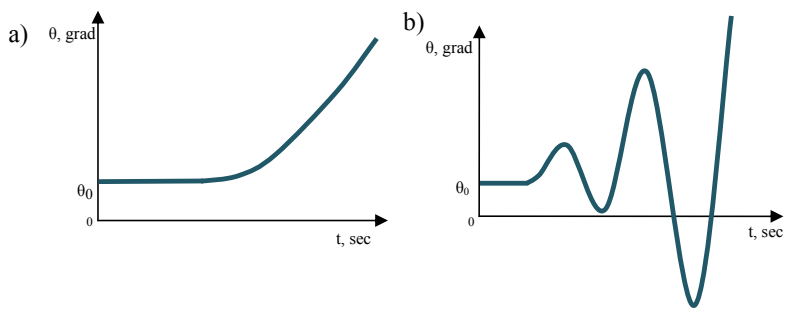

Figure 2-3: Aperiodic and oscillatory rotor angle response for a disturbance

Aperiodic rotor angle instability is triggered by the lack of synchronizing torque. It is characterized by gradual increase of the rotor angel until the synchronous machine goes out of step (Figure.2-3a).

Oscillatory instability may be caused by unfavorable combination of system parameters initiating cumulative hunting or, in the most of the cases, can be provoked by action of voltage regulators. Thus, sufficient damping of system oscillations should be provided to ensure stable operation. The lack of damping torque leads to violation of angular stability appearing as increasing in amplitude periodical oscillation of rotor angle (Figure 2-3b). The problem may have a local or a global character:

Local problems are generally associated with oscillations of a single power plant against the rest of the system, such oscillations are called local mode.
Global problems are referred to the interoscilation between large groups of coupled synchronous generators. Phenomena involves multiple machines and has wide spread effect over power system. These oscillations are called inter-area modes.

2.3.2 Frequency stability

Frequency stability problem is caused by imbalance between generated and consumed active power in the system. At any moment of the operation mechanical torque applied to each machine should be balanced by breaking electromechanical torque. When these two opposing forces are in balance, speed of machine is constant and all machines in the system are supporting the same frequency. Considering torque balance the balance of active power might be used instead [18], the balance between mechanical power applied to the prime mover (turbine) and active power consumed in the system plus losses is meant. Imbalance of power is covered at the expense of kinetic energy stored in the rotating mass of the machine resulting in deceleration or acceleration of the rotor. This type of instability is directly linked to rotational dynamics of the machine, the phenomena develops within time frame of up to several seconds- depending on mass of machines involved. Generally, frequency protection has very narrow dead band diapason of allowable deviation (usually 2 Hz) that leads to disconnection of the units experiencing frequency problems from the grid, by this decreasing active power generated, which cause increase of active power imbalance and worsening of situation. In order to prevent frequency declination the reserve of maneuverable generation participating in frequency control (spinning reserve) is activated, for the emergency situations when the reserve value is not sufficient for reestablishing of power balance such measures as load shedding and in more severe cases islanding operation is forced.

2.3.3 Voltage stability

Voltage stability refers to ability of the system to maintain sufficient level of voltage magnitude at all busses at the system under normal operational conditions and after being exposed to a disturbance. The main factor for this type of instability is inability of the system to meet reactive power demand. As a result progressive drop in voltage magnitude is observed leading to the voltage collapse. One of the main triggering mechanisms for voltage instability is considered to be attempt of the loads to restore power consumption exceeding the limits of deliverable power under given operational conditions [21]. Voltage instability starts as local phenomenon, as it is caused by the lack of reactive power at a certain points in the grid. Reactive power is not easily transmitted over the long distances, respectively the maintenance of voltage stability should be controlled locally. However not being captured at the early stage voltage instability might spread over large territory characterizing by slow continuous voltage drop and eventually resulting in voltage collapse leading to the system blackout. Depending on involved equipment, the time frame for the voltage instability ranges from short term in several seconds up to several minutes. The dynamics of synchronous voltage compensators and induction motors is responsible for the fast development of instability; at the same moment under load tap changers lead to very gradual emergence of voltage instability [22].

Possible countermeasures applicable in real-time for prevention of voltage instability includes reactive device switching, generator reschedule, selective load shedding, etc.

2.4 State-of –the-art for real-time stability assessment methods

This section describes methods allowing real time stability monitoring and control. As it is hardly possible to cover all aspects of instability within one methodology, accordingly separate assessment methods for different types of instability are generally suggested [19].

In order to create crosscutting system realizing all-around monitoring, early prediction and prevention of system instability, multi-module structure is suggested in [23,24]. For this system, PMU are considered to be a trustful source of the data, providing complete information regarding current system operational parameters. The received system data are used as input for a range of stability assessment methods. Each assessment method is realized in independent program module. Each module is responsible for the following functions: detection of certain type of instability, generating early warning messages in case of critical operation and suggestion of relevant remedial action preventing system collapse. The major challenges for bringing such system into operation are the following:

- Derivation of the reliable indicators for each type of instability, which is:
  - Transient angle instability
  - Frequency instability
  - Voltage instability
  - Oscillatory small signal angular instability
  - Aperiodic small signal angular instability
- Calculation and monitoring of derived instability indicator in real time
- Adaptability to changes in operational conditions such as topology variation, generation rescheduling, load fluctuation, availability of control reserves etc.
- Coordination of the actions suggested by each module with other modules and with existing protection and control schemes
- Creation of a fast, secure and reliable network for wide area protection level communications
- Unification of control communications protocols

However it should be admitted, that instability prevention system (IPS) (Figure.2-4) feasibility is narrowed to the operational scenarios providing a sufficient time for instability prevention methods to run, meaning that there should be time of tens of seconds prior to system collapse after emerging of instability [25]. Nevertheless continuous development of IT technologies and improvement of computational facilities gives a hope that the time needed for system state assessment and preventive algorithms run-

ning will continue to reduce more and more hence providing increased scope for IPS applications.

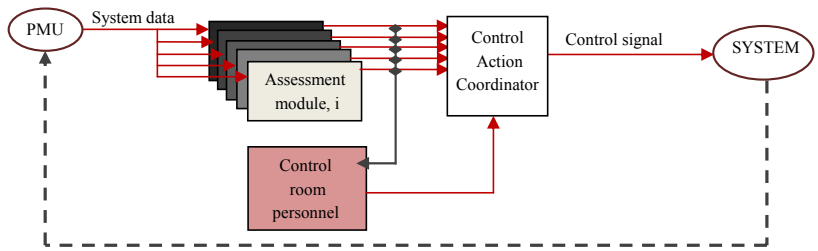

Figure 2-4: Structure of Instability Preventive System

2.4.1 Situational Awareness

Depending on time allowance the control actions suggested by assessment modules after being coordinated are applied either automatically or could be represented as advisory list to the dispatcher in the control room. Inclusion of the human operator into the control loop has both advantages and drawbacks. The drawback is the risk of mistake done due to human factor. For the critical operations the control decision should be done in a short time frame which implies increased psychological pressure and requires extensive professional qualifications. On the other side, having sufficient information regarding system state human operator is able to suggest efficient control measures relying both on experience and intuition, even facing unknown operational conditions. Furthermore, modern power systems being equipped with highly intelligent control automation still require human operator participation for wide range of operational cases. However in order to reduce response time and eliminate risks of operator mistakes the shift to the more and more automated systems is going on [26]. Currently human operator realizes not only supervisory control but plays active role in control actions initiating. Considering this, it is very important to ensure that all the relevant information influencing on the decision making, is explicitly performed to the operator, thus the situational awareness is guaranteed. Following the development in communication and measurement technologies the amount of available data providing information about power system state has increased greatly [27]. Nevertheless, the availability of information does not gain benefits in decision making, unless it is represented in a meaningful way. For the different operational conditions, especially referring to the critical contingency or post-contingency operation, the information which is vital for understanding of the ongoing processes and making adequate control decisions will vary. The amount of information which can be monitored and be effectively perceived by operator is limited, thus it is necessary to sort and combine available information accordingly to the

current needs. Furthermore, proper representation of information is not sufficient for establishing situational awareness, the intelligent system of warning and alarming messages drawing operator's attention to the critical operation should be provided [26], [28].

Instability at the early stage of its emerging is not easily detected from the observation of systems parameters; furthermore the phenomena might have complicated structure when more than one driving force for instability is presented in the system at the same time, making it even worse for appropriate interpretation from system operational data. It is needed that IPS assessment modules provide clear indication of instability mechanisms taking place in the system, are able to capture unsafe operation at the very beginning of its development and allocate the most problematic areas in the grid. Situational awareness depicting full spectrum of system stability problems is crucial issue for the successful prevention of imminent system collapse.

2.4.2 Near real-time stability assesment

Introduction of PMU technology has caused rapid increase of research in the field of real time monitoring and control of power systems. Multiple attempts are taken towards real-time stability assessment and early warning of critical operation conditions. Further in the section, the selected list of suggested approaches will be described.

2.4.3 Stability monitoring and early warning

From the control perspective it is more efficient to monitor different instability mechanisms separately [19], which is in a good agreement with the suggested multi-modular structure of the IPS. Seeing that each assessment module is responsible for the identification of one certain type of instability the methods suggested for monitoring of these instability mechanisms will be considered sequentially below.

2.4.3.1 Transient angle stability

Considering transient angle instability, analysis addressing N-1 criterion assessment is wide spread approach. The time frame between the occurrence of operational conditions awaking transient instability and unit going out of step is up to 10 seconds [19]. The most precise and straightforward methodology utilized for the transient stability assessment is time domain simulation of the power system modeled by non-linear differential equations. However, for the real time assessment this method is unacceptably time consuming, furthermore a precise model of the power system is required both for pre-contingency and post-contingency conditions [19].

Another large group of approaches for transient stability analysis are utilizing transient-energy-function (TEF) method [29]-[34]. The basis of the method is comparison of the difference between the potential and kinetic energy against the reference value regarding certain disturbance. The strong side of these methods is that besides indication of whether the system is transient stable or not, proximity to instability is expressed by means of normalized energy margin. The latest research in this field demonstrates promising potential for TEF based methods to be used for real-time transient stability assessment [31], [33], [34]. However, applying this method faces to considerable modeling limitations, such as higher order generator model, non-linear loads, HVDC, some network controls (Var controls, etc.) [29]. The Approaches, built up on the extended equal area criteria (EEAC) method are based on the same principle of comparison acceleration and deceleration areas [35]-[37]. EEAC is a combination of TEF and step-by –step time domain simulation and allows assessment of the transient stability of multi-machine system. Method provides systems critical clearing time and energy margin for specified contingency. Nevertheless computational efficiency of the method is not sufficient for real-time applications even though the work towards improvement of computational speed is going on it still takes seconds to run the algorithm [37].

Another direction of transient stability analysis is performed by methods based on self-learning techniques such as artificial neural networks [38], decision trees [39], [40], artificial intelligence [41], fuzzy logic [42] and support vector machines [43], [44]. The main advantage of these methods over the computational ones, based on the mathematical interpretation of the physical processes, is fast response. Logic based methods are capable of providing fast solutions within a limited time. However, the major drawback of such methods is necessity to train them on the certain power system before they actually can recognize the patterns of ongoing instability adequately.

2.4.3.2 Oscillatory small signal angular stability

Physical phenomena triggering oscillatory instability is lack of sufficient damping torque. Oscillatory stability is quantified by the Eigen properties of the system state matrix. The instability is essentially induced by Hopf bifurcation of one or more pairs of conjugate eigenvalues. Accordingly monitoring of the system's eigenvalues positions on the complex plane provide information regarding current status of oscillatory stability. However there are serious drawbacks for implementation of eigenvalue monitoring in real time due to the fact that not only complete information regarding power system operational parameters should be available but computation is time consuming (tens of seconds) [45].

For the moment real-time monitoring of oscillatory stability is not full scaled implemented in real power systems, nevertheless intensive research is going on in this field

towards both monitoring and prevention of instability [46]. However, Psymetrix Lmt. claims development of the world-first application allowing continuous real-time tracking of the full characterization of the low-frequency modes of power system oscillation, including damping, amplitude phase and frequency [47].

Another method for real-time oscillatory instability monitoring and prediction has been verified in CRIEPI's Power system Simulator [48], [49]. Real-time Oscillatory Instability Prediction System (ROIPS) based on the multi-layered wide-area monitoring architecture is suggested:
"The oscillatory stability in power system is evaluated based on the already developed scheme applying to two types of time series data; 1) the phase differences of voltages between substations, 2) rotor angles of generators relative to the phases of their terminal voltages. If both time series data sets have same frequency of unstable oscillatory mode, the power system is judged as unstable." [50].

The method is validated on the five machine test system. It is shown that oscillatory instability can be detected several seconds prior critical unit meets out-of-step condition.

Alternative direct method using PMU measurements to assess oscillatory stability is described in [51]. A system identification method described there is proposed to estimate the damping coefficient from low quality ambient noise, which is the natural response of power system due to random load switching. Furthermore, the use of the estimated damping torque coefficient as a stability index is studied.

Among other things usage such methods as Neural Networks, Decision Trees and Neuro-Fuzzy of Computational Intelligence for real-time assessment of oscillatory stability is under consideration [52], [53]. In [52] methodology for computation of countermeasures for prevention of oscillatory instability is proposed suggesting usage of generalized optimal power flow where the target function is defined as the difference between the desired features resulting from the countermeasure computation and the actual load flow. Those methods provides promising results for identification of oscillatory instability on the early stage, however have common drawback of being necessarily intensively trained before adequate functioning is possible.

2.4.3.3 Voltage Instability

The detailed description of voltage instability mechanism is covered in [54]-[57]. A system is voltage unstable if for at least one bus in the system increase of reactive power injection leads to decrease of voltage magnitude. There are several approaches developed for the real-time voltage stability assessment; three main directions of the research

in this field can be mentioned as follows: PV curve monitoring, sensitivities analysis and neural networks application [58].
Voltage stability assessment based on real-time monitoring of PV curves is mostly based on determination of loading margin at an individual load bus. To obtain PV curve, gradual increase of power system load is to be done, for each step of load increment the power flow should be run in order to define bus voltage corresponding to new value of load. The gradual increase of load continues until the nose point of PV curve is reached and system experience voltage collapse. The loading margin between current operational point and the nose point of PV curve is used as stability criteria. Real-time voltage stability assessment based on this approach was suggested in [59]. PV curve analysis is widely used for steady state voltage stability assessment as provides very illustrative and easily interpretive stability criteria. Nevertheless, that means building of the up- to-date PV curve would require a run of serial load flow simulations, leading to huge computational efforts, considering real-time operation. As an alternative pre-calculated PV curves might be used, however it induces noticeable error in actual loading merging as real operational conditions might vary from the one used for off-line pre-calculation of PV curve largely.

Another approach for the real-time voltage stability monitoring is sensitivity analysis which could be applied in various modifications, including voltage stability indexes, contingency ranking and modal analysis. Sensitivity of total reactive power generation to individual load reactive powers is considered in [60], [61]. The presented approach demonstrates that when the operating point crosses PV curve nose point the sign of sensitivity is changed. Combined action of over excitation limiter (OEL) and Load Tap Changer (LTC) is simulated in several study cases and special prerequisites for the tuning of OEL and LTC were derived in order to provide early prediction of voltage instability; however these conditions require coordination of operating time delay for all OEL and LTC what is complicated for large systems. Another drawback for sensitivity analysis approach is that number of equations to solve is increased by additional set of system sensitivity equations [62].

Alternative branch of research aimed on prevention of instability is neural networks [63]-[65], however the necessity to train neural networks still is a major drawback for their implementation to real power systems, as it was mentioned in previous sections.

At the moment, along with above mentioned approaches, method of sequential deterioration of the system is described in [66] for voltage stability assessment. System sequential deterioration deals with systematic sequential application of disturbances to the system, continuously worsening voltage stability conditions, until the system collapse. On the basis of the obtained result ranking of contingencies is realized and current operational conditions are identified either as secure if application of any single contingency

is not leading to voltage collapse or as insecure if at least one of possible contingency leads to instability. Practically this method estimates fulfillment of N-1 criterion for the given operational conditions. Real-time implementation of this approach became possible with increase of computer computational abilities and usage of parallel computing techniques. However the given methodology doesn't provide monitoring of voltage stability margin, as qualitative assessment is suggested manifesting only either system is secure or not. Thus, no any real-time defined margin to instability is available.

2.4.3.4 Frequency Instability

At any moment of power system operation, the frequency is experiencing small deviations, due to natural fluctuations in load and generation. For correction of such a small deviations Automatic Generation Control (AGC) is used [19]. Frequency is real-time monitored and in case if deviations are registered, corrective actions are initiated by AGC, involving generators participating in the frequency control. Some modifications of AGC considering distributed generation and economic load dispatch utilizing genetic algorithms are described respectively in [67], [68].
In case of severe disturbances such as generation, load or HVDC interconnection loss, causing large imbalance between produced and consumed power, emergency control actions should be taken in order to prevent noticeable frequency drop and prevent frequency instability.

Preventive control actions may include [69]:

- Tripping of generators
- Fast generation reduction through fast-valving or water diversion
- HVDC power transfer control
- Load shedding
- Controlled opening of interconnection to neighboring systems to prevent spreading of frequency problems
- Controlled islanding of local system into separate areas with matching generation and load.

Most of the countermeasures apart from automatic load shedding are initiated by operational personnel in the control room [69], [70].

Practically, load shedding is one of the most utilized countermeasures preventing a critical frequency drop. It is activated automatically when frequency falls down to some predefined level with a certain rate of change (most often, combination of two control channels is used: frequency deviation and the first frequency derivative with respect to time [19]). The action is step wise disconnection of the load until the frequency drop is stopped. However, the tripping logic of frequency relay is developed based on off-line system analysis and is not adaptive to actual emergency situation as there is no any on-line coordination. Furthermore this measure is aimed on dealing only with system under

frequency whereas over frequency problem is absolutely uncovered. To overcome these drawbacks a generation rejection and/or remote load shedding system (RLSS) in [71] was introduced. RLSS defines the value of the power to be tripped depending on the severity of contingency and sends the commands to communication processor. Communication processor in its turn interconnects to Programmable Load Shedding Systems (PLSS). PLSS executes the received load shedding commands. Thus, the following advantages are established [71]:

- Coordination remote shedding orders within the same time frame;
- Estimation the load factor of substations equipped with load shedders and estimate in real time the load that can actually be shed;
- Selection of the substations to shed and supervising the proper operation of the shedders

Another advanced algorithm proposing predictive control is presented in [72]. Based on wide area measurements the sensitivity of loads both to voltage and frequency deviation are estimated after the disturbance and load model parameters are determined. Each island of power system is presented as a single machine model with connected load. This model is monitored to determine steady state post contingency frequency rate and identify proper amount of load or generation to be shed. The described approach allows avoiding over shedding as an exact value of frequency deviation to be compensated is predicted immediately after the disturbance.

2.4.3.5 Aperiodic small signal angular instability (ASSAI)

Regarding small signal angular stability, oscillatory angular stability is considered mostly [19]. However, besides oscillatory, aperiodic irregularity of the rotor angle might be triggered by small disturbances as well. As it was mentioned in the section 2.3.1 the reason for commutative aperiodic increase in rotor angle is caused by the lack of synchronizing torque. Such type of instability is typically induced due to increase of loading, generation loss or increase of the system impedance seen from the terminal of the given generator. The blackout 2003 involved Denmark and Sweden might serve as a good example illustrating critical effect of undetected ASSAI development, when following series of contingencies and facing N-3 emergency conditions system collapsed in approximately 80 sec after experienced the last contingency [24]. Depending on system configuration and the extent of synchronizing torque deficit the time frame between emerging instability and system collapse may comprise from few seconds to tens of seconds. In case of small synchronizing torque deficit early stage of instability is not detectable from the monitoring of main system parameters, as their variation is very smooth and gradual. At the same time identification of ASSAI at the very early stage would provide sufficient time for taking appropriate countermeasures. Even so, over the last decade this type of instability was not in the focus of the research addressing real-

time stability assessment. Very few approaches were established for on-line ASSAI assessment.
It was shown in [73] that critical boundaries for steady state stability are close to the boundaries of load flow convergence. Thus the conclusion about steady state stability of the system might be done on the base of power flow calculation. Nevertheless, using this method for stability assessment in real-time is hardly feasible as it requires complete and precise model of the grid at any time of operation, furthermore load flow calculations for the large-scale power systems are excessively time consuming for being applicable to on-line analysis [74].

The early attempt of identification angular stability allowing online applications was suggested in [75]. In [75] a method is described, which is based on real time monitoring of two torque components synchronizing and damping. The method utilizes multilayer feed forward neural network approach. Mainly, the prediction of transient stability is considered in the paper, however monitoring of the synchronizing torque component basing on the real-time measurements of rotor angle, speed and electromagnetic torque makes it potentially applicable for aperiodic small signal angular stability (ASSAS) assessment. Then again there is the necessity to train neural network, which takes time and meets a lot of challenges on the way to its implementation in large scaled power systems [76].

Another method considered in [77] is based on utilizing wide area measurements for defining ASSAS boundary for each generator in the system in terms of maximum injectable power and maximum rotor angle. In order to obtain these critical values, specified operations on the reduced admittance matrix are proposed. The reduced admittance matrix used in [77] is obtained from system admittance matrix by adding generators internal nodes of constant voltage and following eliminating of all the remaining nodes (shrinking of the system admittance matrix to system generator matrix). System admittance matrix, in its turn, is formed and updated on the basis of PMU measurements. The described method demonstrate promising results, however, to obtain system generator matrix number of computational demanding operations should be carried out, such as matrix multiplication and inversion. The feasibility of the real-time realization of the suggested method being applied to the large scale system is not provided.

Alternative method, based on the same principles as [77] and providing real-time ASSAS assessment using wide area measurements is described in [24]. The stability boundary is analytically derived for each of generators of an arbitrary system. The boundary is expressed in terms of injection impedance of the given generator and corresponding Thevenin system impedance. Injection impedance is obtained directly from PMU measurements, while in order to define Thevenin impedance seen by each generator operations on the low-up (LU) decomposed system admittance matrix are proposed.

Method allows identification whether the system is operating in a stable operation area or not, furthermore the distance to the critical boundary might be defined, providing stability margin. The feasibility of the method for the real time application was proved by the simulation of blackout 2003 using Danish power system model which contains 320 busses and 480 branches. It was shown that blackout 2003 was caused by ASSAI as a main driving force.

The method described in [24] gave a basis and inspiration for the current study. The early prevention method for ASSAI is utilizing results from the real-time stability assessment, suggested in [24] as an input signal, which triggers the prevention algorithm when the minimum stability margin is reached. Additionally, the early warning method is used to indicate the efficiency of control actions taken, which in its turn were initiated by the early prevention algorithm.

3
EARLY PREVENTION METHOD−IDEOLOGY AND CONCEPTUAL STRUCTURE

This chapter explains the main context of the suggested approach of early prevention method. Modern power systems control ideology will be presented and the scope of early prevention method specified. This section formalizes the early prevention concept and describes the philosophy staying behind it. Due to the latest tendencies in power systems and new achievements in monitoring and control techniques, the development of the advanced real-time control methods ensuring safety and stability of power system operation under arbitrary conditions is stimulated. Among them, the developed early prevention method, which is aiming to provide early instability prevention under stressed operational conditions, assuming complete system observability available at any time.

3.1 Wide Area Adaptive Emergency Control: power system scope

For the start let's define the term adaptive control:

"Adaptive control is the capability of the system to modify its own operation to achieve the best possible mode of operation. A general definition of adaptive control implies that an adaptive system must be capable of performing the following functions: providing continuous information about the present state of the system or identifying the process; comparing present system performance to the desired or optimum performance and making a decision to change the system to achieve the defined optimum performance; and initiating a proper modification to drive the control system to the optimum [78]. Adaptive control must be implemented under conditions of a continuously changing and unpredictable environment; it therefore requires sensor measurements of the environment [79]."

According to the mentioned definition there are three main components compiling any adaptive control system:

- Identification of the ongoing processes
- Decision of the necessity of interference

- Modification of the system towards optimal operation

Integration of phasor measurement units (PMU) [13] into power systems makes it possible to obtain real-time synchronized system's snapshots, enabling near real-time identification of the processes taking place in power system at the moment. Hence, the technological basis for implementation of a wide area adaptive control is provided.

New capabilities of measuring and monitoring technologies gave a rise to development of methods which are capable to carry out fast analysis of power system on the basis of the data received from PMU. Naturally, various methods for system's analysis are focused on the specific subjects of study. The focus of the current work is placed on the stability problem, thus the availability of the methods aiming on real-time stability monitoring is considered. Lately, few methods capable of early identification of instability were delivered, among them [60]-[61], [80]-[81]. Such methods can be associated with a second component for adaptive control, as awareness of the current stability conditions and specifically information regarding the proximity of a given operational point to the stability boundary can serve as input information for the decision of the preventive control activation.

The next step on the way to realization of wide area adaptive control is development of the last component from the list which is modification of the system on the basis of the obtained information in a way that improves operational conditions. In closer look this component includes several sub-problems to be solved:

- Identification of control action
  - Location of a control action application
  - Identification of the type of control action
  - Pre-assessment of the sufficiency of the suggested countermeasure
- Automatization of the execution of the chosen control action
  - Taking into account communication time delay between the controller and the actuator
  - Coordination of the suggested control with other automation and protection in the system
  - Realization of supervisory control by control room personnel, prioritization of the decision maker (Automated control vs. human operator control)

The first group of problems has a fundamental scientific nature. In order to solve these problems corresponding theoretical and methodological base should be developed, while the second group is mostly reflecting the challenge of practical implementation and is mainly an issue of applied engineering.

This thesis is mainly focused on the development of the theoretical and methodological basis for the algorithms enabling automated self-modification of the system when the

risk of instability occurs. This definition allows relating the method under development to the methodological base supporting the concept of self-healing systems [82]. The Figure 3-1 illustrates the niche which developed method is taking in power systems operation and adaptive control.

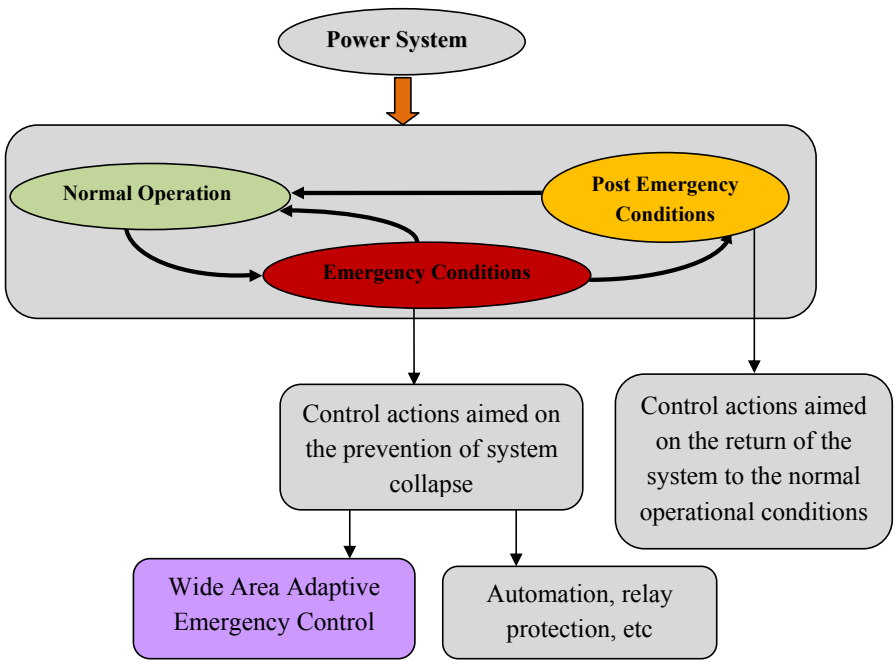

Figure 3-1: Niche for Wide Area Adaptive Emergency Control in power systems.

This thesis is focused on the development of early prevention method. Availability of such methods, capable to define the appropriate countermeasure within restricted time frame will open up the opportunity of implementation of wide area adaptive control aimed on retaining stability of power systems. In order to illustrate the functionality of the early prevention method the detailed structure of wide area adaptive emergency control is presented in Figure 3-2.

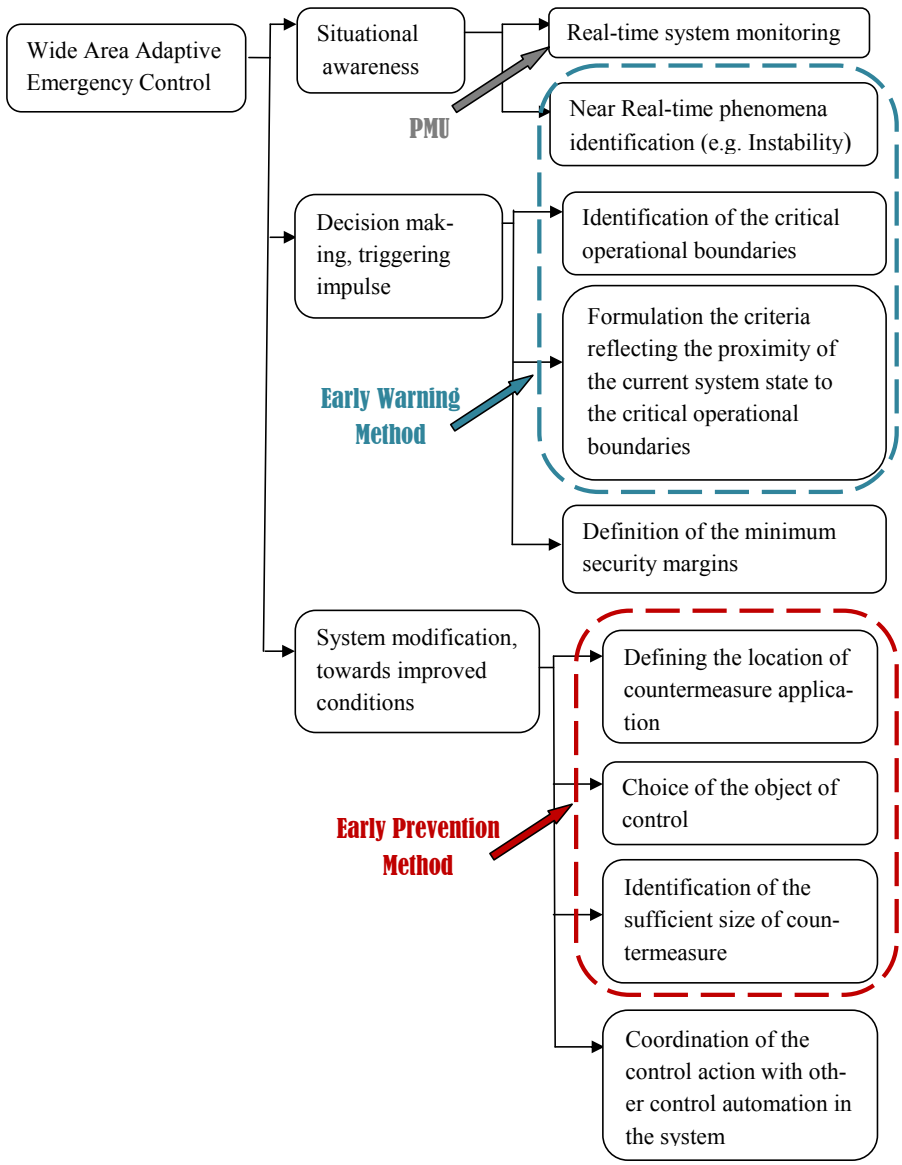

Figure 3-2: Wide Area Adaptive Emergency Control Architecture.

The study is utilizing the results of the previous research, which was aimed on early indication of aperiodic small signal angular instability, utilizing PMU. A short overview of this method is presented in the next section of this chapter.

3.2 Early Warning Method for System Instability

Early warning method was developed within the scope of a PhD project and described in detail in the report [24]. Main achievement of this method is the capability of identification of the aperiodic small signal angular stability (ASSAS) boundary for each synchronous generator in the grid in real-time. The mathematical expression for the stability boundary identification was analytically derived and allows, among other matters, defining how close an operational point of a given generator is to the actual stability boundary at the given moment of observation. Stability boundary is formulated in terms of equivalent two bus system representation, which contains generator under consideration and the remaining system reduced to Thevenin equivalent. Graphical representation of this system can be seen in Figure 3-3.

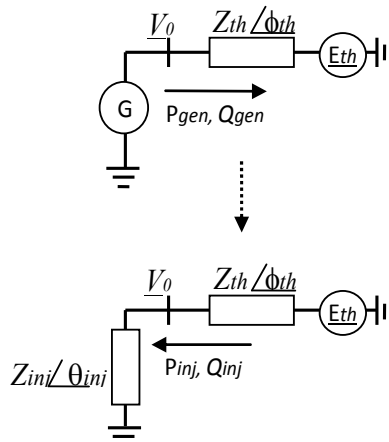

Figure 3-3: Equivalent system representation relatively critical generator.

The power injection from a given generator is represented at a node of constant steady-state voltage magnitude V_0. The mathematical criterion for the aperiodic small signal angular stability given by [24]:

$$Z_{inj} \geq -Z_{th} \cdot \sin(\theta_{inj}) / \sin(\phi_{th}) \qquad \textbf{(3.1)}$$

Where Z_{inj} corresponds to the magnitude of the generators' injection impedance, measured at the node of constant steady state voltage magnitude V_0, Z_{th} is equivalent Thevenin impedance of the system seen from the node of power injection. θ_{inj} and ϕ_{th} are the angles of $\underline{Z}_{inj}$ and $\underline{Z}_{th}$ respectively. The injection impedance is determined as:

$$\underline{Z}_{inj} = -\underline{V}_0^{\,2} / (P_{gen} + j \cdot Q_{gen})^* = \underline{V}_0^{\,2} / \underline{S}^*_{inj} \qquad \textbf{(3.2)}$$

Where P_{gen}, Q_{gen} are an active and reactive power of a generator fed to a grid from the node of constant steady state voltage magnitude and $\underline{S}_{inj}$ is corresponding injection power which equals to $\underline{S}_{gen}$ with opposite sign.

$$\underline{Z}_{inj} = \underline{V}_0 \cdot \underline{Z}_{th} / (\underline{E}_{th} - \underline{V}_0) \tag{3.3}$$

Considering (3.1) and (3.3) one may see that parameters determining the ASSAS boundary are $\underline{Z}_{th}$, $\underline{E}_{th}$ and $\underline{V}_0$. $\underline{Z}_{inj}$ and $\underline{V}_0$ can be easily defined from PMU data, whereas calculation of $\underline{Z}_{th}$ in near real-time required development of an algorithm, capable of determining this value algebraically avoiding computationally consuming operations. Corresponding method was developed in [24] and enables calculation of $\underline{Z}_{th}$ directly from the regularly updated system admittance matrix. Up-to-date system admittance matrix is assumed to be available due to data provided by PMU, meaning complete system observability is required.

The proximity of the current operational point of a generator to its stability boundary is introduced in [24] in terms of active power margin. Active power margin is showing how much more active power can be injected into the node of constant steady state voltage magnitude bevore the out of step conditions would be met. Mathematically, active power margin is expressed as follows (3.4):

$$P_{inj} = \frac{E_{th} \cdot V_0}{Z_{th}} \cos(\gamma + \phi_{th}) - \frac{V_0^2}{Z_{th}} \cdot \cos(\phi_{th}) \,,$$

$$\therefore \quad P_{inj,\max} = -\frac{E_{th} \cdot V_0}{Z_{th}} - \frac{V_0^2}{Z_{th}} \cdot \cos(\phi_{th}) \,, \tag{3.4}$$

$$\%\Delta P_{inj} = \frac{P_{inj,\max} - P_{inj}}{P_{inj,\max}} \cdot 100\%$$

Where (see equivalent system in Figure 3-3) E_{th} and Z_{th} stand for magnitudes of Thevenin voltage and impedance, ϕ_{th} is the angle of the Thevenin impedance, V_0 corresponds to magnitude of constant steady state voltage and γ is an angle between $\underline{V}_0$ and $\underline{E}_{th}$.

Early warning method provided detection of instability on the very early stage of its emergence; furthermore the assessment of proximity of a given operational point to the stability boundary for each synchronous generator was presented. These achievements gave an inspiration for development of the method capable of identification of preventive countermeasure being triggered by early warning message.

The early warning method was taken as a basis for the current study as it provides criterion for ASSAS, which can be monitored in real-time and it can be used to trigger early prevention, when the system is facing risk of instability. Development of the early prevention method, which could provide functionality of an emergency adaptive control was the main goal of current study. Conceptual description of the early prevention method is presented in the next section.

3.3 Early Prevention Method: the concept

Identification of the appropriate and sufficient countermeasure is a crucial issue for the successful localization and elimination of emerging instability in power systems. Unlike system disturbances caused by stepwise events (short circuit, lightning overvoltage, malfunction of equipment. etc) ASSAI develops gradually which makes it possible to reduce an effort needed to prevent its development if appropriate countermeasure would be applied at the early stage of its emergence. Thus, assuming availability of the method reliably detecting risk of upcoming instability, it is required to develop method capable of fast identification of a countermeasure which would lead to escape from critical operational conditions before the situation would evolve to the level were the consumer might suffer from electricity shortages. This thesis is focused on development of such early prevention method. The method is based on solving number of tasks described in the Figure 3-4

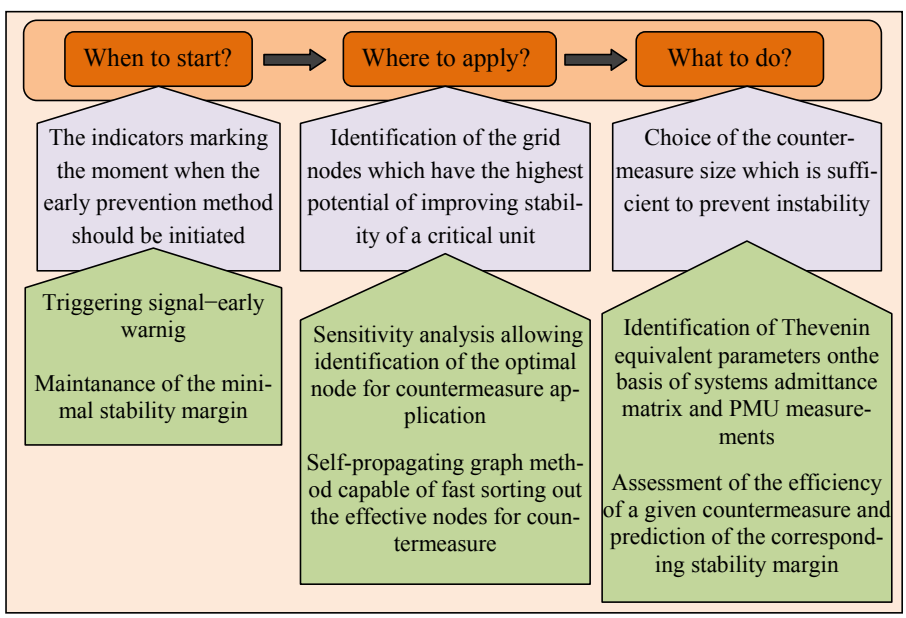

Figure 3-4: List of tasks and solutions proposed by early prevention method.

The early prevention method should provide backup functionality for the control room personnel, advising the most appropriate countermeasure to withstand instability in the given operational conditions, and overtake charge if no countermeasure action is taken by human operator, even though solution itroducing dispatcher ‘s “veto” right should be provided.

The early prevention method is dealing with aperiodic small signal angular instability-instability affecting synchronous machines in the grid, which makes itself felt by gradual monotonic increase of rotor angle up to the point where a unit goes out of step. For the current study the area of countermeasure application was limited to the load nodes in the grid (nodes which contain neither generators nor voltage sources). The chosen scope is reflecting operational conditions when the rescheduling of the generators is not possible, either due to complete loading of the units or insufficient maneuverability of the machines. Both those restrictions reflect the scenario of post contingency stressed operational conditions where the development of instability might have fast avalanche behavior. It should be mentioned that under normal operational conditions the rescheduling of the generators in order to improve stability margins might be more natural solution, even though economical feasibility of rescheduling should be confirmed; furthermore manipulations to the load nodes might have faster effect. Furthermore, flexible controllability of the load nodes is newly introduced control mechanism which may become available due to integration of electrical vehicles, energy storages and smart houses, advantage of which should be utilized.

3.4 Time domain simulation

As it was earlier described the method of early prevention is assuming that the complete observability of the system is available in real-time. In real power systems such data can be provided by wide area measurement systems utilizing PMU as a measuring device. Synchronized by GPS time stamp PMU measurements provide snapshots of the current system state. In order to generate synthetic PMU data time domain simulation of power system was used. As a simulation tool DIgSILENT Power Factory was chosen. Power Factory is software used for modeling and analysis of power systems operation, both in static and dynamic state. This software is actively used to model and analyze real power systems by different TSO among which are French, English and Danish. The advantage of Power factory is that besides static and dynamic simulation it allows script applications written in DigSilent Programming Language. That functionality was used for packing of the synthetic PMU data to the matrix and exporting them to the Matlab where the remaining calculations were carried out.

3.5 Timeline Structure

This section describes the typical time line of aperiodic small signal angular instability and the structure of the early prevention method. As it can be seen from the Figure 3-5 early warning and early prevention algorithms are to be utilized for the ASSAS assessment when the power system enters the quazi-steady state operation. For the certainty the term of quazi steady state operation should be defined.

In the given context the "quazi steady-state operation" stands for the slow dynamics of the system, which can be mathematically described as a sequence of the steady states. Meaning that after an initial transients, one (or more) of the dependent variables can be regarded as in steady state with respect to the instantaneous values of the other dependent variables [83]. Thus the lower limit for the time interval defining early prevention algorithm execution is specified by the time needed for power system to settle down to the quasi steady state operation after the disturbance had been experienced. The upper limit is not as such defined by the time rather than by the moment of ASSAS boundary cross-over. In fact time interval for the early prevention algorithm application needs to be reduced even more, considering the allowance for certain minimal stability margin in order to ensure that there will be time left for actual execution of the countermeasure prior to the instability dramatic development. Eventually, the time interval left for the early prevention algorithm application is enclosed between the moment when the system entered the quasi-steady state and the moment when the minimal stability margin is reached. This period is marked with light green in Figure.3-5.

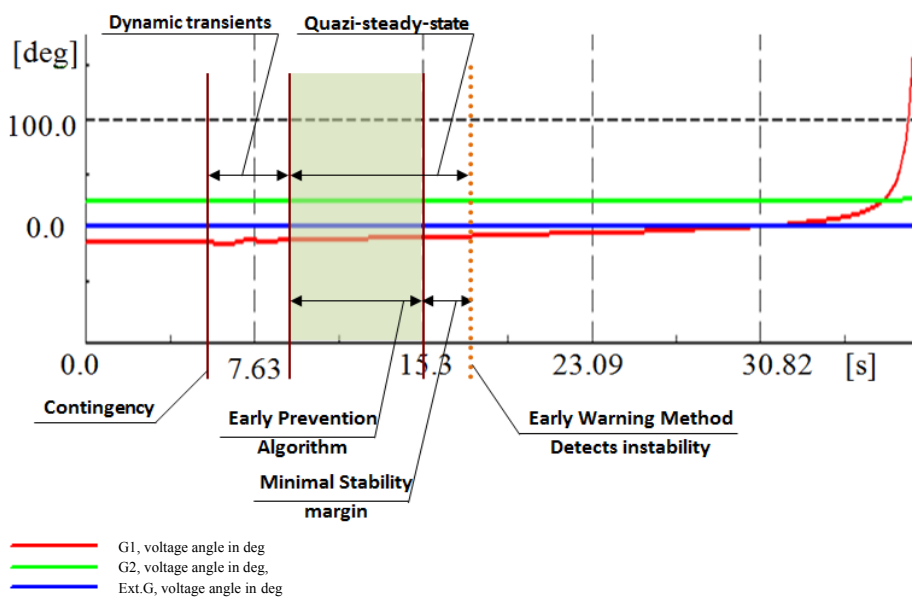

Figure 3-5: Timeline for the application of early prevention method.

On its turn, early prevention method contains several stages of analysis, which are consequently executed. Figure 3-6 presents the schematic timeline for these tasks.

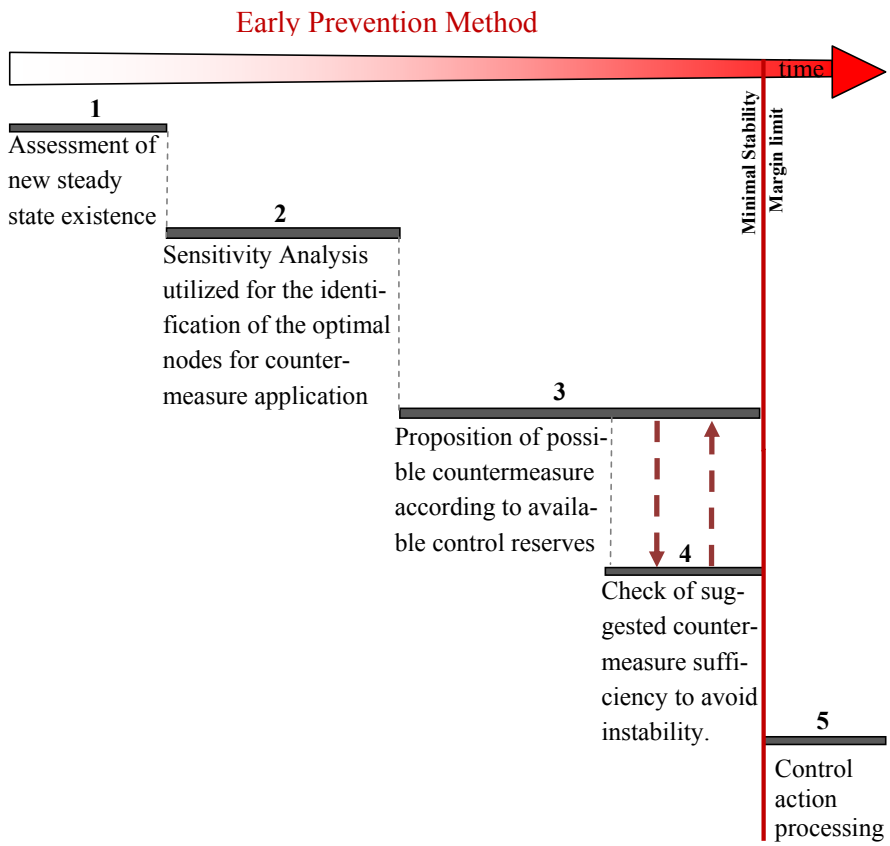

Figure 3-6: Stages of the early prevention algorithm.

Between the stages **3** and **4** at the feedback loop is possible in order to adjust the proposed countermeasure to the sufficient level which will lead to escape from instability.

The next chapters of this thesis will cover each of the stages listed in Figure 3-6 in detail. Firstly the stage number **2** is to be considered, the stage **1** will be considered jointly with the stage **4** as they have common theoretical basis.

4
IDENTIFICATION OF THE OPTIMAL NODE FOR COUNTERMEASURE APPLICATION

When the early warning method indicates that certain generators are approaching stability boundary, the natural step is to prevent the dangerous tendency by applying preventive countermeasure. Generally there might be a number of possible control actions helping the situation; nevertheless it would be beneficial to identify which of possible countermeasures would have the greatest impact on the improvement of critical generators' stability. For the current study, manipulations applied to the load nodes in the grid were studied as possible countermeasures. The nodes containing neither generators nor voltage sources are reffered to as load nodes in the following.

4.1 Sensitivity Analysis for the search of optimal candidates in the grid for the application of preventive countermeasure

To start the discourse concerning the choice of the optimal node for countermeasure application, the mathematical expression for ASSAS boundary derived in [24] and introduced in the section 3.2 is to be considered in detail:

$$Z_{inj} \geq -Z_{th} \cdot \sin(\theta_{inj}) / \sin(\phi_{th}) \tag{4.1}$$

The expression (4.1) can be rewritten the following way:

$$\begin{cases} Z_{inj} / \sin(\theta_{inj}) \geq -Z_{th} / \sin(\phi_{th}) & \text{when } \sin(\theta_{inj}) > 0 \\ Z_{inj} / \sin(\theta_{inj}) \leq -Z_{th} / \sin(\phi_{th}) & \text{when } \sin(\theta_{inj}) < 0 \end{cases} \tag{4.2}$$

Where, the left part of the inequation is dependent on steady state voltage magnitude V_0 and the apparent power of the generator under consideration. Considering the equation 3.3 it can be seen that any change in Thevenin equivalent will result in corresponding change of $\underline{Z}_{inj}$. The more noticeable change happens to Thevenin equivalent seen by critical generator, the more the generator's output is varied. For the current study the assumption that the rescheduling of the generator is restricted (active power output under steady state operation is fixed). The ASSAS conditions of a given generator can be influenced by varying the corresponding Thevenin equivalent. Considering the equation for the ASSAS boundary (4.2) it can be seen that stable operational area is defined by

Thevenin impedance and generator's injection impedance, where the latter is varying when the change in corresponding Thevenin equivalent happens. Thus, in order to identify which node in the grid has the highest potential influence stability conditions of a given generator it is necessary to find out which of the nodes is contributing the most to the corresponding Thevenin equivalent, specifically the Thevenin impedance. To rank the nodes in the grid respectively to their impact to the Thevenin impedance seen by a given generator the sensitivity analysis [84] is utilized.

Referring to the formula for the ASSAS boundary (4.1) the sensitivity of the term Z_{th} /sin(θ_{th}) to a variation of a nodal admittance is to be considered. The variation of nodal admittace is suggested for the analysis as countermeasure application can be interpreted in a form of admittance change, enabling studying of system admittance matrix alteration as a mean of stability improvement. For the further use lets denote $Z_{th}/\sin\phi_{th} = K_{th}$.

Generally, nodal admittance contains both an active and a reactive component. Furthermore, the active and reactive components of the nodal admittance often can be controlled separately. Taking this factor into account, the sensitivity of the K_{th} to the alteration of the active and reactive part of nodal admittance should be established (4.3):

$$S_{Kth\,P} = \left[\frac{\partial(Z_{th} / \sin(\varphi_{th}))_j}{\partial(real(\underline{Y}_{m,m}))}\right] = \left[\frac{\partial(K_{th_j})}{\partial(real(\underline{Y}_{m,m}))}\right]$$
$$S_{Kth\,Q} = \left[\frac{\partial(Z_{th} / \sin(\varphi_{th}))_j}{\partial(imag(\underline{Y}_{m,m}))}\right] = \left[\frac{\partial(K_{th_j})}{\partial(imag(\underline{Y}_{m,m}))}\right] \quad \textbf{(4.3)}$$

The nodal admittance is sequentially altered per the same value ΔY in each load node (Figure 4-1), and corresponding change in K_{th} is defined. Hence the ratio of ΔK_{th} /ΔY defines desired sensitivity.

$$Y_0 = \begin{bmatrix} Y_{11} & \dots & \dots & Y_{1N} \\ \dots & Y_{ii} & \dots & \dots \\ \dots & \dots & Y_{jj} & \dots \\ Y_{N1} & \dots & \dots & Y_{NN} \end{bmatrix} \Rightarrow \begin{cases} Y' = \begin{bmatrix} Y_{11}+\Delta Y & \dots & \dots & Y_{1N} \\ \dots & Y_{ii} & \dots & \dots \\ \dots & \dots & Y_{jj} & \dots \\ Y_{N1} & \dots & \dots & Y_{NN} \end{bmatrix} \\ Y' = \begin{bmatrix} Y_{11} & \dots & \dots & Y_{1N} \\ \dots & Y_{ii}+\Delta Y & \dots & \dots \\ \dots & \dots & Y_{jj} & \dots \\ Y_{N1} & \dots & \dots & Y_{NN} \end{bmatrix} \\ \dots \end{cases}$$

Figure 4-1: Sequential alteration of the nodal admittance for the sensitivity analysis.

The obtained values being normalized with respect to the highest sensitivity are indicating the relative potential effectiveness of the countermeasures applied to a certain node for improving stability conditions of a given generator. The nodes, with the higher sen-

sitivity will provide greater impact on the stability of a considered generator. For the further use, the term for relative effectiveness of countermeasure application is to be introduced as Control Efficiency Factor (CEF) (4.4).

$$CEF_i = \frac{S_{Kth\ i}}{S_{Kth\ \max}}; \qquad S_{Kth\ \max} = \max(S_{Kth\ i})\ ,\ i \in 1..\mathrm{M} \qquad \textbf{(4.4)}$$

Where M=N-Nvs;

Taking into account independent variation of active and reactive component of the nodal admittance, two matrixes $\mathbf{CEF}_P$ and $\mathbf{CEF}_Q$ can be formulated as follows (4.5):

$$[CEF]_Q = \begin{pmatrix} S_{Kth_1\ Q_1} & \cdots & S_{Kth_1\ Q_{(N-N_{VS})}} \\ \vdots & \ddots & \vdots \\ S_{Kth_k\ Q_1} & \cdots & S_{Kth_k\ Q_{(N-N_{VS})}} \end{pmatrix} \qquad [CEF]_P = \begin{pmatrix} S_{Kth_1\ P_1} & \cdots & S_{Kth_1\ P_{(N-N_{VS})}} \\ \vdots & \ddots & \vdots \\ S_{Kth_k\ P_1} & \cdots & S_{Kth_k\ P_{(N-N_{VS})}} \end{pmatrix} \qquad \textbf{(4.5)}$$

k Generators

Load nodes

The prioritized list for the countermeasure application candidates can be formulated on the basis of $\mathbf{CEF}_P$ and $\mathbf{CEF}_Q$ sorting the nodes in descending values of CEF. This approach allows optimizing application of a countermeasure, enabling improvement of stability for a given generator with a minimum effort.

However, high CEF indicating the high potential efficiency of a countermeasure application does not reflect the availability of control reserves at a given node. For clarity, the term "control reserves" should be specified. In the context of this study, "control reserves" are defined by possibility of nodal admittance regulation by means of e.g.: commutation of the reactive power compensation devices, control of the flexible load, variation of power injection (e.g. HVDC control), etc. Generally, allocation and availability of the control reserves in the system would vary depending on current operational conditions, maintenance plan, etc. This factor should be taken into account when creating prioritized list of candidate nodes for countermeasure application. For this purpose the control participation matrix **C**, indicating the availability of the control reserves at a given node is introduced. Matrix **C** is a square matrix sized $\{N - N_{vs}\}$ x $\{N - N_{vs}\}$, where all off-diagonal elements are equal to zero, while elements on the main diagonal are either equal to zero – indicating that there are not control reserves available in a given node , or C_{ii} is equal to 1 reflecting the availability of control reserves in the node i. By multiplying **CEF** matrix and **C** matrix the resulting matrix **CEF2** is obtained. When normalized, elements with higher value of sensitivity are indicating the higher effectiveness of the countermeasure applied to the corresponding node, but the prioritization in this case is carried out only between the nodes containing a control reserve for variation of nodal admittance.

$$[CEF]_Q = \begin{pmatrix} S_{Kth_1 Q_1} & \cdots & S_{Kth_1 Q_{(N-N_{VS})}} \\ \vdots & \ddots & \vdots \\ S_{Kth_k Q_1} & \cdots & S_{Kth_k Q_{(N-N_{VS})}} \end{pmatrix} \qquad [C] = \begin{pmatrix} C_{11} & 0 & 0 \\ 0 & C_{mm} & 0 \\ \cdots & \cdots & \cdots \\ 0 & 0 & \cdots & C_{(N-N_{VS})(N-N_{VS})} \end{pmatrix}$$

$$[CEF2]_Q = [CEF]_Q \cdot [C] = \begin{pmatrix} CEF2_{11} & \cdots & CEF2_{1(N-N_{VS})} \\ \vdots & \ddots & \vdots \\ CEF2_{k1} & \cdots & CEF2_{k(N-N_{VS})} \end{pmatrix} \tag{4.6}$$

4.2 Stability improvement for a number of generators simultaneously, activating minimum of control reserves.

Experiencing post-contingency operation of the power system it might appear that several synchronous generators in the grid are operating close to their stability boundaries. In order to insure safety and reliability of the power supply the stability margin should be maintained at a certain required level. It should be mentioned here that the regulations for minimal stability margin varies from country to country, and nowdays a predefined constant value, often obtained on the basis of N-1 off-line analysis is used.

The possibility of simultaneous improvement of stability for the chosen group of generators will be discussed in this section. The suggestion is to utilize the sensitivity method described above for identification if there is a node in the grid which has a noticeable influence on the stability of a number of generators under consideration.

To begin with the vector containing generators which stability conditions are unsatisfactory is created $k_{gr} = [k_1 \ldots k_m]$, where m is a number of chosen generators. For the selected set of generators the sensitivity analysis described in the section above is carried out, thus the **CEF2** is formulated. On the next step the rows of **CEF2** corresponding to generators from the set k_{gr} are summarized elementwise:

$$for\ k_{gr} = \{k_{gr1}, k_{gr2}, k_{gr3} \ldots k_{grn}\} \subseteq \mathrm{k}$$

$$[GrC] = \left[\sum_{i=k_{gr1}}^{k_{grn}} CEF2_{i,1} \quad \sum_{i=k_{gr1}}^{k_{grn}} CEF2_{i,2} \quad \ldots \quad \sum_{i=k_{gr1}}^{k_{grn}} CEF2_{i,(N-N_{VS})} \right] \tag{4.7}$$

The elements of the resulting vector **GrC** (group control vector) are representing integral control efficiency factor for each of the load nodes in the grid. The higher the integral factor is the more influence a corresponding node has on the stability of the generators set k_{gr}. Nevertheless in order to accomplish the group effect of regulation, the contribution of the control efficiency factor from each of the generators $\subset \mathrm{k}_{gr}$ should be

commensurable. To ensure that participation of each $CEF2_{k,m}$ in the $GrC_{1,m}$ is commeasurable, which means that given load node *m* has influence on the stability of all the generators from the control group, filtering is to be applied. The filter is based on setting the low limit for the weight coefficients *wc* of $CEF2_{k,m}$:

$$wc_{k_{grn},m} = CEF2_{k_{grn},m} \;/\; GrC_{1,m} \quad , \quad \forall wc_{k_{grn},m} \geq \frac{1}{2N_{k_{gr}}} \tag{4.8}$$

Where N_{kgr} is number of the generators in the control group.

The nodes which meet the condition (4.8) are added to the candidate list for the group control. The optimal node for countermeasure application is defined from that list. The higher value of the integral control efficiency factor (ICEF) $\sum CEF2_{1,j}$ corresponds to a higher influence of a given node on the stability of a generators from the control group k_{gr}. Accordingly the optimal countermeasure application node has the maximum ICEF.

$$OptC = \max\left[GrC\right] \tag{4.9}$$

When the condition (4.8) is not satisfied by any load nodes the stability of the critical generators should be improved separately, as there is no node in the grid which can deliver group control functionality for the chosen set of generators. Individual improvement of stability conditions for each of critical generators would require more changes in the grid comparing to the group control, nevertheless in this case the sufficient stability margin increase for each of critical generators can be ensured.

The validation of the suggested methodology is described in the paper “Early Prevention of Instability - Search for Optimal Grid Nodes for Applying Countermeasures” [85], where the application of the method to the test systems is considered.

5
SELF PROPAGATING GRAPH FOR THE FAST SEARCH OF OPTIMAL COUNTERMEASURE APPLICATION NODE

The methodology for the search of the optimal location for the countermeasure application has been described in the previous chapter. The developed algorithm required calculation of the Thevenin impedance sensitivity to the variation of nodal admittance, where consequently all load nodes in the grid were considered. Even though calculation of Thevenin impedance corresponding to a given admittance matrix can be processed fast, utilizing the approach described at [24], there is a wish to reduce the number of nodes processed through sensitivity analysis (SA). Such intention is supported by logical reasoning that there is a limited amount of nodes in the grid which have significant influence on the stability of a given generator, as with increase of electrical distance participation of a given node in the Thevenin impedance seen by generator reduces.To reduce the number of nodes to be processed through SA, avoiding computation of the electrical distance the algorithm based on discrete graphing was developed.

5.1 The background considerations for the self-propagating graph methodology

The approach described in this section was inspired by the observation of propagation of the drop disturbance over the water surface. As it can be seen from Figure 5-1 water drop causes the largest disturbance close to the epicenter while on a certain distance the drop is not causing considerable perturbations. It can be noticed that it is possible to choose a radial closed contour embracing the region where the water drop initiate noticeable surface disturbance, while the remaining water surface which keep being still stays out of chosen contour.

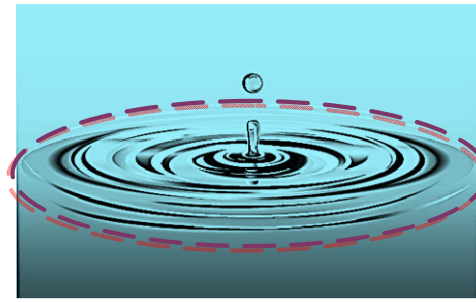

Figure 5-1: Water drop disturbance embraced by closed contour.

As soon as such contour is defined it can be stated that for any point of the water surface lying out of the contour the disturbance caused by water drop is negligible. Meaning that the whole water surface is divided into two areas: the one influenced by disturbance greatly and another where the disturbance courses minor response. Furthermore, for the second area it can be declared a-priory that the disturbance would have minor effect at any point related to this area. It can be noticed that in any point outside of the chosen closed countour the sensitivity to the disturbance would be smaller comparing to the area within the contour.

Applying this reasoning to an electrical grid the following analogy is considered: water drop is representing variation of nodal admittance, while a disturbance on the water surface is representing an influence which given admittance variation has on a generator's stability.

In case of water drop the attenuation gradient is radially distributed from the point of the drop fall, forming "equipotential" surfaces of the disturbance spread. Meanwhile an electrical grid is not homogeneous, considering that the topological structure is uneven, "equipotential" surfaces of the disturbance spread would not appear as an "equi-radial" circles. In fact "equipotential" surface of disturbance propagation in the case of electrical grid is defined by electrical distance between the node to which the variation of nodal admittance was applied and other nodes in the grid. With increase of electrical distance sensitivity to an applied disturbance decreases. In order to avoid calculation of electrical distance, for the first approximation it can be assumed that the electrical distance between given nodes is corresponding to their topological distance. Thus, as a benchmark for the directing of the attenuation gradient a topological distance between nodes is proposed. The term "topological distance" in this context means a number of vertexes on the shortest path between the critical generator and a given node, while a grid is represented as a graph; moreover, the edges in this graph are weightless. Since the interest is a generator's stability, the root of the graph is placed at a terminal of the generator under consideration. When the root vertex is defined the further graphing of the grid should follow the logic described in the next paragraph.

5.2 Creation of self-propagating graph

As it was mentioned earlier the process of graphing starts from a terminal of a generator of interest. Guided by the main purpose to sort out the nodes with the higher sensitivity s_{Kth} and bearing in mind correlation between the sensitivity decrease and topological distance, the natural decision is to start consideration of the nearest nodes in the first order. Thus, the further spread of the graph into the grid is organized in discrete steps, where the reference criterion is a shortest topological distance from a given generator to the considered node. The discretization interval is defined to be one vertex, meaning that the nodes added to the graph on an each successor step are having the shortest path to a root of the graph one vertex longer than the nodes included in the graph on the previous step. The formation of the graph happens stepwise adding a set of the semi-distant nodes on each step (Figure 5-2). When a new set of nodes is added to the graph, the sensitivity of Thevenin impedance to a nodal admittance variation s_{Kth} should be calculated for each of the nodes in the set. In order to sort out the nodes which should be added to the countermeasure candidate list, the value of minimal acceptable sensitivity $s_{Kth\min}$ is introduced.

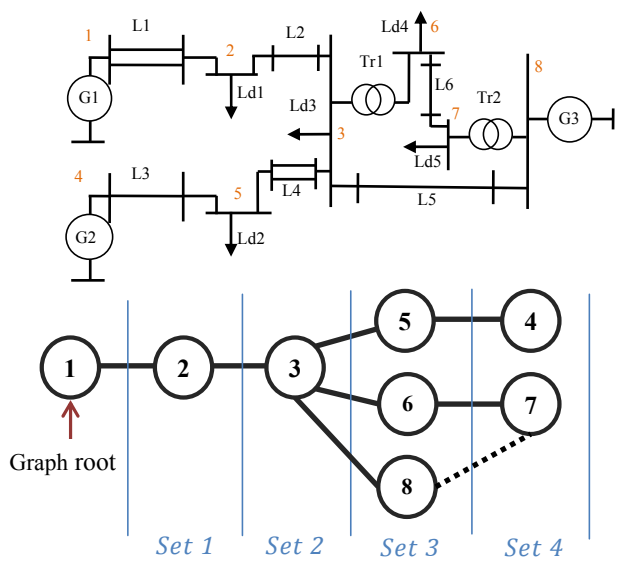

Figure 5-2: Single line diagram of 8 bus system and corresponding graph, with illustrated split per node sets.

$s_{Kth\min}$ is the minimal limit for sensitivity, according to which the part of a grid in which nodal admittance variation has a noticable influence on the stability of a given generator is chosen. This criterion is defining the "depth "of graph propagation into a grid. Generally, this criterion is varying and depends on topology of the grid. In meshed grids the

sensitivity s_{Kth} decreases faster, which means that the minimum acceptable value for $S_{Kth_{\min}}$ can be lowered in this case, to ensure that a sufficient amount of nodes capable of providing positive effect on generator's stability are considered. Furthermore, the sufficiency of number of nodes processed through SA, is dependent on the availability of the control reserves in the nodes with high sensitivity and might vary depending on the current control reserves allocation.

The propagation of the graph into a grid through the considered node continues until the sensitivity in this node s_{Kth} is higher than $S_{Kth_{\min}}$. If $s_{Kth} < S_{Kth_{\min}}$ the node is marked as a dead-end node and further development of the graph through this node is blocked. Thus when the next set is formed, the path to the considered nodes can't lay through the dead-end node. The spread of the graph into the grid continues until one of the two following conditions is satisfied:

- All nodes in the grid are visited;
- The further propagation of the graph is impossible as all nodes in the previous set are marked as dead-end nodes.

Satisfaction of the second criterion means that all unvisited nodes in the grid will have CEF below the defined $S_{Kth_{\min}}$, and should not be processed through SA. Thus the group of nodes is excluded from SA a-priory, gaining savings in computational time.

In order to keep track of the visited nodes, which have been already included in the self-propagating graph, the nodes from the considered set are added to the list **L**, on each step of the propagation; before adding a node to the set the check if the node is already listed in **L** is carried out. Further computational improvement can be achieved if graphing can be organized in a way so that the resulting graph is a tree. By eliminating loops in the graph the double check of sensitivity at the same node can be avoided. Looping can take place when a given node has more than one path with the same number of vertexes on the way to the beginning of the graph. In Figure 5-2 it is shown that there are two pathes to the node 7 with the same amount of the vertexes to the beginning of the graph; they are 1-2-3-6-7 and 1-2-3-8-7, which means that node 7 would be included in the set 4 twice, which consequently will lead to double calculation of sensitivity s_{Kth} at that node. In order to avoid excessive calculations looping in the graph should be eliminated. For this purpose the FIFO (First In First Out) queuing is used, with update of the list **L** in each step of the queue. Such approach allows keeping track of the visited nodes, not only when comparing a set of nodes to the previous sets, but within a set as well.

If those principles of graphing are followed, the resulting graph is a tree and all nodes added to the graph are visited only ones.

5.3 The algorithm for SA realized within self-propagating graph approach

Below the schematic representation of the self-propagating algorithm is presented.

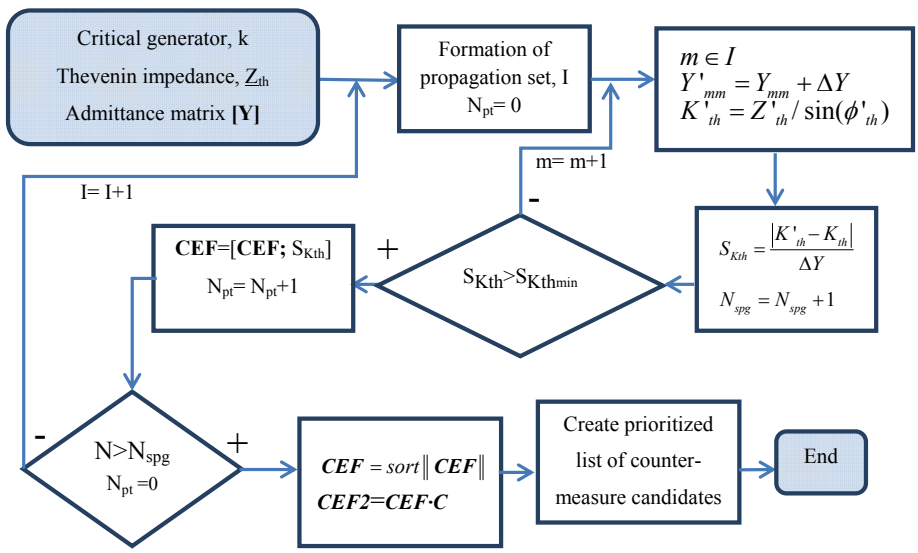

Figure 5-3: Self-propagating graph algorithm

Where:

N_{pt}−the number of nodes in the set through which the further propagation of the graph is allowed;

I− set of the nodes formed on the current step of propagation;

m− node belonging to the set I;

N− total number of load nodes in the grid;

N_{spg}− number of visited nodes, which are added to self-propagating graph;

s_{Kth} −sensitivity of the Thevenin impedance seen by generator k when varying admittance of the node m;

$s_{Kth_{\min}}$ −minimal acceptable value of sensitivity;

C− control participation matrix, reflecting allocation of control reserves in the grid;

$\|CEF\|$− normalized control efficiency factor matrix.

In Figure 5-4 the improvised grid structure is depicted to illustrate the formation of the self-propagating graph. The initial grid is colored in light gray; the root of the graph is located in the node marked in red. Yellow marks the nodes which represent the dead-end nodes, black corresponds to the nodes which are not included into self-propagating graph as it is not possible to reach them from the root of the graph without passing the dead-end nodes.

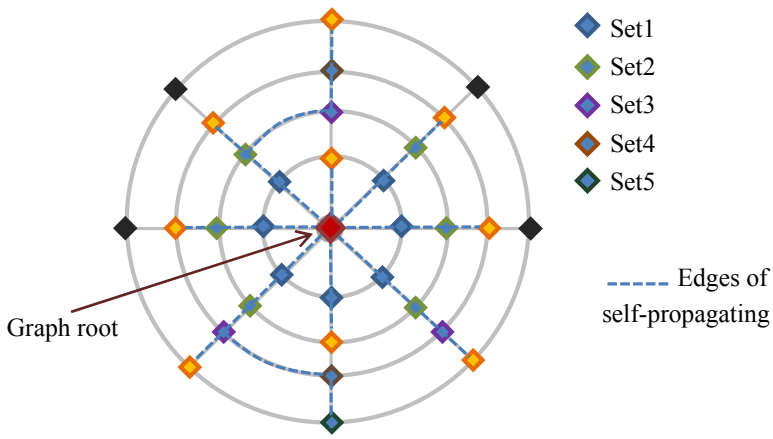

Figure 5-4: Illustration of self-propagating graphing

The described methodology allows eliminating the nodes having low influence on stability of a given generator from being processed through SA. Thus the search of the optimal node for application of the countermeasure is carried out between the reduced number of nodes, reducing computational time. The efficiency of the self-propagating graph algorithm can be assessed using the following expression:

$$\eta = \frac{N - N_{spg}}{N} \cdot 100\% ;$$

Where N stand for total number of load nodes in the grid and N_{spg} is a number of nodes included into self-propagating graph. It can be seen that the less nodes are included in the self-propagating graph the higher the efficiency is, thus reflecting the greater improvement in computational time for the search of the best location for the countermeasure application.

The validation of the considered methodology is covered in [86], where two test systems were studied: the IEEE30 bus test system and the 1648 bus US west coast test system provided in the PSSR E-30.06. It is shown that the efficiency of the self-propagating graph grow with increase of the dimensionality of the system under consideration. For the IEEE30 bus test system the efficiency equaled to 30% meaning that only 0.6·N of the total number of nodes will be processed through SA. For the 1648 bus US west coast test system the efficiency of the longest created self-propagating graph

appeared to be 83.24%, resulting in processing of only ~20% of the nodes through SA. Thus, the suggested methodology provides noticeable reduction of the computational time spent for SA, especially considering large scale systems.

6
DETERMINING THE SUFFICIENT SIZE OF A COUNTERMEASURE

The previous chapter was focused on the fast identification of the optimal location for a countermeasure application. Self-propagating graph algorithm capable of solving this problem has been introduced. The next action on the way of preventing unwished operational conditions leading to aperiodic small signal angular instability is specifying the countermeasure "size", which would be sufficient for avoidance of instability. This chapter will be considering the methodologies allowing assessment of the sufficiency of the suggested countermeasure.

6.1 Stability active power margin as a benchmark for countermeasure efficiency assessment

In order to assess the effectiveness of applied countermeasure a certain benchmark criterion should be set. As such criterion the stability active power margin introduced in [24] has been chosen.

$$\begin{aligned} P_{inj} &= \frac{E_{th} \cdot V_0}{Z_{th}} \cos(\gamma + \phi_{th}) - \frac{V_0^2}{Z_{th}} \cdot \cos(\phi_{th}) \,, \\ \therefore \quad P_{inj,\max} &= -\frac{E_{th} \cdot V_0}{Z_{th}} - \frac{V_0^2}{Z_{th}} \cdot \cos(\phi_{th}) \,, \\ \%\Delta P_{inj} &= \frac{P_{inj,\max} - P_{inj}}{P_{inj,\max}} \cdot 100\% \end{aligned} \tag{6.1}$$

Where (⇒equivalent system (Figure 3-3)) E_{th}, Z_{th} stand for magnitudes of Thevenin voltage and impedance respectively, ϕ_{th} is angle of Thevenin impedance, V_0 corresponds to magnitude of constant steady state voltage and γ is angle between $\underline{V}_0$ and $\underline{E}_{th}$.

When the ASSAS boundary is crossed the stability active power margin $\%\Delta P_{inj}$ is equal to zero. Maintaining stability margin at a certain level ensures stable operation of synchronous generator. In order to define if the countermeasure expressed in terms of nodal admittance variation provides sufficient improvement of stability for the critical generator, it is necessary to determine how change in admittance matrix will influence the Thevenin equivalent parameters, namely $\underline{Z}_{th}$ and $\underline{E}_{th}$ (Figure 6-1).

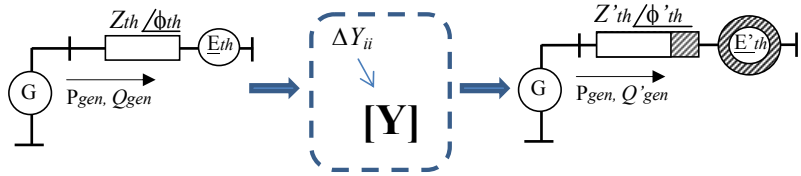

Figure 6-1: Change in Thevenin Equivalent caused by variation in admittance matrix

Utilizing the methodology described in [24] it is possible to calculate $\underline{Z}_{th}$ whenever the system admittance matrix is available. Thus, updating the admittance matrix corresponding to a nodal admittance variation $Y'_{ii} = Y_{ii} + \Delta Y$, new Thevenin impedance can be obtained. The remaining Thevenin equivalent parameter which stays unknown is Thevenin voltage. In the next sections the methodology for identification of the new Thevenin voltage will be presented.

6.2 Split of the Thevenin voltage per components induced by each voltage source in the grid.

Thevenin voltage is an equivalent voltage seen from a given node of the system when reducing remaining system. All voltage sources contained in the reduced system are contributing to the Thevenin voltage. The share of this contribution is dependent both on the value of voltage at the voltage regulated node and on topological structure of the grid.

To begin with, the inference will be carried out for the simple test system depicted in Figure 6-2.

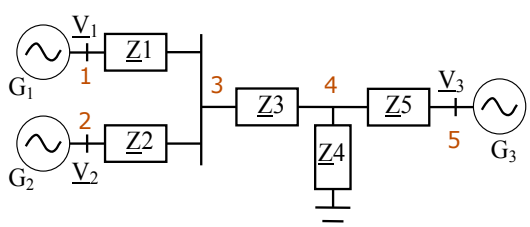

Figure 6-2: Single line diagram of 5 bus example system

Let's consider reduction of the grid with regard to generator G_3. The Thevenin equivalent seen by G_3 is to be defined. Considering system depicted in Figure 6-2 the following expressions for the Thevenin equivalent parameters can be written:

a)

$$\underline{Z}_{th} = \frac{\left(\frac{\underline{Z}_1 \cdot \underline{Z}_2}{\underline{Z}_1 + \underline{Z}_2} + \underline{Z}_3\right) \cdot \underline{Z}_4}{\frac{\underline{Z}_1 \cdot \underline{Z}_2}{\underline{Z}_1 + \underline{Z}_2} + \underline{Z}_3 + \underline{Z}_4} + \underline{Z}_5 \tag{6.2}$$

b)

$$\underline{E}_{th} = \left(\underline{V}_1 \cdot \frac{\underline{Z}_2}{\underline{Z}_1 + \underline{Z}_2} + \underline{V}_2 \cdot \frac{\underline{Z}_1}{\underline{Z}_1 + \underline{Z}_2}\right) \cdot \frac{\underline{Z}_4}{\frac{\underline{Z}_1 \cdot \underline{Z}_2}{\underline{Z}_1 + \underline{Z}_2} + \underline{Z}_3 + \underline{Z}_4} =$$

$$= \underbrace{\left(\underline{V}_1 \cdot \frac{\underline{Z}_2}{\underline{Z}_1 + \underline{Z}_2} \cdot \frac{\underline{Z}_4}{\frac{\underline{Z}_1 \cdot \underline{Z}_2}{\underline{Z}_1 + \underline{Z}_2} + \underline{Z}_3 + \underline{Z}_4}\right)}_{\underline{k}_{tr31}} + \underbrace{\left(\underline{V}_2 \cdot \frac{\underline{Z}_1}{\underline{Z}_1 + \underline{Z}_2} \cdot \frac{\underline{Z}_4}{\frac{\underline{Z}_1 \cdot \underline{Z}_2}{\underline{Z}_1 + \underline{Z}_2} + \underline{Z}_3 + \underline{Z}_4}\right)}_{\underline{k}_{tr32}} =$$

$$= \left(\underline{E}_{th1} + \underline{E}_{th2}\right)$$

It can be noticed from (6.2b) that Thevenin voltage can be represented as a sum of voltage components induced by voltage sources G_1 and G_2. Where each of the components is a product of the voltage at the voltage controlled node and a term, entirely dependent on impedances in the system .The expression (6.2b) can be rewritten in general form as follows:

$$\underline{E}_{th3} = \underline{V}_1 \cdot \underline{k}_{tr31} + \underline{V}_2 \cdot \underline{k}_{tr32} = \underline{E}_{th1} + \underline{E}_{th2} \tag{6.3}$$

According to (6.3) the equivalent Thevenin voltage is a sum of the voltage components induced by voltage sources. The initial voltage at a terminal of a voltage source when is seen by a given generator in form of thevenin voltage component gains magnitude transformation and turn in angle. Graphically the Thevenin equivalent formation can be represented as in Figure 6-3. On the left-hand part of the Figure 6-3 the voltages at a terminal of the voltage sources are depicted, the right hand diagram demonstrates the transformation experienced by voltage vectors when seen by a given generator. It is shown how the voltage components induced by each of the voltage sources in the grid contributes to the equivalent Thevenin voltage.

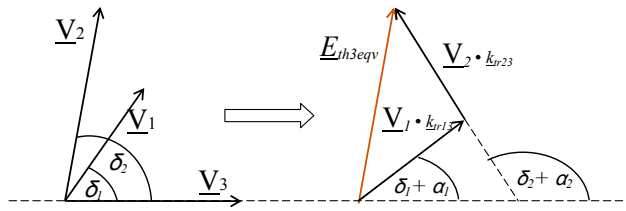

Figure 6-3: Formation of the Thevenin voltage sen by G_3

For the small system in Figure 6-3 the transformation coefficient $\underline{k}_{tr}$ has been defined by applying sequential changes to the system described below. To begin with the assumption that the system is linear and voltage sources are independent is accepted. These assumptions are based on the superposition theorem. This theorem is used for the network analysis including conversion of the system to the Thevenin equivalent. The superposition theorem states that the response in a linear circuit containing multiple voltage sources can be obtained by adding the individual responses caused by the separate independent sources acting alone [87].
Accordingly, the test system can be represented as a sum of two sub-systems presented in Figure 6-4.

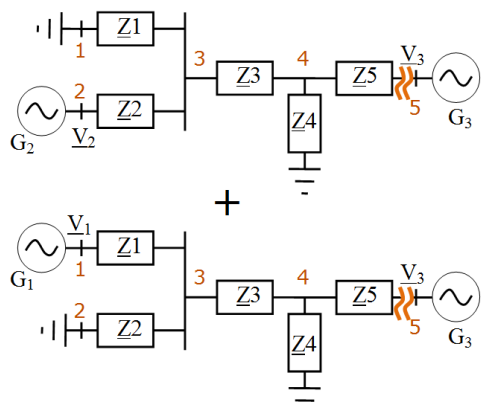

Figure 6-4: Single line diagram of sub-systems split according to the superposition principle

Thevenin voltage equivalent seen by generator G_3 is a voltage appearing at the open end from the grid side when G_3 is open circuited, in studied case it is bus 4. Thus, splitting system per two sub-systems and open-circuiting G_3, the Thevenin component induced by each voltage source appears at bus 4 and can be calculated for example on the basis of network equations.

In order to define $\underline{k}_{tr}$ for the arbitrary power system defining how any voltage source in the grid is seen by any generator the methodology based on availability of complete

system observability has been developed. For certainty let's assume that the arbitrary system under consideration contains N nodes and N_{vs}nodes containing voltage sources, k is a generator regarding which the reduction of the grid is to be studied and Thevenin voltage defined.

An interest is to define Thevenin voltage as a sum of components induced by each of voltage sources; as such representation allows understanding how the equivalent Thevenin voltage is formed and which of the voltage sources are contributing the most to it.
Due to the usage of superposition concept the calculation of each Thevenin component is carried out independently. As complete system observability was claimed as a pre-requisite the value of voltage $\underline{V}_{0,i}$ at the point of constant steady state voltage magnitude is available from PMU measurements, thus the goal is to define transformation coefficient $\underline{k}_{tr,i}$for each of the voltage sources in the reduced grid.

In order to accomplish this task a certain manipulations should be applied to the systems admittance matrix. To determine the Thevenin voltage component induced by voltage source *i* as seen by generator *k*, all the remaining voltage sources should be short circuited. To reflect this operation in admittance matrix the rows and columns corresponding to these voltage sources should be eliminated, which leads to reduction of admittance matrix dimensionality, resulting in $\{N - N_{vs} + 2\}$ x $\{N - N_{vs} + 2\}$. Then the node *k* should be open circuited – resulting in excluding the corresponding row and column from the admittance matrix, as well as deletion of all elements which will remain de-energized when the node *k* is open circuited. That will be all branch elements connected to a node unless there is shunt element at a node, forming closed loop. The adjustment of admittance matrix reflecting the open circuiting of G_3 for the test system is depicted below (Figure 6-5):

	1	2	3	4	5
1	$\underline{Y}_1$	0	$-\underline{Y}_1$	0	0
2	0	$\underline{Y}_2$	$-\underline{Y}_2$	0	0
3	$-\underline{Y}_1$	$-\underline{Y}_2$	$\underline{Y}_1+\underline{Y}_2+\underline{Y}_3$	$-\underline{Y}_3$	0
4	0	0	$-\underline{Y}_3$	$\underline{Y}_3+\underline{Y}_4+\underline{Y}_5$	$-\underline{Y}_5$
5	0	0	0	$\underline{Y}_5$	$\underline{Y}_5$

Figure 6-5: Admittance matrix modification to reflect an open cercuiting of generator G_3.

After all the manipulations related to the reduction of the original admittance matrix are taken, the reordering of it should be done. The column and row corresponding to node *i* should respectively be placed as the last column and row of the final reduced admittance matrix as it shown in Figure 6-6

	1	3	4	2
1	$\underline{Y}_1$	$-\underline{Y}_1$	0	0
3	$-\underline{Y}_1$	$\underline{Y}_1+\underline{Y}_2+\underline{Y}_3$	$-\underline{Y}_3$	$-\underline{Y}_2$
4	0	$-\underline{Y}_3$	$\underline{Y}_3+\underline{Y}_4$	0
2	0	$-\underline{Y}_2$	0	$\underline{Y}_2$

Figure 6-6: The resulting admittance maatrix when allrequired restructuring and reordering is done.

In general form the final structure of admittance matrix can be written as in (6.4):

$$\left[\underline{Y}_{MM}\right]=\begin{pmatrix}\underline{Y}_{11} & \cdots & -\underline{Y}_{1M}\\ \vdots & \ddots & \vdots\\ -\underline{Y}_{M1} & \cdots & \underline{Y}_{MM}\end{pmatrix}=\begin{array}{|c|c|}\hline \underline{Y}_{n\_vc,\,n\_vc} & \underline{Y}_{n\_vc,\,vc}\\ \hline \underline{Y}_{vc,\,n\_vc} & \underline{Y}_{vc,\,vc}\\ \hline \end{array}\quad \text{1} \qquad \textbf{(6.4)}$$

Where M is the size of reduced admittance matrix, index *vc* stands for voltage magnitude controlled nodes, and *n_vc* for non-controlled.

When the properly structured admittance matrix is formed the methodics for $\underline{k}_{tr,i}$ identification is following: at the first order, the nodal equations in matrix form should be written for the obtained admittance matrix(6.5):

$$\boldsymbol{V}=\boldsymbol{Y}^{-1}\cdot\boldsymbol{I};$$

$$\begin{pmatrix}\underline{V}_1'\\ \vdots\\ \underline{V}_q'\\ \\ \vdots\\ \underline{V}_M'\end{pmatrix}=\begin{pmatrix}\underline{Y}_{11} & \cdots & -\underline{Y}_{1M}\\ \vdots & \ddots & \vdots\\ -\underline{Y}_{q1} & \cdots & -\underline{Y}_{qM}\\ \\ \vdots & \ddots & \vdots\\ -\underline{Y}_{M1} & \cdots & \underline{Y}_{MM}\end{pmatrix}^{-1}\cdot\begin{pmatrix}\underline{I}_1\\ \vdots\\ \underline{I}_q\\ \\ \vdots\\ \underline{I}_M\end{pmatrix} \qquad \textbf{(6.5)}$$

When injecting current of 1A to the node M, while the remaining current injections are equal to zero, the voltage at the node M will be numerically equal to Z_{MM}, where

$Z=[Y]^{-1}$ is bus impedance matrix. At the same time the voltage in the arbitrary node *j* appears being numerically equal to Z_{jM}.

$$\begin{pmatrix} \underline{V}_1' \\ \vdots \\ \underline{V}_q' \\ \\ \vdots \\ \underline{V}_M' \end{pmatrix} = \begin{pmatrix} \underline{Z}_{11} & \cdots & \underline{Z}_{1M} \\ \vdots & \ddots & \vdots \\ \underline{Z}_{q1} & \cdots & \underline{Z}_{qM} \\ \\ \vdots & \ddots & \vdots \\ \underline{Z}_{M1} & \cdots & \underline{Z}_{MM} \end{pmatrix} \cdot \begin{pmatrix} \underline{I}_1 \\ \vdots \\ \underline{I}_q \\ \\ \vdots \\ \underline{I}_M \end{pmatrix} = \begin{pmatrix} \underline{Y}_{11} & \cdots & -\underline{Y}_{1M} \\ \vdots & \ddots & \vdots \\ -\underline{Y}_{q1} & \cdots & -\underline{Y}_{qM} \\ \\ \vdots & \ddots & \vdots \\ -\underline{Y}_{M1} & \cdots & \underline{Y}_{MM} \end{pmatrix}^{-1} \cdot \begin{pmatrix} 0 \\ \vdots \\ 0 \\ \\ \vdots \\ 1 \end{pmatrix} \qquad \textbf{(6.6)}$$

Respectively, the voltage at the node where the Thevenin voltage seen by generator *k* appears, for certainty lets denote it as a node *q*, would be numerically equal to Z_{qM}. Accordingly, the following ratio can be written (6.7):

$$\underline{k}_{tr\,Mq} = \underline{V}_q' / \underline{V}_M' = \underline{Z}_{q,M} / \underline{Z}_{M,M} \qquad \textbf{(6.7)}$$

The ratio (6.7) is the desired transformation coefficient between the generator and *q,* which is as expected entirely dependent on reduced system admittance matrix. The voltage transformation coefficient between node *k* and all the remaining voltage sources are calculated following the same methodology. As a result the grid transformation coefficient (GTC) matrix can be defined, which contains the transformation coefficients for each of the voltage source seen by any other voltage source in the grid (6.8).

$$GTC = \begin{pmatrix} 0 & \underline{k}_{tr21} & \cdots & \underline{k}_{trN1} \\ \underline{k}_{tr12} & 0 & \cdots & \underline{k}_{trN2} \\ \cdots & \cdots & \cdots & \cdots \\ \underline{k}_{tr1N} & \underline{k}_{tr2N} & \cdots & 0 \end{pmatrix} \qquad \textbf{(6.8)}$$

Where, the first digit of coefficients' index stands for the voltage source inducing the Thevenin voltage component $\underline{E}_{th,i}$, and the second digit is referring to the generator seeing the Thevenin grid equivalent.

The main diagonal of **GTC**matrix contains only zeros. That happens due to the fact that the generator, for which the reduction of the grid is carried out, doesn't contribute to Thevenin voltage which it sees. Furthermore it should be noted that **GTC** is not symmetrical in general case; that is caused by the fact that the node of appearance of the constant steady state voltage magnitude and the node where Thevenin voltage appears are not the same. For the clarification let's examine the 5 bus example system (Figure 6-7).

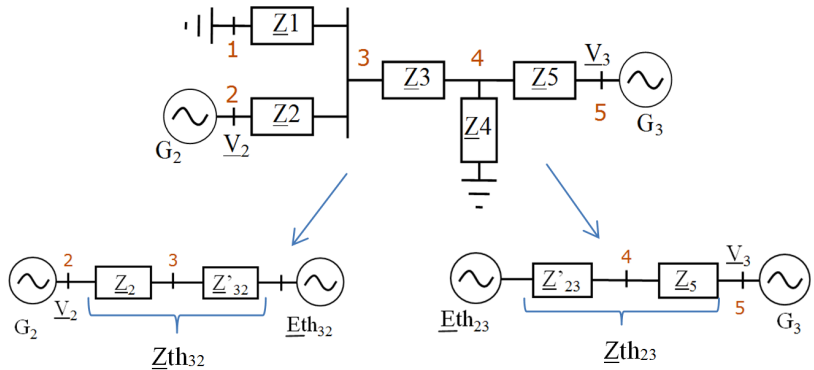

Figure 6-7: The Thevenin equivalet representation of the initial system reduced relatively G2 and G3.

When representing the Thevenin voltages shown in the Figure 6-7 as a product of grid transformation coefficient and the voltage of the voltage source the following can be written

$$\underline{E}_{th23} = \underline{V}_2 \cdot \underbrace{\frac{\underline{Z}_1}{\underline{Z}_1 + \underline{Z}_2} \cdot \frac{\underline{Z}_4}{\frac{\underline{Z}_1 \cdot \underline{Z}_2}{\underline{Z}_1 + \underline{Z}_2} + \underline{Z}_3 + \underline{Z}_4}}_{\underline{k}_{tr23}} \tag{6.9}$$

$$\underline{E}_{th32} = \underline{V}_2 \cdot \underbrace{\frac{\underline{Z}_4}{\underline{Z}_4 + \underline{Z}_5} \cdot \frac{\underline{Z}_1}{\frac{\underline{Z}_4 \cdot \underline{Z}_5}{\underline{Z}_4 + \underline{Z}_5} + \underline{Z}_3 + \underline{Z}_1}}_{\underline{k}_{tr32}}$$

It can be clearly seen from (6.9) that $\underline{k}_{tr23}$ in general is not equal to $\underline{k}_{tr32}$. Similarly, generalizing this observation for the arbitrary system it can be stated that **GTC** matrix isn't symmetrical.

Multiplication of the **GTC** matrix with the vector of voltages appearing at the point of constant steady state voltage magnitude gives the vector of equivalent Thevenin voltages seen by generators (6.10).

$$\begin{pmatrix} \underline{E}_{theqv\ 1} \\ \underline{E}_{theqv\ 2} \\ \cdots \\ \underline{E}_{theqv\ M} \\ \cdots \\ \underline{E}_{theqv\ N} \end{pmatrix} = (GTC) \cdot \begin{pmatrix} \underline{V}_1 \\ \underline{V}_2 \\ \cdots \\ \underline{V}_M \\ \cdots \\ \underline{V}_N \end{pmatrix} \tag{6.10}$$

Thus, Thevenin voltage seen by generator *i* can be calculated as a sum of the components induced by each voltage source in the grid as follows below :

$$\underline{E}_{theqv\ i} = \underline{V}_1 \cdot \underline{k}_{tri1} + \underline{V}_2 \cdot \underline{k}_{tri2} + \ldots + \underline{V}_M \cdot \underline{k}_{triM} + \ldots + \underline{V}_{N-1} \cdot \underline{k}_{tri(N-1)} = \quad \textbf{(6.11)}$$

$$= \left(\underline{E}_{th1} + \underline{E}_{th2} + \ldots + \underline{E}_{thM} + \ldots + \underline{E}_{th(N-1)} \right)$$

Considering the example system (Figure 6-2), the row of the GTC matrix corresponding to generator G3 can be written as (6.12):

$$(GTC) = (\underline{k}_{tr13} \qquad \underline{k}_{tr23} \qquad 0) \quad \textbf{(6.12)}$$

Respectively, the resulting Thevenin voltage seen by generator G3 appears as shown in (6.13):

$$\underline{E}_{th3eqv} = (GTC) \cdot \begin{pmatrix} \underline{V}_1 \\ \underline{V}_2 \\ \underline{V}_3 \end{pmatrix} = \underline{V}_1 \cdot \underline{k}_{tr13} + \underline{V}_2 \cdot \underline{k}_{tr23} = \quad \textbf{(6.13)}$$

$$= \underline{V}_1 \cdot \frac{\underline{V}_A'}{\underline{V}_1'} + \underline{V}_2 \cdot \frac{\underline{V}_A'}{\underline{V}_2'} = \left(\underline{E}_{th1} + \underline{E}_{th2} \right)$$

Expression (6.13) can be rewritten in a way that shows more explicitly the transformation from original voltage vector to the Thevenin voltage component:

$$\underline{E}_{th3eqv} = \left(V_1 \cdot e^{j\delta 1} \right) \cdot \left(k_{tr13} \cdot e^{j\alpha 1} \right) + \left(V_2 \cdot e^{j\delta 2} \right) \cdot \left(k_{tr23} \cdot e^{j\alpha 2} \right) =$$

$$= \left(V_1 \cdot k_{tr13} \cdot e^{j(\delta 1 + \alpha 1)} \right) + \left(V_2 \cdot k_{tr23} \cdot e^{j(\delta 2 + \alpha 2)} \right) \quad \textbf{(6.14)}$$

Where α_i is the angle of $\underline{k}_{tri3}$, δ_i is the voltage angle at the point of the constant steady state voltage magnitude.

In general form, the formula for the definition of the equivalent Thevenin voltage seen by generator *k* can be written as follows:

$$\underline{E}_{th\ k\ eqv} = \sum_{\substack{i=1 \\ i \neq k}}^{Nvs} V_i \cdot k_{trik} = \sum_{\substack{i=1 \\ i \neq k}}^{Nvs} V_i \cdot \frac{V_k^{'}}{V_i^{'}} \quad \textbf{(6.15)}$$

The dashed voltages are the voltages obtained according to expression (6.6), *k* is an index referring to the generator relatively which the calculation of corresponding Thevenin voltage is carried out.

To validate the developed method the IEEE 30 bus test system will be considered in the next section.

6.2.1 IEEE30 bus test system: decomposition of Eth per components induced by each of voltage sources.

Figure 6-8 shows the IEEE 30-bus test system diagram, with the system data borrowed from the power system test archive [88]. Few modifications were done to the system: synchronous compensators in the grid were replaced by generators, three-winding transformers were replaced by two two-winding transformers. The terminal of generator G_1 is chosen as a reference bus.

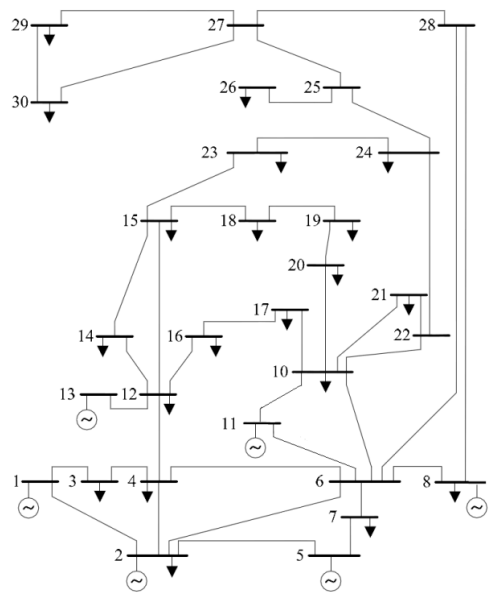

Figure 6-8: Single line diagram of IEEE 30 bus test system [89].

According to the methodology described in the previous section, the reduced admittance matrix for each of the generators should be created to begin with. The reduced matrix is obtained by open-circuiting generator relatively which the system is reduced, and short-circuiting the remaining voltage sources, except for the voltage source which impact to $\underline{E}_{th}$ is to be defined. In the Table 6-1 it is shown in which node the Thevenin voltage appears for each of voltage sources in the grid depicted in Figure 6-8

Table 6-1 Buses where Eth Appears

Gen	G_1	G_2	G_5	G_8	G_{11}	G_{13}
$\underline{E}$th bus	1	2	5	8	11	12

For the current study split of Thevenin equivalent voltage per components induced by each of voltage sources in the grid is carried out, where Thevenin equivalent seen by each of generators in the grid is sequentially considered.

As it was described in the previous section the grid transformation coefficients are to be defined. The obtained **GTC** matrix is provided in the Table 6-2.

Table 6-2 Elements of GTC matrix for IEEE 30 bus test system

	G_1	G_2	G_5	G_8	G_{11}	G_{13}
G_1	0	|0.1322| ang -37.3466	|0.0895| ang -43.3246	|0.1102| ang -41.0637	|0.0541| ang -42.3022	|0.0526| ang -43.0729
G_2	|0.1762| ang -35.5036	0	|0.0866| ang -41.6280	|0.1056| ang -39.4651	|0.0518| ang -40.7694	|0.0501| ang -41.5195
G_5	|0.1471| ang -41.5268	|0.1067| ang -41.6202	0	|0.1007| ang -43.3910	|0.0491| ang -44.9176	|0.0463| ang -45.8760
G_8	| 0.1475| ang -39.4972	|0.1060| ang -39.7571	|0.0820| ang -43.6655	0	|0.0563| ang -40.4577	|0.0516| ang -41.8550
G_{11}	|0.1402| ang -38.5704	|0.1006| ang -38.8287	|0.0776| ang -42.9098	|0.1091| ang -38.2251	0	|0.0513| ang -38.4331
G_{13}	|0.1425| ang -39.3319	|0.1019| ang -39.6256	|0.0763| ang -43.9912	|0.1046| ang -39.6864	|0.0537| ang -38.4931	0

Substituting obtained **GTC** values into (6.10) the following results for Thevenin voltage components and resulting equivalent Thevenin voltage $\underline{E}_{th}$ seen by each generator were obtained (Table 6-3):

Table 6-3 $\underline{E}_{th}$ identified on the basis of admittance matrix

Gen / Eth	G_1	G_2	G_5	G_8	G_{11}	G_{13}
Eth1		|0.296| ang 32.14	|0.247| ang 26.10	|0.248| ang 28.13	|0.236| ang 29.07	|0.239| ang 28.31
Eth2	|0.228| ang -10.66		| 0.184| ang -14.94	|0.183| ang -13.09	|0.173| ang -12.16	|0.176| ang -12.97
Eth5	|0.225| ang -26.61	|0.218| ang -24.85		|0.206| ang -26.92	|0.195| ang -26.13	|0.192| ang -27.27
Eth8	|0.263| ang -25.53	|0.252| ang -23.94	|0.240| ang -27.87		|0.260| ang -22.69	|0.249| ang -24.12
Eth11	|0.119| ang -12.41	|0.115| ang -10.84	|0.109| ang -14.90	|0.123| ang -10.52		|0.119| ang -8.57
Eth13	|0.099| ang -3.17	|0.094| ang -1.64	|0.087| ang -6.03	|0.097| ang -1.94	|0.096| ang 1.44	
Eth, sum	|0.923| ang -18.13	|0.886| ang -3.90	|0.807| ang -6.25	|0.800| ang -3.14	|0.893| ang -6.81	|0.907| ang -8.45

The graphical representation of the obtained componnets allows visualizing the impact which a given Thevenin voltage component impose on the equivalent Thevenin voltage seen by a certain generator. The example of the Thevenin voltage vector diagram is provided in Figure 6-9.

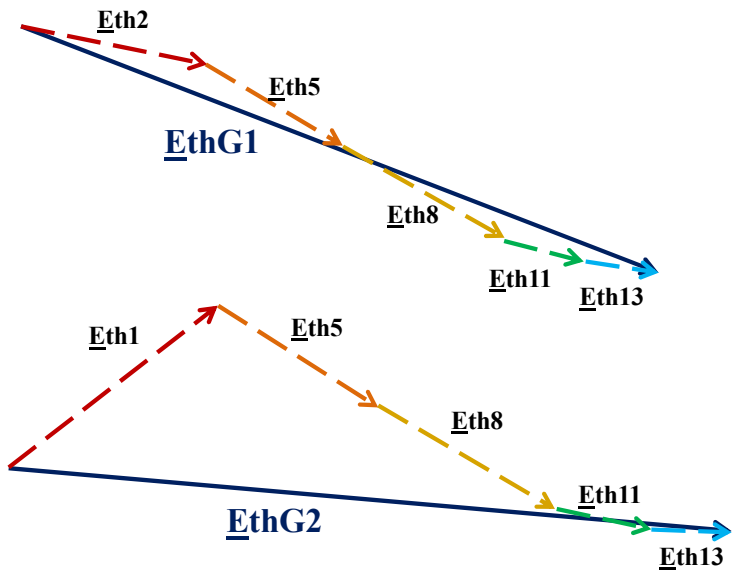

Figure 6-8: Vector diagram for the Thevenin voltages seen by generators G_1 and G_2

To ensure the correctness of the obtained value for the equivalent Thevenin voltage, the results demonstrated in Table 6-3 are compared with values of $\underline{E}_{th}$ obtained by solving circuit equations for the system depicted in Figure 6-8 (Table 6-4).

Table 6-4 $\underline{E}_{th}$ identified on the basis of cirquit equations

Eth \ Gen	G_1	G_2	G_5	G_8	G_{11}	G_{13}
Eth	|0.923| ang -18.13	|0.886| ang -3.90	|0.807| ang -6.25	|0.800| ang -3.14	|0.893| ang -6.81	|0.907| ang -8.45

As can be noticed from Table 6-3 and Table 6-4, $\underline{E}_{th}$ obtained by applying the two different methodologies yields the same results demonstrating the validity of the suggested approach.

By representing $\underline{E}_{th}$ in terms of components induced by individual voltage sources, it helps understanding how much impact a given voltage source can have on ASSAS of a given generator. Furthermore, the **GTC** matrix allows the analysis of how certain variations in the admittance matrix will result in change of impact which voltage sources have on the stability of the given generator. As a result the smart manipulation of the Thevenin voltage can provide advanced capabilities for stability improvement. This

knowledge can be used for the assessment of the efficiency of suggested preventive countermeasures, which will be considered in the next section.

6.3 Pre-Assessment of the resulting steady state stability considering a given countermeasure application

At the previous section the dependency between voltage sources and Thevenin voltage seen by a given generator has been shown. Specifically the influence of grid topology and admittances variation on the impact which certain voltage source has on a Thevenin equivalent seen by the chosen generator has been studied. The key expression describing this dependency is as follows:

$$\left[\underline{\boldsymbol{E}}_{th}\right] = \left[\boldsymbol{GTC}\right] \cdot \left[\underline{\boldsymbol{V}}_{0}\right] \tag{6.16}$$

Where the grid transformation coefficient is defined by grid topology and obtained on the basis of system admittance matrix. Thus Thevenin voltage can be found any time when the corresponding system admittance matrix and measurements of the voltage at the point of constant steady state voltage magnitude are available.

Assuming that the grid is fully observable the derived dependency can help understanding how much different voltage sources in the grid are coupled with each other, and which variations of either admittance matrix or generators' excitation voltage, or the rescheduling of the generators would have the greatest impact on the operational conditions of the generator under consideration. Nevertheless, the derived expression doesn't help identification of the Thevenin voltage when a countermeasure application effect on the systems stability has to be predicted prior actual event appears, as the vector $[\mathbf{V_0}]$ for the new operational conditions is unknown. To be more specific, the voltage magnitudes are known as it is supposed that the voltage magnitude stays the same during steady state operation at the voltage magnitude controlled nodes granting the excitation voltage is constant. The variable which remains undefined is the voltage angles. In order to predict the effect of the suggested countermeasure on the Thevenin equivalent seen by a critical generator, it is necessary to develop the method capable of pre-definition of the voltage angles at the point of constant steady state voltage magnitude which will appear at the new steady state corresponding to the applied system changes.
The next section will present the method allowing prediction of the voltage angles for the new steady state conditions, avoiding load flow or time domain simulation.

6.3.1 Assessment of the resulting steady state stability considering a given countermeasure application

Figure 6-9 shows power−angle characteristic of synchronous generator and is used to illustrate the following discourse. The suggestions and remarks built up for the method

under consideration are carried out following tracking of operational point over P-δ curves (Figure 6-9).

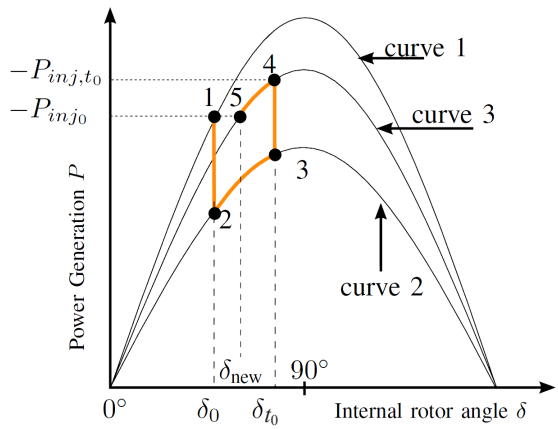

Figure 6-9: Trajectory of the rotor angle δ over P-δ curve when steady state is afflicted by disturbance and followed by countermeasure application.

In the figure point 1 is the initial steady state operational point, point 2 is immediately after disturbance, point 3 is when countermeasure is applied, point 4 is the operational point immediately after the countermeasure has been applied and point 5 is the final equilibrium operational point corresponding to a new steady state. The P-δ curves are corresponding respectively to 1) initial steady state, 2) post-disturbance quasi-steady operation (system gradually is approaching ASSAS boundary), 3) post-countermeasure curve, where the new steady state operational point will be located on.
In order to define if applied countermeasure would have sufficient impact preventing instability the dynamics of δ over P-δ curves corresponding to a given generator from point 3 to point 5 (Figure 6-9) should be predicted for each generator in the grid. For the current study the assumption is made that the time slot between decision about countermeasure application and actual execution of it can be neglected, thus at the moment $t=t_0$ which corresponds to the point 3 the last actual measurements from PMU can be received, based on these measurements the further dynamics of δ is to be predicted for the suggested countermeasure. The countermeasure is represented as corresponding nodal admittance variation in the system admittance matrix.The initial point of consideration starts from the steady state operation described by the first P-δ curve, where point 1 marks initial operational conditions. Assuming some disturbance applied to the grid which leads to resulting aperiodic small signal angular instability the operational point shifts to the second P-δ characteristic. Trying to find new equilibrium point on this characteristic operational point moves from point 2 to point 3. As the new steady state does not exist for the operation described by the second P-δ characteristic, there is a need to take a countermeasure in order to avoid upcoming instability. Thus, at a moment

$t=t_0$ the countermeasure is applied, which reflects in the admittance matrix change and transition to the new P-δ characteristic happens (curve 3). As the change in rotor angles doesn't appear in step due to inertia they remain the same immediately after countermeasure application $\delta_{i,t=t0+}=\delta_{i,t=t0-}$. Due to this, immediate response to the applied variation in terms of injected power $Pinj_{t=t0+}$(point 4) can be defined according to (6.1) , where the values of $\underline{V}_{0i}$ are assumed to be the same as in the latest measurements obtained from PMU corresponding to point 3, and the value of $\underline{Z}_{th}$ and **GTC** are updated accordingly to the suggested admittance variation.

$$P_{inj\,t=t_0+} = \frac{E_{th\,t=t_0+}\cdot V_0}{Z_{th\,t=t_0+}}\cos(\gamma_{t=t_0+}+\phi_{th\,t=t_0+}) - \frac{V_0^{\,2}}{Z_{th\,t=t_0+}}\cdot\cos(\phi_{th\,t=t_0+}) =$$
$$= \frac{E_{th\,t=t_0+}\cdot V_0}{Z_{th\,t=t_0+}}\cos(\delta_{t=t_{0^-}} - \theta_{th\,t=t_0+} + \phi_{th\,t=t_0+}) - \frac{V_0^{\,2}}{Z_{th\,t=t_0+}}\cdot\cos(\phi_{th\,t=t_0+}) \qquad \textbf{(6.17)}$$

Where $\theta_{t=t0+}$ is the angle of corresponding Thevenin voltage.

The further trajectory of δ will lie along the third P-δ characteristic, tending to settle around new equilibrium point, if such exists.

For this study the rescheduling of the generators was restricted. The purpose was to figure out how the load nodes can be utilized for system stabilization. Thus, the power output for the generators is supposed to stay the same for the new steady state operation (point 5). Taking into account all the assumption, the variables remaining unknown in point 5 and needed for the prediction of the resulting active power margin, according to (6.1) are: E_{th}, θ_{th} and δ_i.

Considering that $\underline{E}_{th}$ is dependent on four components (6.18): ktr_{ij}, α_{ij}, V_{0i}, δ_i; and three of them except the voltage angles can be defined for the new P-δ characteristic precisely. While δ_i will experience noticeable change which should be predicted. It is suggested to use the value of $\underline{E}_{th}$corresponding to the point 4for the first approximation when the voltage angles corresponding to the final steady state (point 5) are to be found. Meanwhile the value of the $\underline{E}_{th}$ corresponding to the point 4 can be found precisely as immediately after disturbance $\delta_i$will stay the same due to inertia of the generators, and can be extracted from the measurements taken prior the countermeasure application (point 3).

$$\begin{pmatrix} \underline{E}_{theqv\,1} \\ \underline{E}_{theqv\,2} \\ \cdots \\ \underline{E}_{theqv\,i} \\ \cdots \\ \underline{E}_{theqv\,N} \end{pmatrix} = (\mathbf{GTC})\cdot \begin{pmatrix} \underline{V}_{01} \\ \underline{V}_{02} \\ \cdots \\ \underline{V}_{0i} \\ \cdots \\ \underline{V}_{0N} \end{pmatrix}; \quad \mathrm{GTC}_{i,j} = k_{trij}\cdot e^{j\alpha_{ij}} \qquad \textbf{(6.18)}$$

Besides, one can notice that the second term in (6.1) would remain the same for the immediate post-contingency state and new steady state; furthermore it can be precalculated for the suggested admittance matrix variation in advance. Thus the first ap-

proximation of δ corresponding to the new steady state can be found as it shown in (6.19):

$$\delta = \arccos\left[\left(\frac{E_{th\,t=t_{0+}}\cdot V_0}{Z_{th\,t=t_{0+}}}\cos(\gamma_{t=t_{0+}}+\phi_{th\,t=t_{0+}})-P_{inj\,t=t_{0+}}+P_{inj0}\right)\frac{Z_{th\,t=t_{0+}}}{E_{th\,t=t_{0+}}\cdot V_0}\right]+\theta_{th\,t=t_{0+}}-\phi_{th\,t=t_{0+}} \quad \textbf{(6.19)}$$

The calculation of the first approximation for the voltage angle corresponding to the new steady state should be accomplished for all voltage sources in the grid.

When the first approximation is obtained the value of the Thevenin voltage can be re-calculated according to (6.18) and sequentially used for readjustment of the voltage angles. In order to facilitate this process an iterative approach, based on the Newton method [90], is initiated.

The wish is to solve a system of nonlinear equations (6.20) where the number of equations is equal to the number of voltage sources minus one (the angle of the reference bus is pre-defined):

$$\mathbf{y=f(x)} \quad \textbf{(6.20)}$$

where **x**,**y** and **f** vectors are defined as follows :

$$[\mathbf{x}]=[\boldsymbol{\delta}]=\begin{pmatrix}\delta_2\\ \dots\\ \delta_N\end{pmatrix};\quad [\mathbf{y}]=\left[\mathbf{P}_{gen}\right]=\begin{pmatrix}P_{gen2}\\ \dots\\ P_{genN}\end{pmatrix} \quad \textbf{(6.21)}$$

$$[\mathbf{f(x)}]=[\mathbf{P}(\boldsymbol{\delta})]=\begin{pmatrix}\dots\\ P_{geni}=\dfrac{V_{0i}^{\,2}}{Z_{th_i}}\cdot\cos(\phi_{th_i})-\dfrac{E_{th_i}\cdot V_{0i}}{Z_{th_i}}\cos(\delta_i-\theta_i+\phi_{th_i})\\ \dots\end{pmatrix} \quad \textbf{(6.22)}$$

Graphically the system of equations to be solved can be represented as follows:

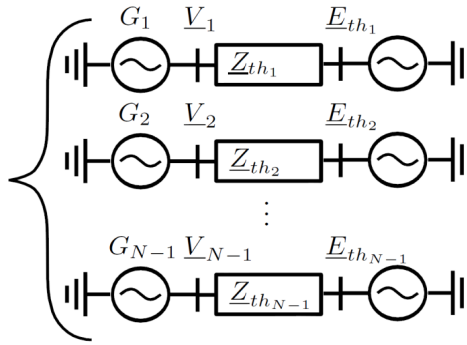

Figure 6-10: Graphical representation of the system of equations each of which describes power flow in the grid containing given generator and corresponding Thevening equivalent, substituting the remaining system.

When (6.20)-(6.22) are defined (6.23) can be obtained:

$$\frac{\mathbf{dy}}{\mathbf{dx}} = \frac{\mathbf{df(x)}}{\mathbf{dx}} = \frac{\mathbf{dP(\delta)}}{\mathbf{d\delta}} = \mathbf{J(\delta)}; \tag{6.23}$$

Where **J(δ)** is the Jacobian matrix of **P(δ)** with respect to **δ**, which being written explicitly appears as in (6.24)

$$J = \begin{bmatrix} \frac{\partial Pgen_1}{\partial \delta_1} & \frac{\partial Pgen_1}{\partial \delta_2} & \vdots & \frac{\partial Pgen_1}{\partial \delta_N} \\ \frac{\partial Pgen_2}{\partial \delta_1} & \frac{\partial Pgen_2}{\partial \delta_2} & \vdots & \frac{\partial Pgen_2}{\partial \delta_N} \\ \cdots & \cdots & & \cdots \\ \frac{\partial Pgen_N}{\partial \delta_1} & \frac{\partial Pgen_N}{\partial \delta_2} & \vdots & \frac{\partial Pgen_N}{\partial \delta_N} \end{bmatrix} \tag{6.24}$$

In order to define elements of the Jacobian matrix the following derivatives are to be specified:

$$\mathrm{J}_{ij}(\delta) = \frac{\mathrm{dP}_i(\delta)}{\mathrm{d}\delta_j};$$

$$\frac{\partial\left(\mathrm{P_i}\left(\delta\right)\right)}{\partial\delta_\mathrm{j}} = \frac{\partial\left(\mathrm{E}_{thi}\left(\delta_{j,j\neq i}\right)\cdot \mathrm{V}_{0i} / \mathrm{Z}_{thi}\cdot cos(\delta_i - \theta_{thi}\left(\delta_{j,j\neq i}\right) + \phi_{thi})\right)}{\partial\delta_j} \tag{6.25}$$

for i = j

$$\frac{\partial\left(\mathrm{P_i}(\delta)\right)}{\partial\delta_{\mathrm{i}}}=\frac{\mathrm{V}_{0i}}{Z_{thi}}\cdot\left[\frac{\partial\left(\mathrm{E}_{thi}\right)}{\partial\delta_{\mathrm{i}}}\cdot cos(\delta_i-\theta_{thi}+\phi_{thi})+\mathrm{E}_{thi}\cdot\frac{\partial\left(cos(\delta_i-\theta_{thi}+\phi_{thi})\right)}{\partial\delta_{\mathrm{i}}}\right]=-\frac{\mathrm{V}_{0i}}{Z_{thi}}\cdot\mathrm{E}_{thi}\cdot\sin(\delta_i-\theta_{thi}+\phi_{thi})$$

for i ≠ j

$$\frac{\partial\left(\mathrm{P_i}(\delta)\right)}{\partial\delta_{\mathrm{j}}}=\frac{\mathrm{V}_{0i}}{Z_{thi}}\cdot\left[\frac{\partial\left(\mathrm{E}_{thi}\right)}{\partial\delta_{\mathrm{j}}}\cdot cos(\delta_i-\theta_{thi}+\phi_{thi})+\mathrm{E}_{thi}\cdot\frac{\partial\left(cos(\delta_i-\theta_{thi}+\phi_{thi})\right)}{\partial\delta_{\mathrm{j}}}\right]$$

$$\frac{\partial\left(\mathrm{E}_{thi}\right)}{\partial\delta_{\mathrm{j}}}=\frac{\mathrm{V}_{0j}\cdot k_{0trij}}{\mathrm{E}_{thi}}\cdot\left[\mathrm{Im}(\underline{\mathrm{E}}_{thi})\cdot\cos(\delta_j+\alpha_{ij})-\mathrm{Re}(\underline{\mathrm{E}}_{thi})\cdot\sin(\delta_j+\alpha_{ij})\right]$$

$$\frac{\partial\left(cos(\delta_i-\theta_{thi}+\phi_{thi})\right)}{\partial\delta_{\mathrm{j}}}=\sin(\delta_i-\theta_{thi}+\phi_{thi})\cdot\frac{V_{0j}\cdot k_{trji}}{Im\left(\underline{\mathrm{E}}_{thi}\right)}\cdot$$

$$\cdot\left[-\sin\left(\delta_j+\alpha_{ji}\right)-\frac{\mathrm{Re}\left(\underline{\mathrm{E}}_{thi}\right)\cdot Im\left(\underline{\mathrm{E}}_{thi}\right)\cdot\cos\left(\delta_j+\alpha_{ji}\right)}{{E_{thi}}^2}+\frac{\mathrm{Re}\left(\underline{\mathrm{E}}_{thi}\right)^2\cdot\sin\left(\delta_j+\alpha_{ji}\right)}{{E_{thi}}^2}\right]$$

Where θ_{th} is the angle of the Thevenin voltage, ϕ_{th} is the angle of the Thevenin impedance, δ is an angle of the voltage at the point of constant steady state voltage magnitude and α_{ji} is the angle of the corresponding GTC. E_{th} is a magnitude of Thevenin voltage, Z_{th} magnitude of the Thevenin impedance, V_{0i} voltage magnitude at the point of constant steady state voltage magnitude and $k_{0trij}$is the magnitude of GTC between nodes *i* and *j*.

The detailed derivation of the formulas (6.25) can be found in the Appendix 1.
It may be noticed that the function P(δ) (6.22) is uninterruptable and differentiable which ensures that J is defined everywhere.
Wherever $\mathbf{J^{-1}}$ exists (6.26) can be rewritten:

$$\Delta\boldsymbol{\delta}=\mathbf{J}^{-1}\cdot\Delta\mathbf{P}(\boldsymbol{\delta}) \qquad \textbf{(6.26)}$$

Respectively, the following iterative process can be initiated in order to define voltage angles at the point of constant steady state voltage magnitude, and afterwards calculate the corresponding active power stability margin:
For each iteration:

$$\begin{aligned}\Delta\mathbf{P}_k&=\mathbf{P}_{gen}-\mathbf{P}_k\\ \Delta\boldsymbol{\delta}_k&=\mathbf{J}^{-1}\cdot\Delta\mathbf{P}_k\\ \boldsymbol{\delta}_{k+1}&=\boldsymbol{\delta}_k+\Delta\boldsymbol{\delta}_k\end{aligned} \qquad \textbf{(6.27)}$$

$$E_{th_{k+1}} = \boldsymbol{GTC} \cdot \begin{pmatrix} V_{01} \cdot e^{j\delta_{1\,k+1}} \\ V_{02} \cdot e^{j\delta_{2\,k+1}} \\ \cdots \\ V_{0i} \cdot e^{j\delta_{i\,k+1}} \\ \cdots \\ V_{0N} \cdot e^{j\delta_{N\,k+1}} \end{pmatrix} \tag{6.28}$$

$$P_{k+1}(\delta) = \frac{V_{0i}^{\,2}}{Z_{th_i}} \cdot \cos(\phi_{th_i}) - \frac{E_{th_i} \cdot V_{0i}}{Z_{th_i}} \cos(\delta_{i\,k+1} - \theta_{i\,k+1} + \phi_{th_i}) \tag{6.29}$$

Where k is a number of iteration

The iterative process continues until the sufficient accuracy $\Delta\delta_i<\varepsilon$ is achieved or the limit for number of iterations is exceeded indicating non convergence. The obtained results would be a solution for the new steady state operational conditions corresponding to point 5 (Figure 6-9).

In case of non-convergence of iterative process ,considering the dependency between load flow calculation and steady state stability limit derived at [73], the conclusion that steady state could not be achieved for the given operational conditions can be made. Thus, based on the suggested admittance matrix variation the assessment of new steady state existence can be carried out and the value of active power stability margin is predicted. Nevertheless few modifications to the suggested algorithm can be proposed in order to reduce its computational burden, which will be considered in the next section.

6.3.2 Improvement of the computational burden of the algorithm for assessment of the proposed countermeasure sufficiency

As it was shown in the previous section Jacobian matrix is used in order to adjust the first approximation of the voltage angles at the point of constant steady state voltage magnitude. Furthermore, in fact the inverted Jacobian matrix is used. Considering large scale power systems, containing hundreds of voltage sources the inversion of the Jacobian matrix $\boldsymbol{J} = \frac{\partial \boldsymbol{P}}{\partial \boldsymbol{\delta}}$ has a considerable computational burden, in general, such methods may require $O(n^3)$ floating point operations. Considering the need to operate early prevention algorithm within near real-time frame, all possible steps reducing the computational effort should be considered.

At the first place the attention is paid to the inversion of **J** as it is the most computational heavy operation in the algorithm. As it was described in the previous section J is up-

dated on each iteration, however assuming that the initial approximation is close enough, a recalculation of the Jacobian matrix on each iteration can be avoided as it will not change considerably (6.30). The utilization of the constant Jacobian matrix calculated on the first iteration is suggested. The proposed simplification might lead to slow-down of convergence of the iterative process, reflected in an increased number of iterations. However, the benefit of avoiding multiple Jacobian matrix inversion outweighes the fact that more iterations are required, as each of the iterations is not computationally heavy.

$$\begin{cases} O_\varepsilon\left(\delta_{0j}\right)=\left\{\delta'_j:\left|\delta'_j-\delta_{0j}\right|<\varepsilon\right\} \\ \left.\dfrac{\partial P_i}{\partial \delta_j}\right|_{\delta'_j}=\left.\dfrac{\partial P_i}{\partial \delta_j}\right|_{\delta_{0j}}=const \\ J\left(\delta\right)=\left.\dfrac{dP_i(\delta)}{d\delta_j}\right|_{O_\varepsilon(\delta_{0j})}=const \end{cases} \tag{6.30}$$

Having a closer look on the Jacobian matrix structure the specific attention is drown to the off-diagonal elements. Comparing diagonal elements and off-diagonal elements in Jacobian matrix (6.31, Appendix1) the hypothesis is suggested that diagonal elements are expected to be fairly greater in absolute value than the off-diagonal ones.

$$\begin{aligned} \frac{dP_i(\delta)}{d\delta_i}&=-\frac{V_{0i}}{Z_{thi}}\cdot E_{thi}\cdot\sin(\delta_i-\theta_{thi}+\phi_{thi}) \\ \frac{dP_i(\delta)}{d\delta_j}&=\frac{V_{0i}}{Z_{thi}}\cdot\frac{V_{0j}\cdot k_{trji}}{E_{thi}}\cdot\Big[Im\left(\underline{E}_{thi}\right)\cdot\cos(\delta_i-\theta_{thi}+\phi_{thi}+\delta_j+\alpha_{ji})- \\ &-\mathrm{Re}\left(\underline{E}_{thi}\right)\cdot\sin(\delta_i-\theta_{thi}+\phi_{thi}+\delta_j+\alpha_{ji})\Big] \end{aligned} \tag{6.31}$$

It is natural to suppose that power injected by a given generator is dependent on δ of this generator to considerably larger extend than on the voltage angles variations of any other voltage source in the grid. If this proposal is fair, the influence of other generators' rotor angle variation can be neglected. Assuming the suggested hypothesis is valid, the Jacobian matrix is simplified to a diagonal matrix:

$$J=\begin{bmatrix} \frac{\partial Pgen_1}{\partial\delta_1} & 0 & \vdots & 0 \\ 0 & \frac{\partial Pgen_2}{\partial\delta_2} & \vdots & 0 \\ \cdots & \cdots & \vdots & \cdots \\ 0 & 0 & \vdots & \frac{\partial Pgen_N}{\partial\delta_N} \end{bmatrix} \tag{6.32}$$

For diagonal Jacobian matrix (6.32) inversion operation can be replaced by simple algebraic operation ~ O(n) (6.33):

$$J^{-1} = \begin{bmatrix} \frac{1}{J_{11}} & 0 & \vdots & 0 \\ 0 & \frac{1}{J_{22}} & \vdots & 0 \\ \cdots & \cdots & \vdots & \cdots \\ 0 & 0 & \vdots & \frac{1}{J_{NN}} \end{bmatrix} \tag{6.33}$$

The suggested approach of the Jacobian matrix modification leads to drastic reduction of computational time while the converged solution is expected to be the same comparing to usage of the complete Jacobian.
The validity of the proposed approach will be considered in the next section, where two study cases will be presented.

6.3.3 Fast Assessment of the Effect of Preventive Wide Area Emergency Control

For the verification of the suggested approach two test systems are considered: 8 bus test system and IEEE 30 bus test system.

6.3.3.1 Instability Prevention by applying control action which efficiency has been pre-defined and resulting active power margins predicted

Simple 8 bus test system was used to prove the validity of the method for prediction of the resulting steady state stability margin when a given countermeasure is suggested. Below the details regarding the system under considerations are provided Figure 6-11, Table 6-5 and Table 6-6:

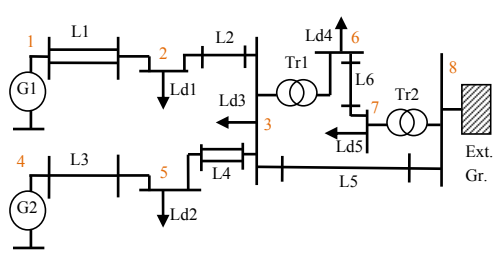

Figure 6-11: Single line diagram of 8 bus test system.

Table 6-5 8-bus System data:branches

Branch	L1	L2	L3	L4	L5	L6
X, Ohm	1.8	6	1.2	7.2	9.6	22.2

Table 6-6 8-bus System data:buses

Bus	Un-om, kV	Pgen, MW	Qgen, MVar	Pload, MW	Qload, MVar
1	10	20	9.81	0	0
2	10	0	0	26	10
3	10	0	0	30	0
4	10	15	6.39	0	0
5	10	0	0	10	2
6	110	0	0	40	10
7	110	0	0	10	20
8	10	81.00	49.94	0	0

For the network shown in Figure 6-11 the study case leading to loss of aperiodic small signal angular stability (ASSAS) is created, using DIgSILENT Power Factory as a simulation tool. For the reference bus the bus of external grid connection (bus 8) is chosen. To initiate instability in the test system the increase of the load Ld1 per 3% is initiated at t=5 seconds, which leads to visible instability at t=38.31 seconds (Figure 6-12). At t=18.6 seconds early warning method [24] detects cross of ASSAS boundary.

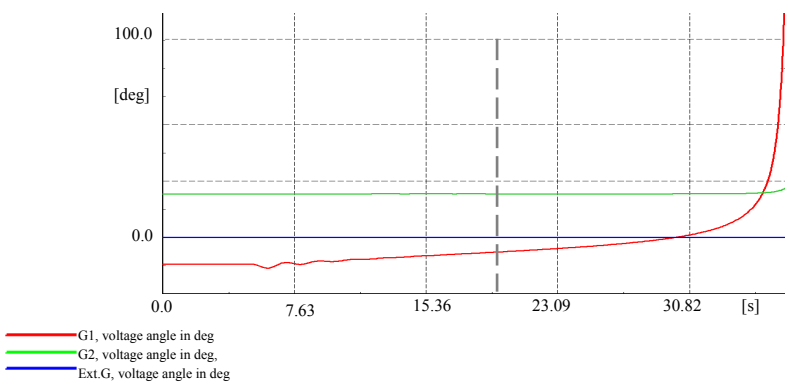

Figure 6-12: Instability caused by increase of the load Ld1 per 3%. Voltage angles at buses 1, 4 and 8.

In order to define the optimal node for countermeasure application the self- propagating graph algorithm is used. The following self- propagating graph with respect to G1 for the system depicted in Figure 6-11 has been formulated:

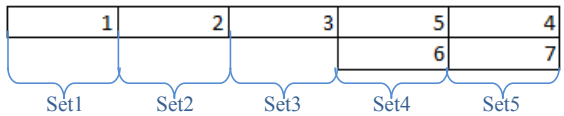

Figure 6-13: Sets of nodes sequentially added to self-propagating graph

Substituting the node names in the Figure 6-13 with corresponding sensitivity value, self-propagating graph appears as shown in Figure 6-14. Minimal acceptable level of sensitivity has been chosen equal to $S_{kth_{\min}}$ =0.33. The corresponding elements of control participation matrix **C** are shown in Figure 6-14 as well.

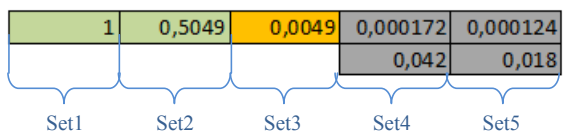

C_{ii}:

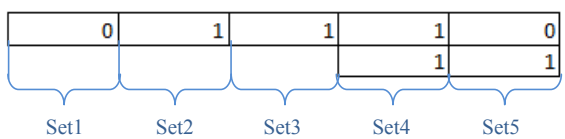

Figure 6-14: Sensitivity values S_{th} corresponding to the nodes added to the self-propagating graph and according to control participation coefficients C_{ii}.

In Figure 6-14 orange color marks the nodes, which were defined as dead-end by self-propagating graph algorithm. The light green color marks the nodes which are added to the candidate list for countermeasure application. Gray color refers to the nodes which were not included into the candidate list for countermeasure application. The nodes having local load connected were considered to have control reserves, and been included in the control participation matrix **C** with control index equal to 1.

According to obtained result, the optimal node for countermeasure application which has a control reserve available is the bus number 2.Therefore, the preventive countermeasure in form of injection of reactive power into the bus2, resulting in decrease of nodal admittance Y_{22} per 0.005j pu is suggested. The assessment of effectiveness of the suggested countermeasure is carried out following the steps described in the previous section. The accuracy $\Delta\delta_i<10^{-5}$ is set as criterion for ending of iterative process. The following results are obtained:

Table 6-7 Prediction of active power stability margin

Gen	δpred	δsim	$P_{marg-pred,\%}$	$P_{marg-sim,\%}$	Er-ror,%	N iteration
G1	19.8139	19.8427	0.6302	0.6261	0.64	27
G2	50.1667	50.1925	0.6371	0.6328	0.68	

The elements of Jacobian matrix obtained during iterative process for the first 3 iterations appear as follows:

Table 6-8 Elements of Jacobi matrix

Niter	$J_{1,1}$	$J_{1,2}$	$J_{2,1}$	$J_{2,2}$
1	0.0432	-0.0094	-0.0056	0.0772
2	0.0432	-0.0094	-0.0056	0.0772
3	0.0432	-0.0094	-0.0056	0.0772

It can be noticed that elements of Jacobian matrix doesn't noticeably change from iteration to iteration, thus the recalculation of Jacobi matrix at each iteration is not needed. The error caused by such simplification is in 10^{-5} degree of order. As inversion of matrix is computationally heavy operation, the conclusion made allows saving computational time considerably. Furthermore, as the diagonal elements are noticeably greater than off-diagonal elements, replacement of off-diagonal elements with zero is considered. Table 6-9 shows the results of preventive countermeasure assessment based on the proposed simplifications – calculation of Jacobian matrix only once at the beginning of iterative process where off-diagonal elements are accepted to be equal to zero.

Table 6-9 Prediction of active power stability margin

Gen	δpred	δsim	$P_{marg-pred,\%}$	$P_{marg-sim,\%}$	Er-ror,%	N iteration
G1	19.8134	19.8427	0.6302	0.6261	0.65	27
G2	50.1668	50.1925	0.6371	0.6328	0.67	

As one can see the introduced simplifications doesn't increase the error of assessment at the same time allowing great improvement of computational efficiency.

According to obtained prediction of resulting active power stability margin the suggested countermeasure should lead to stabilization of the system, even though the value of the active power stability margin is expected to be low. Figure 6-15 shows the effect of the suggested countermeasure application which is in a good agreement with the predicted one.

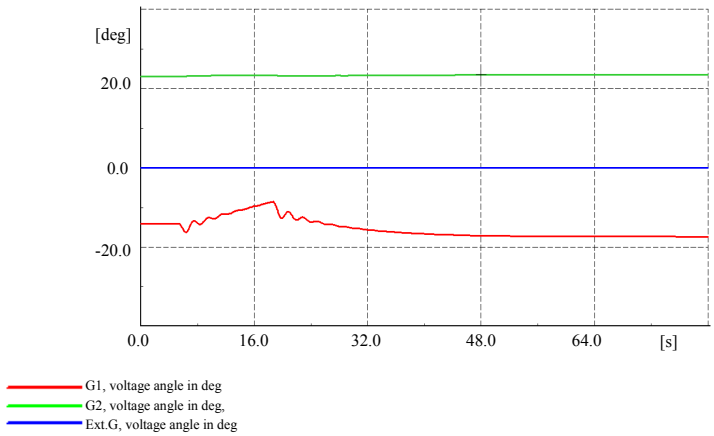

Figure 6-15: System response on application of the suggested countermeasureper.

Voltage angles at buses 1, 4 and 8.

The dependency of the active power stability margin prediction on the accuracy $\Delta\delta_i<\varepsilon$ set as a criterion of iterative process interruption, has been considered in the Table 6-10. It can be seen, when the higher error ε is allowed, number of iterations needed to reach required precision drops significantly. However this error, besides direct participation in the calculation of $P_k(\delta)$ (6.29), is included in calculation of Thevenin voltage. Thus, error in angle calculation leads to noticeable lowering in the precision of active power stability margin prediction.

Table 6-10 The dependency of required precision and number of iterations

Presision, ε		10^{-1}	10^{-3}	10^{-5}	10^{-10}
$N_{iteration}$		1	3	27	88
Pmarg-pred Er-ror,%	**G1**	1.20	1.29	0.65	0.64
	G2	9.3	6.48	0.67	0.61

6.3.3.2 IEEE 30 bus test system, prediction of the resulting active power margin, when a number of disturbances are applied at a time

Figure 6-14 shows IEEE 30-bus test system diagram where the elements influenced by applied disturbances are marked in red. The data for power production and corresponding active power margins are provided in the Table 6-11- Table 6-12.

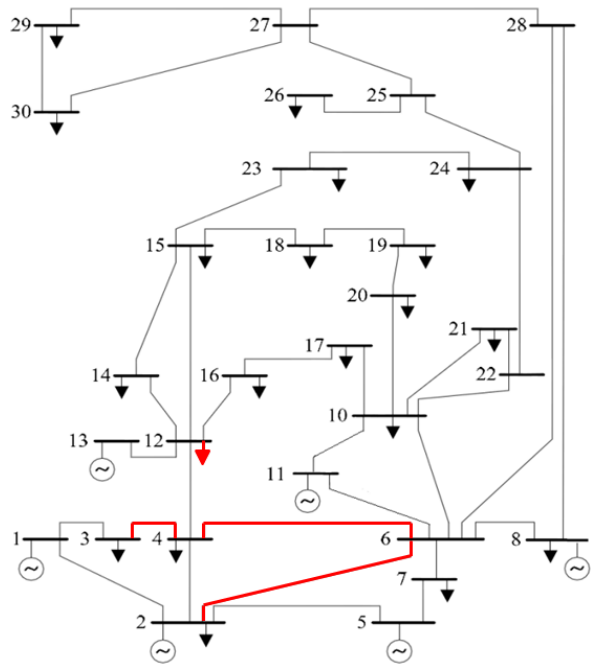

Figure 6-14: Single line diagram of IEEE 30 bus test system, in red the elements experiencing the disturbance are marked.

Table 6-11 Generator data

Gen	G1	G2	G5	G8	G11	G13
P_G,MW	108.75	40	40	40	30	30

Table 6-12 Initial active power stability margin

Gen	G1	G2	G5	G8	G11	G13
$\%\Delta P_{inj}$	80.04	53.04	60.47	63.65	41.21	27.42

The goal of current study is to determine whether after series contingencies applied to the system the new steady state can be achieved and what would be the resulting active power stability margins. For this purpose the following disturbances were applied to IEEE 30 bus test system at a time: increase of load12 per 300%; trip of: line3_4, line2_6 and line4_6. The contingencies are applied at t=5 seconds, immediately after this the assessment of the new resulting steady state starts.
Table 6-13 demonstrates the elements of complete Jacobian matrix. For the calculations both the complete Jacobian matrix and the simplified one where off-diagonal elements are equal to zero were used. The obtained results are compared below.

Table 6-13 Elements of Jacobian matrix

	$J_{i,1}$	$J_{i,2}$	$J_{i,3}$	$J_{i,4}$	$J_{i,5}$
$J_{1,j}$	0.8416	- 0.0131	-0.0109	- 0.0055	-0.0054
$J_{2,j}$	-0.0139	0.8980	-0.1183	-0.0494	-0.0201
$J_{3,j}$	-0.0127	-0.1210	0.8657	-0.1054	-0.0380
$J_{4,j}$	-0.0059	-0.0515	-0.1102	0.4506	-0.0188
$J_{5,j}$	-0.0058	-0.0220	-0.0427	-0.0213	0.3706

Results shown in the Table 6-14 demonstrate the predicted new steady state when the complete Jacobian matrix was used for the calculations. The comparison of the predicted new steady state and time domain simulation are presented. It can be seen that the resulting new steady state was predicted with a high accuracy.

Table 6-14 Prediction of the resulting active power stability margin

Gen	δpred	δsim	$P_{marg-pred,\%}$	$P_{marg-sim,\%}$	Error,%	N iterations
G2	26.30	26.22	52.73	52.63	0.18	11
G5	9.78	9.69	59.40	59.34	0.11	
G8	5.67	5.58	60.06	60.01	0.09	
G11	20.97	20.91	38.54	38.45	0.21	
G13	34.64	34.61	23.03	23.91	0.50	

Table 6-15 contains the results for the new steady state prediction when the diagonal Jacobian matrix was used. It is seen that the obtained solution in Table 6-14 and Table 6-15 is similar, meaning that the iterative process converges to the same solution regardless whether the complete or diagonal Jacobian was used. It can be noticed that the suggested modification of the Jacobian doesn't lead to reduction of the prediction accuracy, even though more iterations are needed. However the computational gain achieved by avoiding Jacobian inversion overcomes the running time caused by increased number of iterations.

Table 6-15 Prediction of the resulting active power stability margin

Gen	δpred	δsim	$P_{marg-pred,\%}$	$P_{marg-sim,\%}$	Error,%	N iterations
G2	26.30	26.22	52.73	52.63	0.18	14
G5	9.78	9.69	59.40	59.34	0.11	
G8	5.67	5.58	60.06	60.01	0.09	
G11	20.97	20.91	38.54	38.45	0.21	
G13	34.64	34.61	23.03	23.91	0.50	

In order to assess the error of active power stability margin prediction depending on both the precision of the voltage angles identification $\Delta\delta i$ and the size of the system the Table 6-10 and Table 6-16 should be compared.

Table 6-16 The dependency of precision and number of iterations

Presision, ε	**10^{-1}**	**10^{-3}**	**10^{-5}**	**10^{-10}**
$N_{iteration}$	4	9	14	26
Max Pmarg-pred Error,%	7.43	0.50	0.50	0.50

One can notice that with increase of the system size the early prediction method demonstrates higher efficiency. High accuracy of the active power stabilitymargin prediction requires less precision in $\Delta\delta_i$ identification, which respectively results in the fewer number of iterations needed. This tendency is explained by a fact that in the larger system the number of components contributing to the Thevenin voltage is larger, meaning that the error in identification of a single component has reduced influence in the equivalent Thevenin voltage calculation. This results in higher accuracy of the new steady state prediction being achieved faster comparing to small systems.

7
LARGE SCALE TEST OF THE EARLY PREVENTION METHOD

In order to further test the early prevention method described in the previous chapters a detailed model of a real power system was used. The model was provided by Danish TSO Energinet.dk and represents the Western Danish Power System. Danish Power System contains two subsystems connected by HVDC line: the Western Danish Power System and the Eastern Danish Power System. The Eastern Danish Power System is a part of and synchronized to the Nordic Power System, geographically it is covering Zealand. The Western Danish Power System is synchronized with Germany, geographically covering Funen and Jutland.

7.1 West Danish Power System description

In the Western Denish Power System the transmission system voltage levels are 400 kV and 150 kV. The distribution system runs at 60 kV, 10 kV and finally at 0.4 kV at households. 6 HVDC interconnections are operated (3 to Norway, 2 to Sweden and 1 to Zealand), as well as an AC interconnection to Germany. West Denmark being synchronised with Germany is a part of the UCTE system (Figure 7-1).

The loads in the model are aggregated at 60 kV and 150 kV level. For the provided network model, the total load is 3.7 GW. Installed capacity of the central power plants is 1.8 GW, while local CHP plants accounts for 2 GW of power. A significant amount of wind power units are installed in the system as well. For the considered case study, wind power production accounts for 2.9 GW of power.

The system voltage is maintained by tap changing transformers and shunt components, as well as voltage control by the main power plants. The distributed units are modelled as PQ buses. The system has a few phase shifting transformers and also 3-winding transformer units.

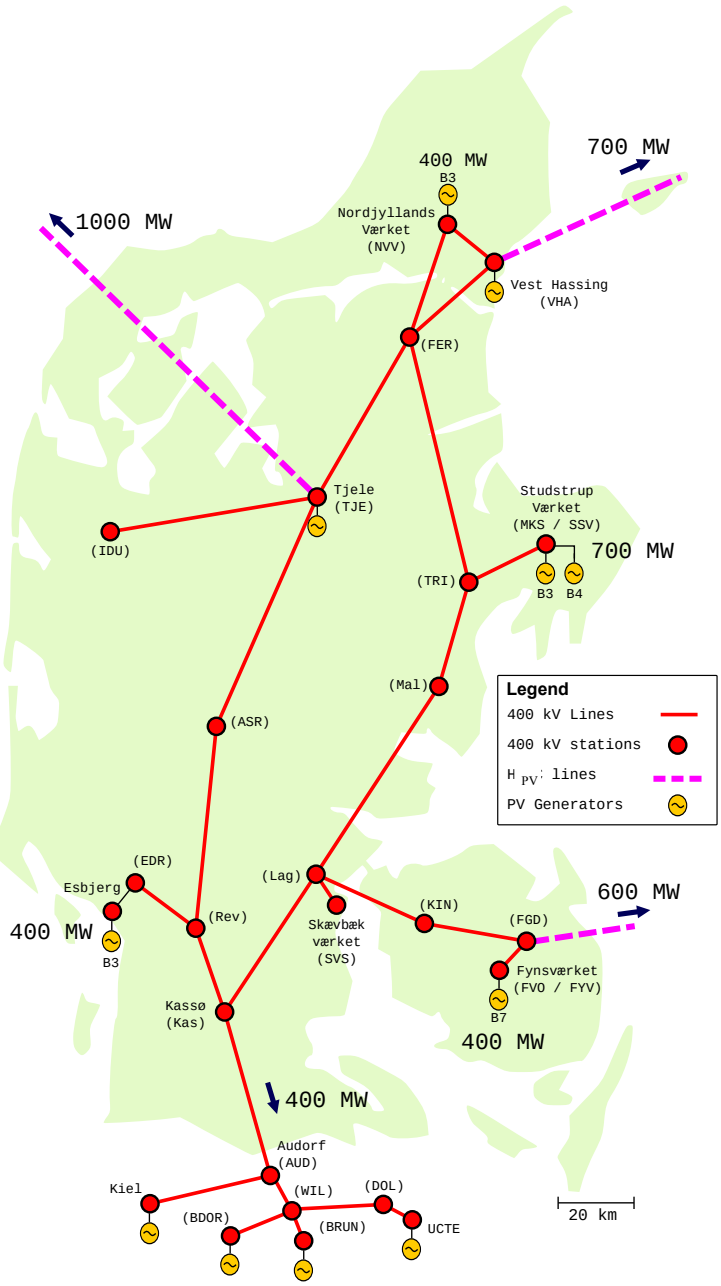

Figure 7-1: 400 kV grid of the Western Danish Power System. The power exchange with the 4 interconnections is indicated, as well as the power generation of the most significant units. The geographical positions are schematically represented, specifically for the part of the grid representing Germany.

7.2 The operational conditions of the case study

A DIgSILENT PowerFactory model of the Western Danish power system is used by Energinet.dk for power system studies. The provided model contains 464 nodes, 162 lines, 377 2-winding transformers, 10 3-winding transformers, 56 asynchronous machines, 150 synchronous machines, 68 shunt units and 29 static generators. Wind turbines and farms are modelled as asynchronous machines and static generators with custom dynamic models written in PowerFactory's DSL language. Interconnections are modelled as static loads.

Full dynamic models of all generation units are included and have been written specifically for the Western Danish system, including protection, frequency control, emergency shutdown, prime movers, voltage control and power system stabilizers.

The provided case is a study of the system under a stressed condition where a large power exchange with the interconnected neighbours occurs, as well as high production at main plants and a significant production of wind power. This results in a large amount of power flowing out of the system. The voltage level of the 400 kV system varies between 1.04 pu and 0.98 pu. Five 400 kV lines are loaded above 40% of rated capacity and three 150 kV lines are loaded above 85%, with 14 150 kV lines running above 50%.

7.3 Creating a case of aperiodic small signal angular instability

To test the developed algorithms, it is neccesarry to perturbate the model in such a manner that aperiodic small signal angular instability (ASSAI) is provoked. 11 generators in the system provide voltage control. In [24] the graphical representation of the stability margins considering specifically ASSAI has been presented. This graphical representation will be used for illustrating of the considered case study (Figure 7-2).In general – the green circle is marking instable operational area, while the distance to this circle is representing the stability margin.

At the initial operational conditions all PV regulated generators are equipped with automatic voltage regulators, which results in quite large stability margins. In order to find the unit most vulnerable to instability, the stability margins of generators when they are swithed to manual excitation were studied. The results of such study are shown in Figure 7-2., where the generators closest to their stability boundary are depicted.

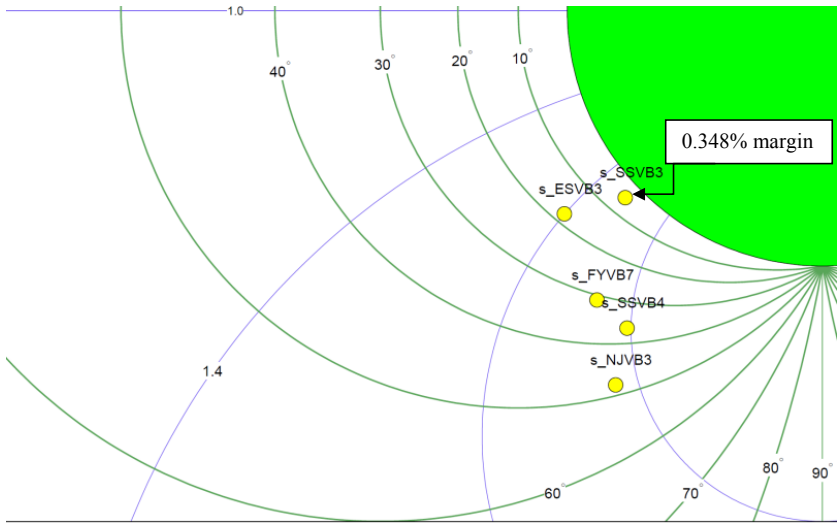

Figure 7-2: Operational points of generators on the injection impedance plane when manual excitation of the machines is used.

It is seen that the machine s_SSVB3 (Studstrup Værket, block 3) would be very close to the stability boundary in the injection impedance plane [82]. Hence, assuming manual excitation for this machine would put the system in an unsafe operation, in which a small contingency can be expected to trigger aperiodic instability. s_SSVB3 will be targeted to initiate ASSAI.

Thus, at first the initial operational conditions are modified by switching the generator s_SSVB3 to the manual excitation regulation. This action as it was shown earlier moves the operational point of this generator close to the stability boundary. However, to push system into unstable operation another contingency is need.
In order to provide more leverage for instability initiation further modification of the initial model was carried out: transformer MKS_150_019A_MT31 of 455 MVA rated power connecting generator s_SSVB3 to the grid has been replaced by three transformers each 260 MVA rated power as it is shown in Figure 7-3.

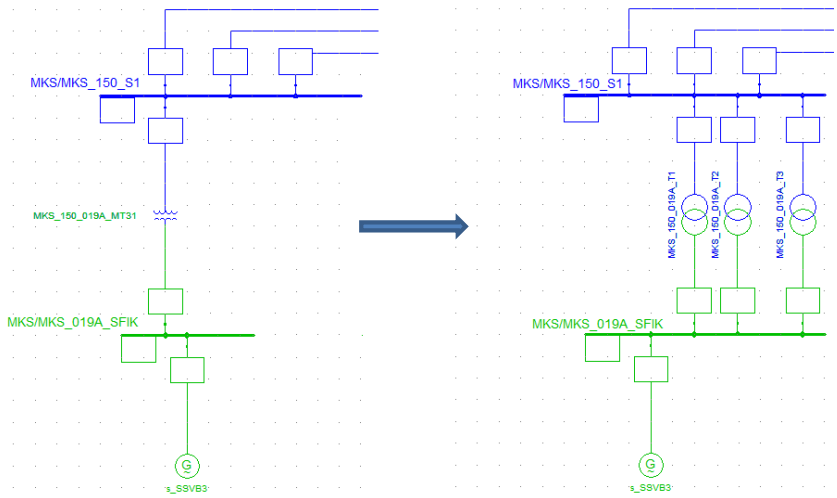

Figure 7-3: Replacement of the transformer MKS_150_019A_MT31 connecting the generator s_SSVB3 to the grid with three transformers each 260 MVA rated power.

With the above mentioned model modification the instability is triggered by tripping of one of the transformers connecting generator s_SSVB3 to the grid.This disturbance leads to emerge of aperiodic small signal angular instability in 156 sec. Figure 7-4 is demonstrating the change of the rotor angle of s_SSVB3 over a time while the described disturbance is applied.

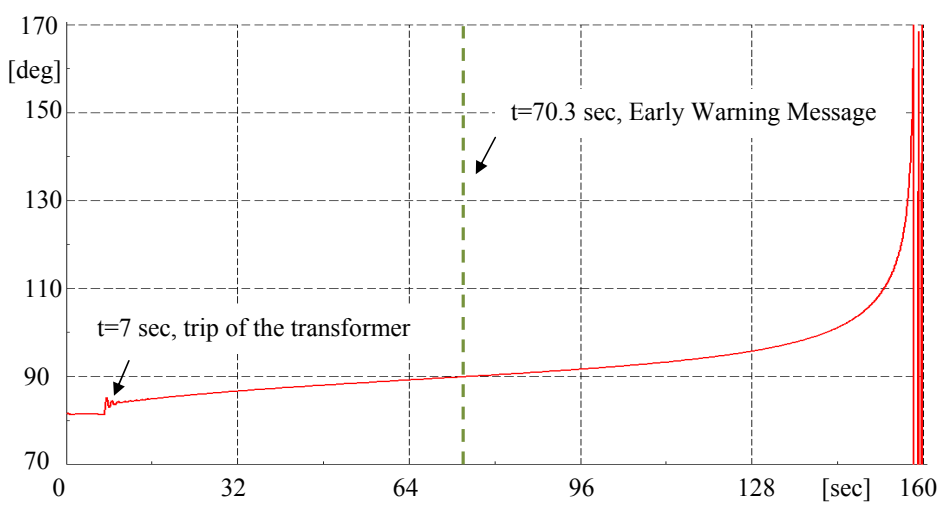

Figure 7-4: Rotor angle s_SSVB3, time domain simulation

As it can be seen from the Figure 7-4 the desired phenomena is provoked, thus the developed scenario is accepted as a case study for further validation of early prevention method.

7.4 Early prevention method implementation onto West Danish Power System model

Utilizing the method developed in [24], the early warning message of upcoming instability is received at a time t_{warn}=70.3 sec. This message is a triggering signal for the initiation of the early prevention algorithm.

7.4.1 Identification of the candidate nodes for the countermeasure application

It was described in chapters 4 and 5 that in order to define the nodes in the grid which are noticeably influencing the stability of the generator s_SSVB3 the self-propagating graph algorithm with embedded sensitivity analysis should be deployed.

For the given study the minimum acceptable value of sensitivity $S_{th_{\min}} = S_{th_{\max}} / 10 = 0.1$ has been chosen. The choice of this value is picked in order to ensure that sufficient number of nodes which have potential to influence the stability of the critical generator are added into the candidate list for countermeasure application. Corresponding to this value of $S_{th_{\min}}$ the self-propagating graph has been created.

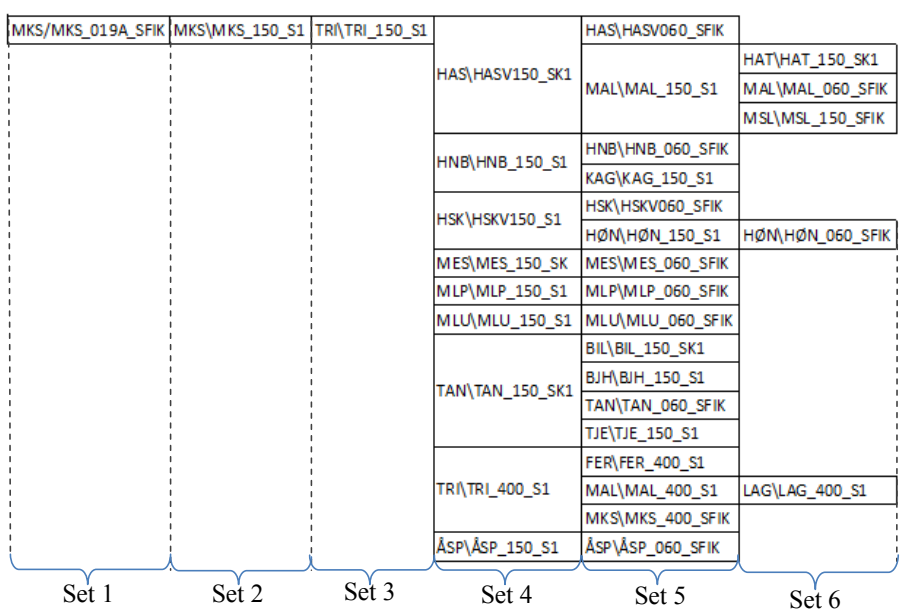

Figure 7-5: Sets of nodes sequentially added to self-propagating graph

The total number of load nodes in the model of the Western Danish power system equals to 425. After application of the self-propogating graph algorithm to this system the resulting amount of nodes added to the candidate list for countermeasure application equaled to 34. The obtained graph in form of sequentially added sets of nodes is depicted in Figure 7-5.

Substituting the node names in Figure 7-5 with corresponding value of sensitivity self-propagating graph appears as shown in Figure 7-6. The orange color marks the nodes, which were defined as dead-end by the self-propagating graph algorithm. The light green color marks the nodes which are added to the candidate list for countermeasure application. The turquois contour is marking the node which is actual dead ends in the grid, thus even though the sensitivity in this nodes is higher than the pre-set minimal limit further propagation of the graph into the grid is not possible.

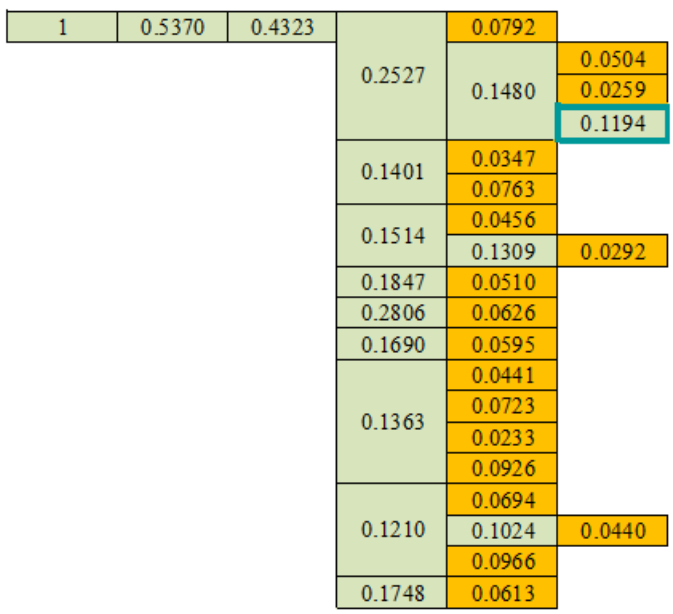

Figure 7-6: Sensitivity values S_{th} corresponding to the nodes added to the self-propagating graph.

In order to create candidate list for countermeasure application it is necessary to take into account actual control reserves allocation. For the current study, the nodes were considered participating in the prevention control if there are either reactive power compensation devices, such as shunt reactors and capacitors, or there is a local load connected. The load variation is considered as a controllable reserve, assuming its control range reaches ΔS=+/-20% from the initial operational point.

The control participation matrix **C** (4.6) containing the information regarding control reserves allocation in the Western Danish Power System was formulated following the rules described at section 4.1.
The elements of control participation matrix **C** corresponding to the nodes included into self-propagating graph in Figure 7-5 are presented in Figure 7-7.

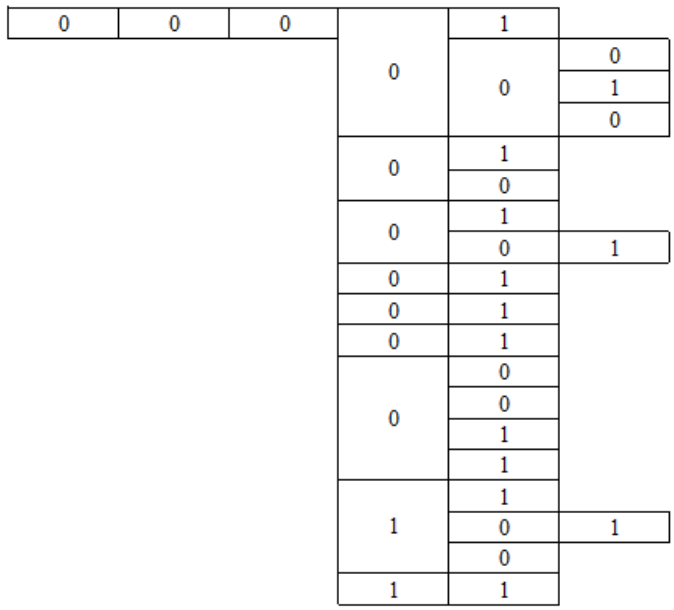

Figure 7-7: Control participation coefficients C_{ii} corresponding to the nodes at Figure 7-5

Multiplying the obtained sensitivity with the control participation coefficient (4.6) the resulting prioritised candidate list for countermeasure application can be formulated. Considering Figure 7-4 and Figure 7-5 the prioritized candidate list for the countermeasure application containing the nodes which have the highest potential of stability influence for generator s_SSVB3 appears as follows:

1. ÅSP\ÅSP_150_S1
2. TRI\TRI_400_S1
3. TJE\TJE_150_S1
4. HAS\HASV060_SFIK
5. FER\FER_400_S1
6. MLP\MLP_060_SFIK
7. ASP\ASP_060_SFIK
8. MLU\MLU_060_SFIK
9. MES\MES_060_SFIK
10. HSK\HSKV060_SFIK

11. LAG\LAG_400_S1
12. HNB\HNB_060_SFIK
13. MAL\MAL_060_SFIK
14. TAN\TAN_060_SFIK

As the next step of the early prevention algorithm, the assessment of the efficiency of the suggested countermeasure for the instability prevention is conducted. As the first step the efficiency of the countermeasure applied to the first node in the prioritized candidate list is to be accomplished. In case the assessment discovers insufficiency of the proposed countermeasure, application of the countermeasure to the next node from the prioritized candidate list is to be done. The assessment continues until a sufficient rate of countermeasure to prevent instability is achieved. The next section will describe the assessment algorithm in detail.

7.4.2 Assessment of the efficiency of the suggested countermeasure

According to the sensitivity analysis carried out in the previous section, the node having the highest potential to influence the aperiodic small signal angular stability of the generator s_SSVB3 is ÅSP\ÅSP_150_S1. The control reserve available at this node is reactor ÅSP_150-ZL1 of 60Mvar nominal power, with no step regulation. The trip of this reactor is suggested as a countermeasure and efficiency of this action for instability prevention is to be assessed.

7.4.2.1 Identification of the GTC corresponding to the admittance matrix, when countermeasure is applied

The actual admittance matrix corresponding to the post-contingency operation is obtained from PMU measurements. The latest measurements which are used for post-contingency admittance matrix formulation are received at a time of early warning message delivery (t=70.3seconds, Figure 7-4). For further use let's denote this admittance matrix as **Y1**.

When a given countermeasure is suggested, it can be represented as corresponding change in admittance matrix. Considering the suggested reactor trip the corresponding nodal admittance change can be defined using the expression (7.1):

$$Y_r = \frac{S_r}{U^2} = \frac{Q_r}{U^2}; \qquad \textbf{(7.1)}$$

For the current study the nodal admittance variation for the bus ÅSP\ÅSP_150_S1 when the reactor is tripped is resulting in $\Delta Y_{ASP\backslash ASP\_150\_S1} = Y_r = 55.0444i$ p.u. Let's denote the matrix corresponding to suggested countermeasure as **Y2**. Then the change of the admittance matrix over time line can be schematically represented as follows:

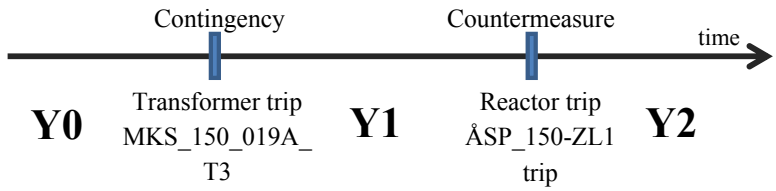

The admittance matrix reflecting the countermeasure application is needed in order to pre-define the grid transformation coefficients GTC which would appear when the countermeasure is actually applied. Later the **GTC** matrix will be needed to define the corresponding Thevenin voltage according to the expression (7.2).

$$\left[\underline{E}_{th}\right] = \left[GTC\right] \cdot \left[\underline{V}_{0}\right] \tag{7.2}$$

In Table 7-1 the grid transformation coefficiens obtained for the Western Danish Power system, when taking into account the change in admittance matrix caused by suggested countermeasure application are shown.

For demonstrating the further assessment let's refer to the P-δ characteristics in Figure 7-8:

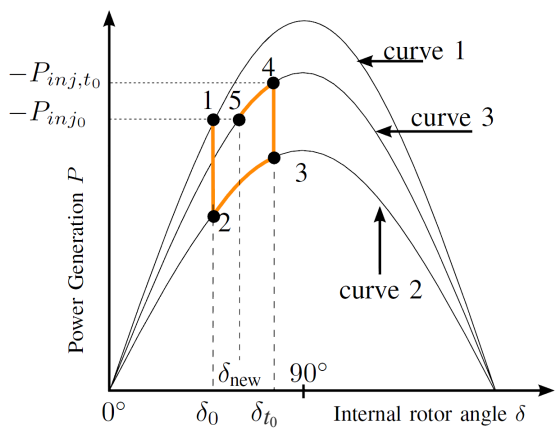

Figure 7-8: Trajectory of the rotor angle δ over P-δ curve when steady state is afflicted by disturbance followed by countermeasure application.

After the trip of the transformer, the operational point of the generator s_SSVB3 moves to point 2 (t=7sec) and starts drifting towards the point 3 in the attempt to retain the power balance. At point 3 (t=72.3sec) the early warning message is received. Up to that point the trajectory of the system is monitored in real time using PMU data. The further movement of the operational point corresponding to the suggested countermeasure application is to be pre-defined, and the resulting active power stability margins should be predicted – characterizing the effectiveness of instability prevention.

Table 7-1 Grid transformatin coefficients corresponding to admittance matrix **Y2**

	s_BDOR	**s_BRUN**	**s_FYVB7**	**s_KIEL**	**s_SSVB 4**	**s_NJVB 3**	**s_TJE1**	**s_UCTE**	**s_VHA1**	**s_ESVB 3**	**s_SSVB 3**
s_BDOR	0	-0.2091+ +0.0144i	-0.0334+ +0.0038i	-0.0348+ +0.0015i	-0.0233+ +0.0023i	-0.0236+ +0.0027i	-0.0175+ +0.0015i	-0.6079+ +0.0167i	-0.0058+ +0.0003i	-0,0310- -0.0007i	-0.0012+ +0.0002i
s_BRUN	-0.2866+ 0.0177i	0	0,0277- -0.0031i	0,0327- -0.0015i	0,0194- -0.0019i	0,0196- -0.0022i	0,0146- -0.0012i	0,5559- -0.0150i	0,0048- -0.0003i	0.0259+ +0.0006i	0,0010- -0.0002i
s_FYVB7	-0.1141+ +0.0149i	0,0692- -0.0092i	0	0,0408- -0.0020i	0,1554- -0.0319i	0,1217- -0.0292i	0,0873- -0.0183i	0,2109- -0.0179i	0,0297- -0.0055i	0,1023- -0.0072i	0,0074- -0.0022i
s_KIEL	-0.1717+ +0.0334i	0,1178- -0.0230i	0,0572- -0.0181i	0	0,0386- -0.0117i	0,0388- -0.0123i	0,0295- -0.0080i	0,4662- -0.0642i	0,0098- -0.0024i	0,0692- -0.0111i	0,0020- -0.0008i
s_SSVB4	-0.0705+ +0.0064i	0,0427- -0.0039i	0,1376- -0.0244i	0,0242- -0.003i	0	0,2410- -0.0379i	0,1511- -0.0213i	0,1297- -0.0059i	0,0562- -0.0067i	0,0888- -0.0003i	0,0141- -0.0032i
s_NJVB3	-0.0625+ +0.0087i	0,0379- -0.0053i	0,0941- -0.0229i	0,0214- -0.0012i	0,2106- -0.0397i	0	0,1867- -0.0359i	0,1152- -0.0107i	0,1007- -0.0173i	0,1052- -0.0044i	0,0108- -0.0029i
s_TJE1	-0.0582+ +0.0078i	0,0352- -0.0048i	0,0844- -0.0206i	0,0202- -0.0009i	0,1653- -0.0334i	0,2335- -0.0520i	0	0,1072- -0.0094i	0,0839- -0.0098i	0.1151+ +0.0003i	0,0162- -0.0036i
s_UCTE	-0.4626+ +0.0803i	0,3085- -0.0556i	0,0465- -0.0107i	0,0715- -0.0110i	0,0325- -0.0070i	0,0328- -0.0076i	0,0245- -0.0048i	0	0,0081- -0.0014i	0,0448- -0.0040i	0,0017- -0.0005i
s_VHA1	-0.0437+ +0.0015i	0,0265- -0.0009i	0,0660- -0.0095i	0.0150+ +0.0008i	0,1409- -0.0147i	0,2889- -0.0367i	0,1911- -0.0082i	0.0803+ +0.0091i	0	0.0824+ +0.0091i	0,0097- -0.0013i
s_ESVB3	-0,1089- -0.0066i	0.0664+ +0.0040i	0,1054- -0.0026i	0.0484+ +0.0079i	0.1036+ +0.0017i	0.1398+ +0.0011i	0.1212+ +0.0098i	0.2037+ +0.0226i	0.0384+ +0.0044i	0	0,0066- -0.0001i
s_SSVB3	-0.0494+ +0.0026i	0,0300- -0.0016i	0,0885- -0.0138i	0.0172+ +0.0006i	0,1898- -0.0206i	0,1670- -0.0205i	0,1982- -0.0098i	0,0909- -0.0006i	0,0514- -0.0017i	0.0742+ +0.0060i	0

The last real data obtained from the PMU measurements are received at point 3. In order to trace transition of the system from point 3 to point4, caused by the switch of the reactor, the new admittance matrix is defined, where the suggested countermeasure in form of nodal admittance change is taken into account. Considering that the rotor angle doesn't change in step, the injected power P_{inj} at point 4 can be defined according to formula (6.17), the corresponding Thevenin voltage is defined using data from the Table 7-2 and (7.2).

The following values for P_{inj} have been obtained for all PV generators in the West Danish Power System:

Table 7-2 Pinj and Eth coresponding to operational point 4

Gen name	**s_BDOR**	**s_BRUN**	**s_FYVB7**	**s_KIEL**	**s_SSVB4**	**s_NJVB3**
P_{inj}	– 1,655	– 0,995	–375,144	– 0,608	–355,615	– 384,0634
$\underline{E}_{th}$	– 0,980+ +0,029i	0,978– –0,034i	0,931– –0,057i	0,995 – –0,144i	0,947 – –0,006i	0,934 – – 0,041i

Gen name	**s_TJE1**	**s_VHA1**	**s_ESVB3**	**s_SSVB3**	**s_UCTE**
P_{inj}	– 3,793	– 1,601	– 382,061	– 355,004	– 1500,500
$\underline{E}_{th}$	0,918 – – 0,003i	0,937 + +0,044i	0,934 + +0,107i	0,959 + +0,018i	0,994 – – 0,175i

After the operational point 4 has been defined the transition from point 4 to the point 5 should be obtained. For the current study the rescheduling of the generators was restricted, thus the assumption is that the power production for the new steady state will stay the same as it was in the initial operational conditions, so $P_{gen_{point1}}=P_{gen_{point5}}$. Generally, the change in power production can be considered, however this study is focused on the involvement of load nodes for the power system stability management.

Taking into account this assumption the first approximation to the operational point 5 can be found according to the following expression:

$$\begin{cases} P_{inj_{t=t0}} = P_{inj_{t=t+steady}} \\ P_{inj_{t=t+}} - \dfrac{E_{th_{t=t+}} \cdot V_0}{Z_{th_{t=t+}}} \cos(\delta_{t=t+} - \theta_{th_{t=t+}} + \phi_{th_{t=t+}}) = P_{inj_{t=t0}} - \dfrac{E_{th_{t=t+}} \cdot V_0}{Z_{th_{t=t+}}} \cos(\delta_{t=t+steady} - \theta_{th_{t=t+}} + \phi_{th_{t=t+}}) \\ \delta_{t=t+steady} = \arccos\left[\left(\dfrac{E_{th_{t=t+}} \cdot V_0}{Z_{th_{t=t+}}} \cos(\delta_{t=t+} - \theta_{th_{t=t+}} + \phi_{th_{t=t+}}) - P_{inj_{t=t+}} + P_{inj_{t=t0}}\right) \dfrac{Z_{th_{t=t+}}}{E_{th_{t=t+}} \cdot V_0}\right] + \theta_{th_{t=t+}} - \phi_{th_{t=t+}} \end{cases} \quad \textbf{(7.3)}$$

The rotor angles corresponding to the first approximation and obtained following the expression (7.3) are shown in the Table 7-3.

Table 7-3 The first approximation of the rotor angles corresponding to operational point 5

Gen name	**s_BDOR**	**s_BRUN**	**s_FYVB7**	**s_KIEL**	**s_SSVB4**	**s_NJVB3**
$\boldsymbol{\delta_{gen}}$, **grad**	178,302	-1,967	8,241	-7,871	9,069	6,008

Gen name	**s_TJE1**	**s_VHA1**	**s_ESVB3**	**s_SSVB3**	**s_UCTE**
$\boldsymbol{\delta_{gen}}$, **grad**	-0,622	2,516	20,048	81,509	0

To define the first approximation of rotor angles for the new steady state the value of equivalent Thevenin voltage corresponding to point 4 was used. However, the equivalent Thevenin voltage seen by generators will change while the system is drifting from point 4 to point 5 as it is directly dependent on the rotor angles as can be seen from the expression **(7.4)**

$$\begin{pmatrix} \underline{E}_{theqv\ 1} \\ \underline{E}_{theqv\ 2} \\ \cdots \\ \underline{E}_{theqv\ \mathrm{i}} \\ \cdots \\ \underline{E}_{theqv\ \mathrm{N}} \end{pmatrix} = (\mathbf{GTC}) \cdot \begin{pmatrix} V_{01} \cdot e^{j\delta_1} \\ V_{02} \cdot e^{j\delta_2} \\ \cdots \\ V_{0i} \cdot e^{j\delta_i} \\ \cdots \\ V_{0N} \cdot e^{j\delta_N} \end{pmatrix}; \qquad \textbf{(7.4)}$$

In order to adjust the obtained rotor angles the iterative process is initiated described in section 6.3.1, where the Thevenin voltage is recalculated in each iteration; this leads to further adjustment of the rotor angle and process repeats. The calculation continues until the required precision $\Delta\delta<\varepsilon$ is achieved.
For the given study case the initial conditions for the iterative process are taken from Table 7-3, the elements for **GTC** matrix are taken from Table 7-1.
Using the formulas (6.28) the Jacobian matrix is defined. As it was described in section 6.3.2 for reducing the computational burden the Jacobian matrix is calculated only ones on the first iteration, furthermore it is simplified to diagonal matrix. The obtained Jacobian matrix is shown in Figure 7-9.

$$\boldsymbol{J} = diag\begin{bmatrix} 6209{,}82 \\ 4492{,}37 \\ 1776{,}95 \\ 1243{,}77 \\ 2094{,}16 \\ 2413{,}04 \\ 1760{,}23 \\ 842{,}28 \\ 1601{,}16 \\ 351{,}02 \end{bmatrix}$$

Figure 7-9: Jacobian matrix calculated at a point of the first approximation.

Following the iterative algorithm described in (6.27)− (6.29) the resulting rotor angles are defined and corresponding active power stabilitymargin calculated. Below the results for the precision $\Delta\delta<10^{-1}$ are presented:

Table 7-4 Prediction of the resulting rotor angle and active power stability margin

Gen name	δpred	$P_{marg\text{-}pred,\%}$	N iteration
s_BDOR	178.182	100.00	14
s_BRUN	-2.0847	100.00	
s_FYVB7	7.8106	80.5509	
s_KIEL	-8.0604	100.00	
s_SSVB4	8.5170	84.0582	
s_NJVB3	5.4431	85.4456	
s_TJE1	-1.1822	99.9999	
s_VHA1	1.9215	99.9974	
s_ESVB3	19.6286	77.2982	
s_SSVB3	85.1026	0.4691	
s_UCTE	0	84.8826	

Where $P_{marg\_pred,\%}$ is predicted active power stability margin , calculated using expression (6.1). According to the results presented in Table 7-4 the early prevention algorithm indicates that the proposed countermeasure (trip of the 60MVar reactor ÅSP\ÅSP_150_S1) leads to stabilization of the system, even though the resulting active power stability margin for the critical generator s_SSVB3 is low.

In order to validate the obtained result, the time domain simulation reflecting the effect of the suggested countermeasure is to be carried out and the actual rotor angles and resulting active power stability margin to be compared with the results obtained by early prevention method.

The result of the time domain simulation carried out using DigSilent PowerFactory is presented in Figure 7-10.The countermeasure in form of reactor trip is applied in 18,5 sec. after the cross of the stability boundary by generator s_SSVB3 has been detected by early warning method [24].

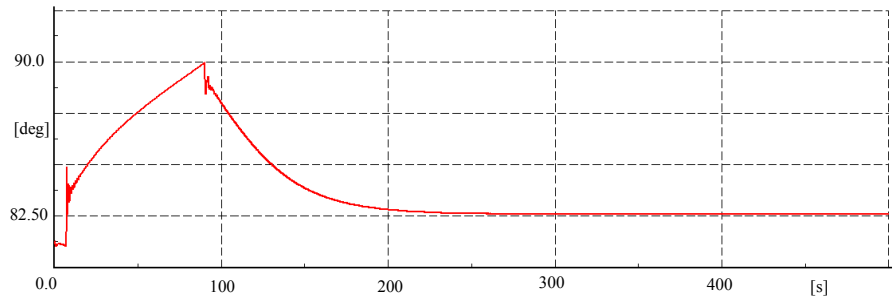

Figure 7-10: Rotor angle s_SSVB3 with reference to the reference machine angle, countermeasure application effect

As it can be seen, the simulation demonstrates that after application of the proposed countermeasure the critical generator stabilizes, settling at the new steady state.
The movement of the operational point of the generator s_SSVB3 corresponding to the points 3-5 on the P-δ curve (Figure 7-8) when visualized using injection impedance plane [81] is shown in Figure 7-11.

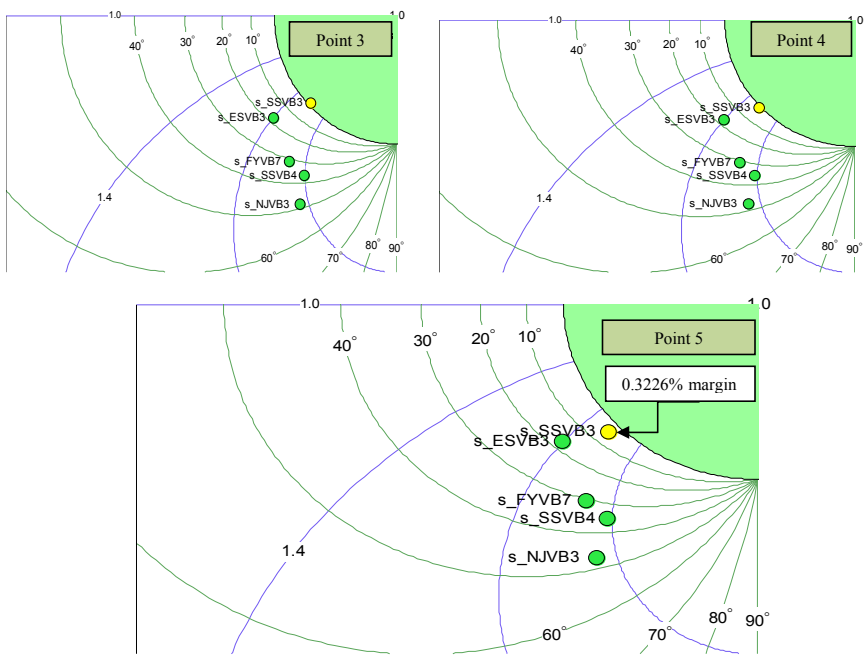

Figure 7-11: Operational points of generators on the injection impedance plane corresponding to points 3-5 of the P-δ curve characteristics (Figure 7-8).

Table 7-5 demonstrates the comparison of the results obtained on the basis of RMS dynamic simulation in PowerFactory and the predication made using early prevention method. It can be seen that the predicted results are in a good agreement with the ones obtained by simulation.

Table 7-5 Comparison of simulation results with the predicted values of rotor angles and actve power margin

Gen name	δ_{sim}	δ_{pred}	$P_{marg\text{-}sim,\%}$	$P_{marg\text{-}pred,\%}$	Pmarg prediction abs. error,Δ
s_BDOR	178.1490	178.182	100.00	100.00	0.00
s_BRUN	-2.1173	-2.0847	100.00	100.00	0.00
s_FYVB7	7.7803	7.8106	80.54	80.5509	0.0109
s_KIEL	-8.0932	-8.0604	100.00	100.00	0.00
s_SSVB4	8.4827	8.5170	84.05	84.0582	0.0082
s_NJVB3	5.3895	5.4431	85.43	85.4456	0.0156
s_TJE1	-1.2154	-1.1822	99.99	99.9999	0.0099
s_VHA1	1.8824	1.9215	100.00	99.9974	0.0026
s_ESVB3	19.5943	19.6286	77.29	77.2982	0.0082
s_SSVB3	85.8851	85.1026	0.3226	0.4691	0.1465
s_UCTE	-0.0328	0	84.89	84.8826	0.0074

The presented example demonstrates that early prevention method is capable of fast identification of the appropriate countermeasure allowing avoidance of upcoming aperiodic small signal angular instability.
The main advantage of the developed methodology is that assessment is done for the actual operation conditions, utilizing PMU data, while modeling of the system and time consuming load flow and EMT/RMS simulations are avoided.

7.4.3 Early prevention method applied for identification of upcoming instability

Current section will consider the possibility of utilizing early prevention method for early indication if a given system disturbance leads to aperiodic small signal angular instability.It the previous section it was shown that it is possible to predict the resulting steady state operational conditions when a given countermeasure, expressed in the form of nodal admittance variation, is suggested. As a triggering signal for the activation of the early prevention method the early warning message was used. This message is generated when the stability criterion derived in [24] indicates crossing of the stability boundary by the most critical generator. However the disadvantage of this criterion is that it is not possible to predict if the machine will cross the stability boundary or it will stabilize after a certain rotor angle increase adjusting to the new operational conditions. Thus, the impossibility of the new steady state is indicated by fact of boundary cross. In

this section an attempt to indicate early the impossibility of the new steady state utilizing early prevention algorithm will be considered.

Both countermeasure application and disturbance occuring in the grid can be interpreted by means of system admittance matrix alteration. Thus the same algorithm for the prediction of the resulting rotor angles and active power stability margin can be utilized. In section 6.3.3.2 the prediction of the new steady state after a series of disturbances being applied is shown on the example of the IEEE30 bus test system.
In this chapter it will be investigated if early prevention method is capable of adequate identification of the upcoming instability, when disturbance applied to the grid leads to emergence of instability.

The same study case as in section 7.4.2 is to be considered. As it is seen from Figure 7-4 that trip of the transformer MKS_150_019A_T3 leads to aperiodic small signal angular instability for the generator s_SSVB3. Introducing trip of transformer as a corresponding change in admittance matrix the intension is to run the early prevention algorithm to predict the resulting system state if no counteractions will be taken.
At the first step the new **GTC** corresponding to changed admittance matrix due to transformer trip is to be defined. Following the methodology described in section 6.2 of the current report **GTC** corresponding to admittance matrix **Y1**are defined and presented in the Table 7-6.

Table 7-6 Grid transformatin coefficients corresponding to admittance matrix **Y1**.

	s_BDOR	**s_BRUN**	**s_FYVB7**	**s_KIEL**	**s_SSVB 4**	**s_NJVB 3**	**s_TJE1**	**s_UCTE**	**s_VHA1**	**s_ESVB 3**	**s_SSVB 3**
s_BDOR	0	-0.2091+ +0.0144i	-0.0333+ +0.0037i	-0.0348+ +0.0015i	-0.0232+ +0.0023i	-0.0236+ +0.0027i	-0.0174+ +0.0014i	-0.6079+ +0.0166i	-0.0058+ +0.0003i	-0,0309- -0.0007i	-0.0012+ +0.0002i
s_BRUN	-0.2866+ 0.0177i	0	0,0277- -0.0031i	0,0327- -0.0014i	0,0193- -0.0018i	0,0196- -0.0022i	0,0145- -0.0011i	0,5559- -0.0149i	0,0048- -0.0003i	0.0259+ +0.0007i	0,0010- -0.0002i
s_FYVB7	-0.1140+ +0.0148i	0,0691- -0.0091i	0	0,0408- -0.0020i	0,1548- -0.0315i	0,1212- -0.0288i	0,0867- -0.0180i	0,2107- -0.0176i	0,0296- -0.0054i	0,1021- -0.0070i	0,0073- -0.0022i
s_KIEL	-0.1717+ +0.0334i	0,1178- -0.0230i	0,0572- -0.0180i	0	0,0385- -0.0115i	0,0387- -0.0121i	0,0294- -0.0079i	0,4663- -0.0641i	0,0097- -0.0023i	0,0692- -0.0110i	0,0020- -0.0008i
s_SSVB4	-0.0702+ +0.0062i	0,0425- -0.0038i	0,1370- -0.0240i	0,0241- -0.003i	0	0,2399- -0.0373i	0,1498- -0.0207i	0,1291- -0.0056i	0,0559- -0.0065i	0,0883- -0.0000i	0,0140- -0.0031i
s_NJVB3	-0.0623+ +0.0085i	0,0377- -0.0052i	0,0937- -0.0226i	0,0213- -0.0012i	0,2097- -0.0391i	0	0,1856- -0.0353i	0,1147- -0.0105i	0,1005- -0.0171i	0,1048- -0.0041i	0,0107- -0.0029i
s_TJE1	-0.0578+ +0.0076i	0,0350- -0.0047i	0,0838- -0.0202i	0,0201- -0.0008i	0,1639- -0.0326i	0,2321- -0.0511i	0	0,1065- -0.0091i	0,0835- -0.0095i	0.1145+ +0.0007i	0,0160- -0.0035i
s_UCTE	-0.4627+ +0.0803i	0,3085- -0.0555i	0,0465- -0.0106i	0,0715- -0.0110i	0,0323- -0.0069i	0,0327- -0.0075i	0,0243- -0.0047i	0	0,0081- -0.0013i	0,0448- -0.0040i	0,0017- -0.0005i
s_VHA1	-0.0435+ +0.0014i	0,0264- -0.0009i	0,0657- -0.0093i	0.0150+ +0.0009i	0,1402- -0.0143i	0,2882- -0.0362i	0,1902- -0.0077i	0.0799+ +0.0012i	0	0.0820+ +0.0093i	0,0096- -0.0012i
s_ESVB3	-0,1088- -0.0068i	0.0664+ +0.0041i	0,1051- -0.0024i	0.0484+ +0.0080i	0.1031+ +0.0019i	0.1394+ +0.0014i	0.1206+ +0.0101i	0.2035+ +0.0229i	0.0382+ +0.0045i	0	0,0065- -0.0001i
s_SSVB3	-0.0489+ +0.0023i	0,0296- -0.0015i	0,0875- -0.0133i	0.0170+ +0.0006i	0,1877- -0.0197i	0,1652- -0.0196i	0,1958- -0.0090i	0,0898- -0.0002i	0,0508- -0.0015i	0.0734+ +0.0063i	0

As the intension is to predict if given disturbance leads to system instability the transition from point 1 to point 2 (Figure 7-8) is defined at the first step. In the next step, the transiton to point 3 is to be assessed. The first approximation of the resulting rotor angles is obtained using expression (7.3). The first approximation of the rotor angles corresponding to operational point 3 is shown in Table 7-7.

Table 7-7 The first approximation of the rotor angles corresponding to operational point 3

Gen name	**s_BDOR**	**s_BRUN**	**s_FYVB7**	**s_KIEL**	**s_SSVB4**	**s_NJVB3**
$\delta_{gen,}$ **deg**	178,264	-2,006	8,159	-7,922	8,964	5,890

Gen name	**s_TJE1**	**s_VHA1**	**s_ESVB3**	**s_SSVB3**	**s_UCTE**
$\delta_{gen,}$ **deg**	-0,751	2,386	20,000	91,673	0

When the first approximation of the resulting rotor angle is defined (Table 7-7), the iterative process for further rotor angles adjustment should be initiated as described in section 6.3.1. The Jacobian matrix defined at the first approximation to the point 3 is presented in Figure 7-11.

$$\boldsymbol{J} = diag\begin{bmatrix} 6206{,}08 \\ 4490{,}39 \\ 1764{,}82 \\ 1242{,}54 \\ 2071{,}04 \\ 2388{,}67 \\ 1737{,}04 \\ 833{,}88 \\ 1592{,}36 \\ 342{,}97 \end{bmatrix}$$

Figure 7-11: Jacobian matrix calculated at a point of the first approximation.

Following the iterative algorithm described in (6.27)− (6.29) the resulting rotor angles are to be defined. As it can be seen from the Table 7-8 iterative process doesn't converge. Specifically rotor angle of the generator s_SSVB3 continues to increase from iteration to iteration. This perfectly reflects the behavior pattern of the rotor angle when the uncompensated mismatch of mechanical and electrical torques on the shaft leads to increase of rotor angle until the machine goes out of step. Hence, non- convergence of the iterative process serves as an indicator of unreachability of the new steady state under new operational conditions. As a criterion for iterative process interruption the angle separation in 180 degrees between considered generator and corresponding Thevenin voltage equivalent is used.

Table 7-8 Rotor angles defined on the different iterations

N	s_BDOR	s_BRUN	s_ FYVB7	s_KIEL	s_ SSVB4	s_NJVB3	s_TJE1	s_ VHA1	s_ ESVB3	s_SSVB3	s_UCTE
iter	δ, deg	δ, deg	δ, deg	δ, deg	δ, deg	δ, deg	δ, deg	δ, deg	δ, deg	δ, deg	δ, deg
1	178,258	-2,012	8,128	-7,927	8,934	5,845	-0,777	2,347	19,978	**91,584**	0
2	178,267	-2,004	8,176	-7,920	9,015	5,892	-0,740	2,368	20,012	**92,130**	0
3	178,276	-1,995	8,209	-7,906	9,051	5,933	-0,700	2,411	20,044	**92,682**	0
4	178,283	-1,989	8,234	-7,895	9,085	5,966	-0,669	2,445	20,069	**93,243**	0
5	178,289	-1,983	8,256	-7,886	9,113	5,994	-0,643	2,472	20,091	**93,821**	0
6	178,294	-1,978	8,275	-7,878	9,137	6,017	-0,622	2,495	20,109	**94,419**	0
7	178,298	-1,974	8,291	-7,872	9,159	6,037	-0,603	2,515	20,125	**95,046**	0
8	178,301	-1,971	8,306	-7,866	9,178	6,055	-0,588	2,532	20,139	**95,709**	0
9	178,304	-1,968	8,319	-7,861	9,195	6,071	-0,574	2,547	20,151	**96,416**	0
10	178,307	-1,965	8,332	-7,857	9,212	6,086	-0,562	2,560	20,163	**97,181**	0
11	178,309	-1,963	8,343	-7,853	9,227	6,100	-0,551	2,573	20,174	**98,016**	0
12	178,312	-1,960	8,355	-7,849	9,242	6,114	-0,542	2,584	20,184	**98,939**	0
13	178,314	-1,958	8,365	-7,846	9,256	6,126	-0,533	2,594	20,194	**99,975**	0
14	178,316	-1,957	8,376	-7,843	9,270	6,138	-0,526	2,603	20,204	**101,154**	0
15	178,317	-1,955	8,386	-7,840	9,284	6,149	-0,521	2,611	20,213	**102,518**	0
16	178,319	-1,954	8,396	-7,838	9,296	6,160	-0,518	2,617	20,221	**104,126**	0
17	178,320	-1,953	8,405	-7,837	9,308	6,169	-0,519	2,621	20,229	**106,064**	0
18	178,320	-1,952	8,413	-7,836	9,317	6,175	-0,524	2,622	20,235	**108,456**	0
19	178,320	-1,952	8,419	-7,837	9,323	6,177	-0,538	2,617	20,239	**111,498**	0
20	178,318	-1,954	8,420	-7,840	9,320	6,172	-0,566	2,602	20,238	**115,506**	0
21	178,313	-1,958	8,412	-7,848	9,303	6,151	-0,619	2,569	20,227	**121,019**	0
22	178,304	-1,967	8,385	-7,864	9,255	6,102	-0,718	2,504	20,198	**129,027**	0
23	178,285	-1,984	8,317	-7,896	9,140	5,989	-0,913	2,371	20,129	**141,491**	0
24	178,244	-2,020	8,154	-7,964	8,864	5,733	-1,319	2,091	19,970	**162,654**	0
25	178,154	-2,100	7,742	-8,115	8,177	5,116	-2,226	1,458	19,580	**202,402**	0

The demonstrated case study showed that the early prevention method can be used for the assessment of the reachability of the new steady state after the system has been exposed to a disturbance. The assessment can be carried out immediately after the system has entered quasi-steady state operation. Thus, there is no need to wait until the stability boundary will be crossed in order to make a conclusion if the system can't settle down to a steady state under new operational conditions. That provides greater time allowance for the search of the appropriate countermeasure.

8
CONCLUSION

In the scope of this work a method capable of fast identification of appropriate preventive countermeasure allowing avoidance of the upcoming instability has been developed. The main purpose was to develop early prevention method which could solve the problem of identifying proper countermeasure in the near-real time.

The inspiration for this work was triggered by the fact that new monitoring technologies have resulted in the methods capable of detecting instability at the early stage of its emergence have started to appear. Integration of PMU into power systems will allow obtaining up-to date information about system parameters and operational conditions. This leads to the opportunity to carry out an analysis of various system problems on the basis of measured data, hence considering an actual operational situation, instead of using control regulations derived on the basis of pre-simulated cases.

The developed monitoring and control methods, which utilize wide area measurements, has a number of perspectives: real-time monitoring of the actual operational conditions, integration of the adaptive control systems which are addressing specifically given critical conditions, introduction of preventive control systems enabling concept of self-healing power systems.

In order to demonstrate new possibilities for the preventive control when wide area measurements are integrated into the power system, the ideas expressed at the given project have been based on the perspective of the real-time complete system observability.The latest ideas concerning integration to the system such controllable load as: electric vehicles, smart houses, and energy storages were specifically addressed in the project.

Manipulation of the load nodes in the grid for stability problems management was studied in the project. Conventional passive regulation devices as shunt reactors and condensers were as well considered as a means of preventive control for avoiding instability. Overall, the potential of the future grid flexibility for smart control targeted to keep system in stable operation was the the main focus of the project.

8.1 Results

Power systems stability is a broad research area as different types of instability have different triggering phenomena. This project was focused on a particular type of instability−aperiodic small signal angular instability (ASSAI). The choice of this type of instability for the study was defined by the fact, that the method enabling early detection of ASSAI utilizing PMU measurements has been available. This method has been used as a triggering signal for the early prevention method.

For achieving the main ambition of the project, which is to develop early prevention method for systems instability, a number of goals have been set. Among them: finding of the optimal node for applying countermeasure, pre-identification of the equivalent Thevenin voltage which will be seen by a given generator when a certain change in the grid is to be applied, assessment of the existence of the new steady state after a suggested countermeasure has been applied and finally prediction of the resulting active power stability margin.

In order to define the optimal node for applying a countermeasure, sensitivity analysis was utilized, where the sensitivity of the Thevenin impedance seen by a given generator to a variation of the nodal admittance was suggested as a criterion determining the effectivity of a considered node to influence stability of a given generator. In order to reduce the number of nodes for which sensitivity analysis should be carried out, the self-propagating graph algorithm was developed.

It was noticed that only in a few nodes alteration of a nodal admittance lead to high sensitivity of the Thevenin impedance seen by a considered generator, while for the vast majority of the nodes alteration of admittance doesn't lead to a noticeable change in Thevenin impedance. At the same time the correlation between topological distance and sensitivity decay has been noticed. This factor was used to develop the algorithm which enables discrete supplementing of the nodes to be processed through sensitivity analysis, in a way that topologically nearest nodes are added at the first order. Adding of nodes is organized in sets. Each set contains nodes which have similar length of the shortest pass to the considered generator. Each next set added to sensitivity analysis contains nodes which shortest distance to the considered generator is one vertex longer comparing to the nodes from previous set.When the sensitivity analysis is carried out, the nodes which appeared to have low sensitivity are marked as a dead-end and further propagation of the graph through this node is restricted. Thus when the sensitive of all nodes added on the last step of algorithm appears to be below a pre-set level the search for the candidates for the optimal location ofapplying a countermeasure stops. This method enables significant reduction of the number of nodes to be processed through sensitivity analysis, eliminating large part of the grid from the consideration on the a-

priory basis. Self-propagating graph algorithm reduces the computational time for the identification of the candidates for the optimal location of countermeasure application.

The next step of the Early Prevention Algorithm provides identification of equivalent Thevenin voltage seen by a given generator on the basis of system admittance matrix and voltages of the voltage sources. Equivalent Thevenin voltage seen by a given generator is represented as a sum of the components induced by each voltage source in the grid. The value of each induced component is defined as a product of the voltage at a terminal of the voltage source and grid transformation coefficient (GTC), where the latest is calculated on the basis of the system admittance matrix. Such representation allows predicting how the equivalent Thevenin voltage will be affected when a certain countermeasure is applied. This knowledge is essential for the assessment of the new steady state existence and the resulting stability margin prediction.

Finally, when a certain countermeasure is suggested to be applied at a chosen, on the basis of sensitivity analysis, node, and the change in equivalent Thevenin voltage seen by considered generator is predicted the assessment of the existence of the new steady state is to be carried out. For this purpose the solution of the system of non-linear equations is initiated. Each equation is describing a power flow in the system containing a generator and the corresponding Thevenin equivalent. The number of equations equals to the number of voltage controlled synchronous machines in the grid. The solution of the system with respect to rotor angles is utilizing Newton approach for system linearization and iterative solution. When iterative process converges the obtained solution is a new steady state operational point. Prediction of the resulting stability margin is based on the obtained solution. The non-convergancy of the iterative process indicates unreachability of the new steady state for the proposed operational conditions. Thus, the functionality of the efficiency prediction for the suggested countermeasure is realized.

The large scale validation of the early prevention method was realized on the Western Danish Power System model. This system contains 464 nodes, 162 lines, 377 2-winding transformers, 10 3-winding transformers, 56 asynchronous machines, 150 synchronous machines among which 11 voltage controlled, 68 shunt units and 29 static generators. The instability case causing slip of the rotor poles in 156 seconds after application of the disturbance has been created. As a disturbance triggering instability, the trip of one of the transformers connecting critical generator to the grid was used. The task for early prevention method was to suggest the effective countermeasure leading to escape from instability and predict the resulting active power stability margin.

Early prevention algorithm has suggested as a countermeasure the trip of the 60 MVar reactor, and predicted that new steady state will be reached granting the suggested countermeasure is performed, even though the resulting stability margin for the critical gen-

erator will stay low and be equal to 0.47%. The time domain simulation of the proposed countermeasure application demonstrated the stabilization of the system; resulting stability margin for the critical generator appeared to be 0.32%. Thus, the absolute error of predicted stability margin comparing to one obtained on simulation basis amounts to 0.1465.This result gives promising perspectives that the presented method can be used for the fast identification of the appropriate countermeasure for the instability avoidance. Method contains algorithms enabling complete cycle analysis starting from proposition of the optimal location of the countermeasure application, assessment of the sufficiency of the proposed countermeasure for the system stabilization and prediction of the resulting stability margin.

The main advantage of the developed early prevention method is that no computer simulation is required in order to assess the sufficiency of the proposed countermeasure; furthermore each step of the method doesn't contain computationally heavy operations enabling applicability of this method for the near real-time application.

8.2 Further work

Considering the results achieved in this project, the perspective of the next research steps can be defined.

First of all, further development of the early prevention method is a natural direction of the future research. Other preventive control actions, besides the nodal admittance variation, are to be studied. Using the same methodological basis, the early prevention realized by means of generator rescheduling and smart excitation control can be considered. Another challenging topic is enhancement of the early prevention method to deal with other instability types apart from ASSAI. The crucial issue for the success of this task is derivation of the corresponding stability criteria which could be monitored in real-time, utilizing PMU data.

In this thesis synthetic PMU data were used for the analysis, thus data were complete and precise. However, in real power systems, PMU data can contain bad measurements or be incomplete. In order to make the early prevention method implementable in real power systems, special solutions to deal with bad data should be developed. As part of this task, the influence of measurement error on the effectiveness of the early prevention method should be stadied.

Considering the near real-time scope of the early prevention method, the activity focused on improving the computational efficiency of the suggested method and the proposition of better algorithmical solutions should be part of the future work.

REFERENCES

[1] O. P. Veloza, and R.H. Cespedes “Regulatory Mechanisms to Mitigate the Vulnerability of Power Systems to Blackouts”, Transmission & Distribution Conference and Exposition: Latin America, 2006. TDC '06. IEEE/PES, April 2007.

[2] R. Gutman, “Application of Line Loadability Concepts to Operating Studies”, IEEE Transactions on Power Systems, Vol. 3, No. 4, November 1988

[3] Savu Crivat Savulescu, “Real-time stability assessment in modern power system control centres”, Piscataway, NJ : IEEE Press [u.a.], 2009.

[4] H.K. Temraz, M.M.A. Salama, A.Y. Chikhani, “Review of electric load forecasting methods”, Canadian Conference on Electrical and Computer Engineering, Engineering Innovation: Voyage of Discovery. IEEE, 1997

[5] Y. Chakhchoukh, P. Panciatici and L. Mili, “Electric Load Forecasting Based on Statistical Robust Methods”, ”, IEEE Transactions on Power Systems, Vol. 26, No. 3, August 2011

[6] P. R. J. Campbell, and K. Adamson, “Methodologies for Load Forecasting”,3rd International IEEE Conference Intelligent Systems, pp. 800-806, London, September, 2006

[7] D. S. Callaway, I. A. Hiskens, “Achieving Controllability of Electric Load”, Proceedings of the IEEEP, Vol. 99, No. 1, January 2011

[8] V.H.M. Quezada, J.R. Abbbad and T.G.S. Roman, “Assessment of Energy Distribution Losses for Increasing Penetration of Distributed Generatio”, IEEE Transactions on Power Systems, VOL. 21, NO. 2, May, 2006

[9] E. Lannoye, D. Flynn, M. O’Malley, “The Role of Power System Flexibility in Generation Planning”, Power and Energy Society General Meeting, 2011 IEEE

[10] R. Karki, “Wind Power in Power Generation Planning”, Canadian Conference on Electrical and Computer Engineering, VOL. 3, pp. 1511-1514, 2004

[11] Z. Styczynski et al.,“Electric Energy Storage Systems”, Working Group C6.15, Cigre, April 2011

[12] A. G. Phadke, J. S. Thorp, and M. G. A. Adamiak, “New measurement technique for tracking voltage phasors, local system frequency, and rate of change of frequency,” IEEE Trans. Power App. Syst., vol. PAS-102, no. 5, pp. 1025–1038, May 1983.

[13] W. Sattinger,”Application of PMU Measurements in Europe TSO Approach and Experienc”, Trondheim PowerTech, 2011.

[14] B. Singh, N.K. Sharma, A.N. Tiwari, K.S. Verma and S.N. Singh,”Applications of phasor measurement units (PMUs) in electric power system networks incorporated with FACTS controller”, International Journal of Engineering, Science and Technology , Vol. 3, No. 3, pp. 64-82, 2011

[15] K. Uhlen, D. Cirio,”IEA Implementing Agreement on Electricity Networks Analysis, Research&Development (ENARD)”, Sintef Energy Research, 2012

[16] A.G. Phadke, J. S. Thorp and M.G. Adamiac, “A New Measurement Technique for Tracking Voltage Phasors, Local System Frequency, and Rate of Change of Frequency ”, ” IEEE Trans. on Power Apparatus and Systems, vol. PAS-102, pp. 1025-1038, May 1983

[17] A.G. Phadke, B. Kasztenny, “Synchronized Phasor and Frequency Measurement Under Transient Conditions ”, IEEE Transactions on Power Delivery, VOL. 24, NO. 1, pp. 89-95, January, 2009

[18] P. Kundur, G. Anderson “Definition and Classification of Power System Stability”, IEEE Trans., vol. 19, NO. 2, pp. 1387–1401, May 2004.

[19] P.Kundur, “Power System Stability and Control”, The EPRI Power System Engineering Series, 1993

[20] Y. Yu, “Electric Power Systems Dynamics”, Academic Press, 1983

[21] T.Van Cutsem “Voltage Instability: Phenomenon, Countermeasures and Analysis Methods”, Proc IEEE, vol. 88, pp. 208-227, 2000

[22] C. O. Heyde “Dynamic Voltage Stability Assessment for On-Line Control Room Application”, Magdeburg University, 2010

[23] C. Rehtanz, J. Bertsch,” Wide Area Measurement and Protection System for Emergency Voltage Stability”, Power Engineering Society Winter Meeting, 842-847 vol.2, 2002.

[24] Hjortur Jóhannsson “Development of Early Warning Methods for Electric Power Systems”, PhD thesis, Denmark University of Technology, 2010

[25] P. W. Oman, J. Robert, “Barriers to a Wide-Area Trusted Network Early Warning SystemFor Electric Power Disturbances”, Proceedings of the 35th Hawaii International Conference on System Sciences, 2002

[26] G. Gross, A. Bose,C. DeMarco, M. Pai, J. Thorp and P. Varaiya, “Grid of the Future White Paper on Real Time Security Monitoring and Control of Power System” , Consortium for Electric Reliability Technology Solution, PSERC, December 1999

[27] R. Hoffmann, F. Promel, F. Capitanescu, G. Krost, and L. Wehenkel,” Situation Adapted Display of Information for Operating Very Large Interconnected Grid”, PowerTech, 2011 IEEE Trondheim

[28] R.T. Guttromson, F.L. Greitzer, M.L. Paget, A. Schur, “Human Factors for Situation Assessment in Power Grid Operation”, PNNL-16780, August 2007

[29] A.A. Fouad and V.Vittal, “The transient energy function method” , International Journal of Electrical Power & Energy Systems, vol.10, iss. 4, pp. 233-246, October,1988

[30] M.A. Pai, “Energy Function Analysis for Power System Stability”, Boston, Kluwer Academic, Publishers,1989

[31] Y.Chen, K. Zhou, “A New Energy Function Based Power System Stability Control Scheme Using Real-time data”, Power System Technology, 2000. Proceedings. PowerCon 2000. International Conference on Power System Technology, vol.1, pp.163-168, December 2000

[32] S. E. Stanton, C. Slivinsky, K. Martin, and J. Nordstrom, “Application of phasor measurements and partial energy analysis in stabilizing large disturbances,” IEEE Trans. Power Syst., vol. 10, pp. 297–306, Feb. 1995

[33] J.H. Chow, A. Chakrabortty, M. Arcak, B. Bhargava and A. Salazar,”

Synchronized Phasor Data Based Energy Function Analysis of Dominant Power Transfer Paths in Large Power System”, IEEE Trans. Power Syst., vol. 22, pp. 727–734, May, 2007

[34] Y. Yare, G.K. Venayagamoorth,” Real-Time Transient Stability Assessment of a Power System during Energy Generation Shortfall”, IEEE 978-1-4244-6266-7/10, 2010

[35] Y. Xue, T.V. Cutsem, M. Ribbens-Pavella, “Extended Equal Area Criterion: Jastifications, Generaizations, Applications”, IEEE Trans. Power Syst., vol. 4, pp. 44–52, February, 1989

[36] Y. Xue, L. Wehenkel, R. Belhomme, P. Rousseaux, M. Pavella, E. Euxibie,.B. Heilbronn and J.F. Lesigne, “Extended equal area criterion revisit-

ed [EHV power systems]", IEEE Trans. Power Syst., vol. 7, pp. 1012-1022, August, 1992

[37] Z. Qinyong, T. Fang, W. Zhongxi," A method to Speed up Transient Stability Assessment", ICEE conference, 2003

[38] D. J. Sobajic and Y.-H. Pao, "Artificial neural-net based dynamic security assessment for electric power systems," IEEE Power Eng. Rev., vol. 9, no. 1, p. 55, Feb. 1989

[39] L. Wehenkel, M. Pavella, E. Euxibie, and B. Heilbronn, "Decision tree based transient stability method a case study," IEEE Trans. Power Syst., vol. 9, no. 1, pp. 459–469, Feb. 1994

[40] S. Rovnyak, S. Kretsinger, J. Thorp, and D. Brown, "Decision trees for real-time transient stability prediction" IEEE Trans. Power Syst., vol. 9, no. 3, pp. 1417–1426, Aug. 1994

[41] L. Wehenkel, T. van Cutsem, and M. Ribbens-Pavella, "An artificial intelligence framework for on-line transient stability assessment of power systems," IEEE Power Eng. Rev., vol. 9, no. 5, pp. 77–78, May 1989.

[42] A. E. Gavoyiannis, D. G. Vogiatzis, D. R. Georgiadis, and N. D. Hatziargyriou, "Combined support vector classifiers using fuzzy clustering for dynamic security assessment," in Proc. IEEE Power Eng. Soc. Summer Meeting, 2001, vol. 2, pp. 1281–1286.

[43] L. S. Moulin, A. P. da Silva, M. A. El-Sharkawi, and R. J. Marks, II, "Support vector machines for transient stability analysis of large-scale power systems," IEEE Trans. Power Syst., vol. 19, no. 2, pp. 818–825,May 2000

[44] F. R. Gomez, A. D. Rajapakse, U. D. Annakkage, and I. T. Fernando, "Support Vector Machine-Based Algorithm for Post-Fault Transient Stability Status Prediction Using Synchronized Measurement", IEEE Trans. Power Syst., vol. 26, no. 3, pp. 1474–1483, Aug. 2011

[45] L. Wang, A. Semlyen, "Application of Sparse Eigenvalue Techniques to the Small Signal Stability Analysis of Large Power Systems",0885-8950/90/0500-0635, 1990 IEEE

[46] J. Dagle, "Grid Oscillations. Limiting your Power", CEC/CIEE Review Meeting Sacramento, California, October, 2010

[47] Psymetrix Limited, official web-site available online http://www.psymetrix.com/hot-topics/oscillatory-stability.html

[48] K. Yamashita, et.al., "Development of Step-out prediction through Oscillation Mode Detection based on Time Series Analysis", CRIEPI Report T00026 (in Japanese), 2001

[49] K. Yamashita, et. al., "Experimental Verification of Real-time Oscillatory Stability Assessment in CRIEPI's Power System Simulator –Developme, 2005

[50] Central Research Institute of Electric Power Industry, Japan, "Experimental Verification of Real-time Oscillatory Instability Prediction Scheme in CRIEPI's Power System Simulator －Development of Oscillatory Instability Prediction System for Multi-machine Syste", 2006 available online http://criepi.denken.or.jp/en/publications/annual/2006/036.pdf

[51] H. Ghasemi and C. Caizares, "On-line Damping Torque Estimation and Oscillatory Stability Margin Prediction", IEEE Trans. Power Syst., vol. 22, no. 2, pp. 667–674, May. 2007

[52] S.P. Teeuwsen, "Oscilattory Stability Assesment of Power Systems using Computational Intelligence", Doktors der Ingenieurwissenschaften Dissertation, University of Duisburg-Essen, March, 2005

[53] S.P. Teeuwsen, I. Erlich, M.A. El-Sharkawi, "Decision tree based oscillatory stability assessment for large interconnected power systems", Power Systems Conference and Exposition, 2004, IEEE PES

[54] Y.V. Makarov, V.I. Reshetov, "Blackouts in North America and Europe: Analysis and Generalization", Power Tech, 2005 IEEE Russia, pp. 1-7, 2005

[55] T.Van Cutsem ,"Voltage Instability: Phenomenon, Countermeasures and Analysis Methods", Proc IEEE, vol. 88, pp. 208-227, 2000

[56] L. Chao, Y. Rongxiang "Analysis of Mechanisms of Mid and Longer Term Voltage Instability", International Conference on Power System Technology, 2006

[57] N. Yorino, H. Sasaki, Y. Masuda, Y. Tamura, M. Kitagawa and A. Oshimo, "On voltage stability from the viewpoint of singular perturbation theory", International Journal of Electrical Power & Energy Systems, vol. 16, no. 6, pp. 409–417, Dec.1994

[58] J.H. Eto, M. Parashar, A. Agarwal, Y. Makarov, I. Dobson, "Real time system operation, 2006-2007. Real-time Voltage Security assessment. Report on Algorithms and Framework", Lawrence Berkeley National Laboratory, CERTS, 2008

[59] Y.N.N. Tchokonte "Real-time identification and monitoring of the voltage stability margin in electric power transmission systems using synchronized phasor measurements", University of Kassel, 2009

[60] M. Glavic, T. Van Cutsem "Wide-Area Detection of Voltage Instability from Synchronized Phasor Measurements. Part I: Principle", IEEE Transactions on Power Systems, VOL. 24, NO. 3, pp. 1408-1416, August 2009

[61] M. Glavic, T. Van Cutsem “Wide-Area Detection of Voltage Instability from Synchronized Phasor Measurements. Part II: Simulation results”, IEEE Transactions on Power Systems, VOL. 24, NO. 3, pp. 1417-1425, August 2009

[62] Savu C. Savulescu, “Real-Time Stability in Power Systems: Techniques for Early Detection of the Risk of Blackout (Power Electronics and Power Systems)”, Springer, 2006

[63] Y. Mansour, “Dynamic Security Contengency Screening and Ranking Using Neural Networks”, IEEE Transaction on Neural Networks, VOL. 8, NO. 4, pp. 942-950 , July 1997

[64] S. Repo, “On-line Voltage Stability Assessment of Power Systems- An Approach of Black-Box Modeling ”, Tampere University of Technology, 2001

[65] R. Diao, “Decision Tree-Based” Online Voltage Security Assessment Using PMU Measurements”, IEEE Transactions on Power Systems, VOL. 24, NO. 2, May 2009

[66] C. O. Heyde “Dynamic Voltage Stability Assessment for On-Line Control Room Application”, Magdeburg University, 2010

[67] S. Matsushita, K. Yukita, Y. Goto , K.Ichiyanagi, H. Aoki and Y. Mizutani, “Automatic Generation Control using GA considering Distributed Generation”, Transmission and Distribution Conference and Exhibition 2002: Asia Pacific. IEEE/PES

[68] G.K. Joshi, “Automatic Generation Control of Power using Genetic Algorithm”, Computer Research and Development, Second International Conference, 2010

[69] M. Zima, “Special Protection Schemes in Electric Power Systems .Literature survey”, Swiss Federal Institute of Technology , Zurich, June 2002

[70] RAO EES official edition, “Instructions for prevention and liquidation of abnormal operational conditions of Power Systems”, (in Russian), 2008

[71] G. Trudel, S. Bernard, G. Scott: “Hydro-Québec’s defence plan against

extreme contingencies”, IEEE Transactions on Power Systems, Vol. 14, No. 3, August 1999

[72] M. Larsson, C. Rehtanz,” Predictive Frequency Stability Control based on Wide-area Phasor Measurements”, Power Engineering Society Summer Meeting, 2002 IEEE

[73] V.A. Venikov, V.A. Stroev, V.I. Idelchik and V.I. Tarasov, “Estimation of Electrical Power System Steady-State Stability in load flow calculations”, IEEE Transactions on Power Systems, VOL. 94, NO. 3, pp. 1034-1041, 1975

[74] A. Mohamed, “Performance comparisons of AC load-flow techniques for real time applications”, Generation, Transmission and Distribution, IEE Proceedings C, 1991

[75] E. Abu-Al-Feilat, M. Bettayeb, H. Al-Duwaish, M. Abido, A. Mantawy, “A neural network-based approach for on-line dynamic stability assessment using synchronizing and damping torque coefficient”, Electric Powr Systems Research, No39, pp. 103-110, 1996

[76] K. Warwick, A. Ekwue and R. Aggarwal, “Artificial intelligence techniques in power systems”, IEE Power Engineering Series 22, 1988

[77] Y. Yuan, P. Ju, Q. Li, Y. Wang, H. Hu and H. Sasaki, “A Real-time Monitoring Method for Power System Steady State Angle Stability Based on WAM”, The 7th International Power Engineering Conference, VOL. 2, pp. 761-764, 2005

[78] “Control System. Basic Principles”, Encyclopedia Brittanica Inc.,2013, http://www.britannica.com/EBchecked/topic/135480/control-system/1512/Basic-principles

[79] “Automation. Modern Developments”, Encyclopedia Brittanica Inc.,2013, http://www.britannica.com/EBchecked/topic/5303/adaptive-control

[80] H. Jóhannsson, R. Garcia-Valle, J. T. G. Weckesser, A. H. Nielsen and J. Østergaard, “Real-Time stability assessment based on synchrophasors”, IEEE PES Trondheim PowerTech,2011

[81] H. Jóhannsson, J. Østergaard and A. H. Nielsen, “Identification of critical transmission limits in injection impedance plane”, Int J Electr Power Energ Syst, 2012, http://dx.doi.org/10.1016/j.ijepes.2012.05.050

[82] K. Moslehi, A.B. R. Kumar and P. Hirsch, ” Feasibility of a Self-Healing Grid – Part I Methodology and Cost Models”, IEEE PES General Meeting, Montreal, Que., 2006.

[83] L. A. Segel, M. Slemrods, “The Quasi-Steady-State Assumption: a Case Study in Perturbation”, Society for Industrial and Applied &Mathematics, Val. 31, No. 3, pp. 446-477, September, 1989

[84] H. W. Bode, “Network Analysis and Feedback Amplifier Design”, D. Van Nostrand Co., Inc., New York, N. Y.; 1915.

[85] E. Dmitrova, H. Jóhannsson and A.H. Nielsen, “Early prevention of instability - search for optimal grid nodes for applying countermeasures”, International Conference on Environment and Electrical Engineering EEEIC, 2012.

[86] E. Dmitrova, H. Jóhannsson and A.H. Nielsen, “Early Prevention of Instability-Use of Self Propagating Graph for the Fast Search for Optimal Grid Nodes to Apply Countermeasures”, PowerTech, Grenoble, 2013.

[87] R. Boylestad , L. Nashelsky, “Electronic Devices and Circuit Theory (9th edition)”, Prentice Hall, 2005

[88] Power System Test Archive, available online http://www.ee.washington.edu/research/pstca, Aug.1993.

[89] Single line diagram of IEEE 30 bus test system, available online http://een.iust.ac.ir/profs/jadid/SCPM.pdf

[90] D. E. Whitney, “Comparative study of Various Minimization Techniques Used in Mathematical Programming”, IEEE Transactions on Automatic Control, October 1969.

A
DETAILED DERIVATION OF THE FORMULA 6.25, 6.31

In this appendix the derivation of the elements of Jacobian matrix $\boldsymbol{J}=\frac{\boldsymbol{dP}}{\boldsymbol{d\delta}}$ is carried out:

$$P_{inj} = \frac{E_{th}\cdot V_0}{Z_{th}}\cos(\gamma+\phi_{th}) - \frac{V_0^{\,2}}{Z_{th}}\cdot\cos(\phi_{th})$$

$$\mathrm{J}_{ij}(\delta)=\frac{\mathrm{dP}_i(\delta)}{\mathrm{d}\delta_j};$$

$$\frac{\partial\left(\mathrm{P_i}\left(\delta\right)\right)}{\partial\delta_{\mathrm{j}}} = \frac{\partial\left(\mathrm{E}_{thi}\cdot\mathrm{V}_{0i}/\mathrm{Z}_{thi}\cdot cos(\delta_i-\theta_{thi}+\phi_{thi})\right)}{\partial\delta_j}$$

for i = j

$$\frac{\partial\left(\mathrm{P_i}\left(\delta\right)\right)}{\partial\delta_{\mathrm{i}}} = \frac{\mathrm{V}_{0i}}{\mathrm{Z}_{thi}}\cdot\left[\frac{\partial\left(\mathrm{E}_{thi}\right)}{\partial\delta_{\mathrm{i}}}\cdot cos(\delta_i-\theta_{thi}+\phi_{thi}) + \mathrm{E}_{thi}\cdot\frac{\partial\left(cos(\delta_i-\theta_{thi}+\phi_{thi})\right)}{\partial\delta_{\mathrm{i}}}\right] = -\frac{V_{0i}}{Z_{thi}}\cdot E_{thi}\cdot\sin(\delta_i-\theta_{thi}+\phi_{thi})$$

for i ≠ j

$$\frac{\partial\left(\mathrm{P_i}\left(\delta\right)\right)}{\partial\delta_{\mathrm{j}}} = \frac{\mathrm{V}_{0i}}{\mathrm{Z}_{thi}}\cdot\left[\frac{\partial\left(\mathrm{E}_{thi}\right)}{\partial\delta_{\mathrm{j}}}\cdot cos(\delta_i-\theta_{thi}+\phi_{thi}) + \mathrm{E}_{thi}\cdot\frac{\partial\left(cos(\delta_i-\theta_{thi}+\phi_{thi})\right)}{\partial\delta_{\mathrm{j}}}\right] \qquad \textbf{(A.1)}$$

$$\underline{\mathrm{E}}_{thi} = V_{01}\cdot k_{tr1i}\cdot\left[\cos\left(\delta_1+\alpha_{1i}\right)+j\cdot\sin\left(\delta_1+\alpha_{1i}\right)\right]+$$

$$+V_{02}\cdot k_{tr2i}\cdot\left[\cos\left(\delta_2+\alpha_{2i}\right)+j\cdot\sin\left(\delta_2+\alpha_{2i}\right)\right]+$$

$$\ldots+V_{0j}\cdot k_{trji}\cdot\left[\cos\left(\delta_j+\alpha_{ji}\right)+j\cdot\sin\left(\delta_j+\alpha_{ji}\right)\right]+$$

$$\ldots+V_{0N}\cdot k_{trNi}\cdot\left[\cos\left(\delta_N+\alpha_{Ni}\right)+j\cdot\sin\left(\delta_N+\alpha_{Ni}\right)\right]=$$

$$=\sum_{\substack{k=1\\k\neq i}}^{N}V_{0k}\cdot k_{trki}\cdot\left[\cos\left(\delta_k+\alpha_{ki}\right)+j\cdot\sin\left(\delta_k+\alpha_{ki}\right)\right]$$

$$\mathrm{Re}\left(\underline{\mathrm{E}}_{thi}\right)=\sum_{\substack{j=1\\ i\neq j}}^{N} V_{0j}\cdot k_{trji}\cdot\cos\left(\delta_j+\alpha_{ji}\right)$$

$$Im\left(\underline{\mathrm{E}}_{thi}\right)=\sum_{\substack{j=1\\ i\neq j}}^{N} V_{0j}\cdot k_{trji}\cdot\sin\left(\delta_j+\alpha_{ji}\right)$$

$$\frac{\partial E_{thi}}{\partial\delta_j}=\frac{\partial\sqrt{\mathrm{Re}\left(\underline{\mathrm{E}}_{thi}\right)^2+Im\left(\underline{\mathrm{E}}_{thi}\right)^2}}{\partial\delta_j}=\frac{1}{2\cdot\underbrace{\sqrt{\mathrm{Re}\left(\underline{\mathrm{E}}_{thi}\right)^2+Im\left(\underline{\mathrm{E}}_{thi}\right)^2}}_{\mathbf{E}_{thi}}}\cdot\left[\frac{\partial\left\{\mathrm{Re}\left(\underline{\mathrm{E}}_{thi}\right)^2\right\}}{\partial\delta_j}+\frac{\partial\left\{Im\left(\underline{\mathrm{E}}_{thi}\right)^2\right\}}{\partial\delta_j}\right] \quad \textbf{(A.2)}$$

$$\frac{\partial\left\{\mathrm{Re}\left(\underline{\mathrm{E}}_{thi}\right)^2\right\}}{\partial\delta_j}=2\cdot\mathrm{Re}\left(\underline{\mathrm{E}}_{thi}\right)\cdot\frac{\partial\left\{\mathrm{Re}\left(\underline{\mathrm{E}}_{thi}\right)\right\}}{\partial\delta_j}=2\cdot\mathrm{Re}\left(\underline{\mathrm{E}}_{thi}\right)\cdot V_{0j}\cdot k_{trji}\cdot(-1)\cdot\sin\left(\delta_j+\alpha_{ji}\right) \quad \textbf{(A.3)}$$

$$\frac{\partial\left\{Im\left(\underline{\mathrm{E}}_{thi}\right)^2\right\}}{\partial\delta_j}=2\cdot Im\left(\underline{\mathrm{E}}_{thi}\right)\cdot\frac{\partial\left\{Im\left(\underline{\mathrm{E}}_{thi}\right)\right\}}{\partial\delta_j}=2\cdot Im\left(\underline{\mathrm{E}}_{thi}\right)\cdot V_{0j}\cdot k_{trji}\cdot\cos\left(\delta_j+\alpha_{ji}\right) \quad \textbf{(A.4)}$$

Substituting (A.3) and (A.4) into (A.2) we obtain:

$$\frac{\partial\left(\mathrm{E}_{thi}\right)}{\partial\delta_{\mathrm{j}}}=\frac{\mathrm{V}_{0j}\cdot k_{0trij}}{\mathrm{E}_{thi}}\cdot\left[\mathrm{Im}(\underline{\mathrm{E}}_{thi})\cdot\cos(\delta_j+\alpha_{ji})-\mathrm{Re}(\underline{\mathrm{E}}_{thi})\cdot\sin(\delta_j+\alpha_{ji})\right] \quad \textbf{(A.5)}$$

$$\frac{\partial\cos\left(\delta_i-\theta_{thi}+\phi_{thi}\right)}{\partial\delta_j}=-\sin(\delta_i-\theta_{thi}+\phi_{thi})\cdot(-1)\cdot\frac{\partial\theta_{thi}}{\partial\delta_j}=\sin(\delta_i-\theta_{thi}+\phi_{thi})\cdot\frac{\partial\theta_{thi}}{\partial\delta_j} \quad \textbf{(A.6)}$$

$$\theta_{thi}=\arccos\frac{\mathrm{Re}\left(\underline{E}_{thi}\right)}{E_{thi}}$$

$$\frac{\partial \theta_{thi}}{\partial \delta_j} = \frac{\partial \left\{ \arccos \frac{\mathrm{Re}\left(\underline{E}_{thi}\right)}{E_{thi}} \right\}}{\partial \delta_j} = \frac{-1}{\sqrt{1-\left(\frac{\mathrm{Re}\left(\underline{E}_{thi}\right)}{E_{thi}}\right)^2}} \cdot \frac{\partial \frac{\mathrm{Re}\left(\underline{E}_{thi}\right)}{E_{thi}}}{\partial \delta_j} =$$

$$= \frac{E_{thi}}{Im\left(\underline{E}_{thi}\right)} \cdot \left[\frac{\frac{\partial \mathrm{Re}\left(\underline{E}_{thi}\right)}{\partial \delta_j} \cdot E_{thi} - \frac{\partial E_{thi}}{\partial \delta_j} \cdot \mathrm{Re}\left(\underline{E}_{thi}\right)}{{E_{thi}}^2} \right] = \frac{\frac{\partial \mathrm{Re}\left(\underline{E}_{thi}\right)}{\partial \delta_j}}{Im\left(\underline{E}_{thi}\right)} - \frac{\mathrm{Re}\left(\underline{E}_{thi}\right) \cdot \frac{\partial E_{thi}}{\partial \delta_j}}{Im\left(\underline{E}_{thi}\right) \cdot E_{thi}} = \qquad \textbf{(A.7)}$$

$$= \frac{V_{0j} \cdot k_{trji} \cdot (-1) \cdot \sin\left(\delta_j + \alpha_{ji}\right)}{Im\left(\underline{E}_{thi}\right)} - \frac{\mathrm{Re}\left(\underline{E}_{thi}\right) \cdot \frac{V_{0j} \cdot k_{trji}}{E_{thi}}}{Im\left(\underline{E}_{thi}\right) \cdot E_{thi}} \cdot$$

$$\cdot \left[Im\left(\underline{E}_{thi}\right) \cdot \cos\left(\delta_j + \alpha_{ji}\right) - \mathrm{Re}\left(\underline{E}_{thi}\right) \cdot \sin\left(\delta_j + \alpha_{ji}\right) \right] = \frac{V_{0j} \cdot k_{trji}}{Im\left(\underline{E}_{thi}\right)} \cdot \left[-\sin\left(\delta_j + \alpha_{ji}\right) - \right.$$

$$\left. - \frac{\mathrm{Re}\left(\underline{E}_{thi}\right) \cdot Im\left(\underline{E}_{thi}\right) \cdot \cos\left(\delta_j + \alpha_{ji}\right)}{{E_{thi}}^2} + \frac{\mathrm{Re}\left(\underline{E}_{thi}\right)^2 \cdot \sin\left(\delta_j + \alpha_{ji}\right)}{{E_{thi}}^2} \right]$$

Substituting (A.7) into (A.6) we obtain:

(A.8)

$$\frac{\partial \cos\left(\delta_i - \theta_{thi} + \phi_{thi}\right)}{\partial \delta_j} = \sin(\delta_i - \theta_{thi} + \phi_{thi}) \cdot \frac{V_{0j} \cdot k_{trji}}{Im\left(\underline{E}_{thi}\right)} \cdot \left[-\sin\left(\delta_j + \alpha_{ji}\right) - \right.$$

$$\left. - \frac{\mathrm{Re}\left(\underline{E}_{thi}\right) \cdot Im\left(\underline{E}_{thi}\right) \cdot \cos\left(\delta_j + \alpha_{ji}\right)}{{E_{thi}}^2} + \frac{\mathrm{Re}\left(\underline{E}_{thi}\right)^2 \cdot \sin\left(\delta_j + \alpha_{ji}\right)}{{E_{thi}}^2} \right]$$

Substituting (A.4) and (A.7) into (*) we obtain:

$$\frac{dP_i(\delta)}{d\delta_j} = \frac{V_{0i}}{Z_{thi}} \cdot \left(\begin{array}{l} \frac{V_{0j} \cdot k_{trji}}{E_{thi}} \cdot \left[Im\left(\underline{E}_{thi}\right) \cdot \cos\left(\delta_j + \alpha_{ji}\right) - \mathrm{Re}\left(\underline{E}_{thi}\right) \cdot \sin\left(\delta_j + \alpha_{ji}\right) \right] \cdot \cos\left(\delta_i - \theta_{thi} + \phi_{thi}\right) + \\ + \sin(\delta_i - \theta_{thi} + \phi_{thi}) \cdot \frac{V_{0j} \cdot k_{trji}}{Im\left(\underline{E}_{thi}\right)} \cdot \left[-\sin\left(\delta_j + \alpha_{ji}\right) - \right. \\ \left. - \frac{\mathrm{Re}\left(\underline{E}_{thi}\right) \cdot Im\left(\underline{E}_{thi}\right) \cdot \cos\left(\delta_j + \alpha_{ji}\right)}{{E_{thi}}^2} + \frac{\mathrm{Re}\left(\underline{E}_{thi}\right)^2 \cdot \sin\left(\delta_j + \alpha_{ji}\right)}{{E_{thi}}^2} \right] \cdot E_{thi} \end{array} \right) =$$

$$= \frac{V_{0i}}{Z_{thi}} \cdot \frac{V_{0j} \cdot k_{trji}}{E_{thi}} \cdot \begin{pmatrix} \left[Im\left(\underline{E}_{thi}\right) \cdot \cos\left(\delta_j + \alpha_{ji}\right) - \mathrm{Re}\left(\underline{E}_{thi}\right) \cdot \sin\left(\delta_j + \alpha_{ji}\right) \right] \cdot \cos\left(\delta_i - \theta_{thi} + \phi_{thi}\right) + \\ + \sin(\delta_i - \theta_{thi} + \phi_{thi}) \cdot \left[-\sin\left(\delta_j + \alpha_{ji}\right) \cdot \frac{E_{thi}{}^2}{Im\left(\underline{E}_{thi}\right)} - \right. \\ \left. - \frac{\mathrm{Re}\left(\underline{E}_{thi}\right) \cdot Im\left(\underline{E}_{thi}\right) \cdot \cos\left(\delta_j + \alpha_{ji}\right)}{Im\left(\underline{E}_{thi}\right)} + \frac{\mathrm{Re}\left(\underline{E}_{thi}\right)^2 \cdot \sin\left(\delta_j + \alpha_{ji}\right)}{Im\left(\underline{E}_{thi}\right)} \right] \end{pmatrix} =$$

$$= \frac{V_{0i}}{Z_{thi}} \cdot \frac{V_{0j} \cdot k_{trji}}{E_{thi}} \cdot \begin{pmatrix} Im\left(\underline{E}_{thi}\right) \cdot \cos\left(\delta_j + \alpha_{ji}\right) \cdot \cos\left(\delta_i - \theta_{thi} + \phi_{thi}\right) - \\ - \mathrm{Re}\left(\underline{E}_{thi}\right) \cdot \sin(\delta_i - \theta_{thi} + \phi_{thi} + \delta_j + \alpha_{ji}) + \\ + \sin(\delta_i - \theta_{thi} + \phi_{thi}) \cdot \left[-\sin\left(\delta_j + \alpha_{ji}\right) \cdot \frac{E_{thi}{}^2}{Im\left(\underline{E}_{thi}\right)} + \frac{\mathrm{Re}\left(\underline{E}_{thi}\right)^2 \cdot \sin\left(\delta_j + \alpha_{ji}\right)}{Im\left(\underline{E}_{thi}\right)} \right] \end{pmatrix} =$$

$$= \frac{V_{0i}}{Z_{thi}} \cdot \frac{V_{0j} \cdot k_{trji}}{E_{thi}} \cdot \begin{pmatrix} Im\left(\underline{E}_{thi}\right) \cdot \cos\left(\delta_j + \alpha_{ji}\right) \cdot \cos\left(\delta_i - \theta_{thi} + \phi_{thi}\right) - \\ - \mathrm{Re}\left(\underline{E}_{thi}\right) \cdot \sin(\delta_i - \theta_{thi} + \phi_{thi} + \delta_j + \alpha_{ji}) + \\ + \sin(\delta_i - \theta_{thi} + \phi_{thi}) \cdot \left[\sin\left(\delta_j + \alpha_{ji}\right) \cdot \left(\frac{\mathrm{Re}\left(\underline{E}_{thi}\right)^2}{Im\left(\underline{E}_{thi}\right)} - \frac{E_{thi}{}^2}{Im\left(\underline{E}_{thi}\right)} \right) \right] \end{pmatrix} =$$

$$\frac{V_{0i}}{Z_{thi}} \cdot \frac{V_{0j} \cdot k_{trji}}{E_{thi}} \cdot \begin{pmatrix} Im\left(\underline{E}_{thi}\right) \cdot \cos\left(\delta_j + \alpha_{ji}\right) \cdot \cos\left(\delta_i - \theta_{thi} + \phi_{thi}\right) - \\ - \mathrm{Re}\left(\underline{E}_{thi}\right) \cdot \sin(\delta_i - \theta_{thi} + \phi_{thi} + \delta_j + \alpha_{ji}) + \\ + \sin(\delta_i - \theta_{thi} + \phi_{thi}) \cdot \sin\left(\delta_j + \alpha_{ji}\right) \cdot \left(-Im\left(\underline{E}_{thi}\right)\right) \end{pmatrix} =$$

$$= \frac{V_{0i}}{Z_{thi}} \cdot \frac{V_{0j} \cdot k_{trji}}{E_{thi}} \cdot \left(Im\left(\underline{E}_{thi}\right) \cdot \cos(\delta_i - \theta_{thi} + \phi_{thi} + \delta_j + \alpha_{ji}) - \mathrm{Re}\left(\underline{E}_{thi}\right) \cdot \sin(\delta_i - \theta_{thi} + \phi_{thi} + \delta_j + \alpha_{ji}) \right)$$

B
FAST ASSESSMENT OF THE EFFECT OF PREVENTIVE WIDE AREA EMERGENCY CONTROL

This paper was published in the proceedings of the 4th European Innovative Smart Grid Technologies (ISGT) Conference, October 2013, Copenhagen

Fast Assessment of the Effect of Preventive Wide Area Emergency Control

Evgenia Dmitrova, Hjörtur Jóhannsson and Arne Hejde Nielsen
Elektro, Technical University of Denmark
Center for Electric Power and Energy
Kgs. Lyngby, Denmark
ed@elektro.dtu.dk, hj@elektro.dtu.dk, ahn@elektro.dtu.dk

***Abstract*—This paper describes an approach to quick assessment of the effect that a suggested countermeasure would have on the system generators stability margins in respect to aperiodic rotor angle small signal stability. The approach ensures that computational demanding simulations can be avoided to determine whether the suggested counteraction is sufficient to avoid system instability during severely critical operating conditions. The fast assessment of the effect that a countermeasure has on system stability provides an important decision support for the control room personnel in emergency situations. The validity of the suggested approach is proved on the 8 bus test system and IEEE30 bus test system.**

***Index Terms*- adaptive control; Newton method; Phasor measurement units; power systems; stability;**

I. INTRODUCTION

Research and development of applications for the real-time monitoring and control became a popular topic for the last decade aligned with increased integration of wide area measurement systems (WAMS) throughout the world [1]. Methods providing early warning through real-time assessment of system stability have been introduced [2-4]. Approaches, enabling early warning for an emerging stability problems motivated development of the method capable of fast identification of appropriate countermeasures leading to instability prevention. The assessment of the impact that individual voltage source in the grid has on a given generators stability has been considered in [5]. This paper presents an approach for the fast assessment of the effect which a given preventive countermeasure would have on the generators aperiodic small signal rotor angle stability (ASSAS).

II. PREDICTING THE EFFECT OF A SUGGESTED COUNTERMEASURE AND ASSESSMENT OF ITS EFFICIENCY

The methodology for the assessment of the sufficiency of the suggested countermeasure is covered in this section. The countermeasures considered are expressed in terms of nodal admittance variation as suggested in [5]. The effect of a countermeasure is assessed in terms of active power margin to the boundary of ASSAS, which was derived in [4] (1):

$$P_{inj} = \frac{E_{th} \cdot V_0}{Z_{th}} \cos(\gamma + \phi_{th}) - \frac{V_0^2}{Z_{th}} \cdot \cos(\phi_{th}) ,$$

$$\therefore \quad P_{inj,\max} = -\frac{E_{th} \cdot V_0}{Z_{th}} - \frac{V_0^2}{Z_{th}} \cdot \cos(\phi_{th}) , \tag{1}$$

$$\%\Delta P_{inj} = \frac{P_{inj,\max} - P_{inj}}{P_{inj,\max}} \cdot 100\%$$

The derivations were made for two bus system representation where one bus is representing a given generator and the rest of the system is reduced to Thevenin equivalent. E_{th} and Z_{th} stand for magnitudes of Thevenin voltage and impedance respectively, ϕ_{th} is the angle of the Thevenin impedance and V_0 corresponds to the steady state constant voltage magnitude at the generator's node of injection. γ is the angle between $\underline{V}_0$ and $\underline{E}_{th}$, P_{inj} is the power injected into the point of steady state constant voltage magnitude and is equal to generated power with opposite sign. When the ASSAS boundary is crossed the active power margin equals to zero, thus maintaining certain active power margin can help to ensure that all generators are operating on the sufficient distance to the stability boundary. In order to keep active power margin on the certain level it is vital to develop an approach for fast prediction of the resulting active power margin when applying certain changes in the grid. To be able to predict what would be the resulting active power margin, it is necessary to define what would be the value of the parameters which affect this margin. The method for calculation of $\underline{Z}_{th}$ is described in [3]. Thus the focus of this paper will be placed on the identification of the $\underline{V}_0$ and $\underline{E}_{th}$ corresponding to the suggested change in the system admittance matrix. The linkage between $\underline{E}_{th}$ and voltage sources in the reduced grid was considered in [5]. It was shown that knowing the value of voltage at the points of constant steady state voltage magnitude $\underline{V}_{0i}$ for all voltage sources in the reduced grid the equivalent Thevenin voltage can be obtained by multiplying the vector of voltages with **GTC** (grid transformation coefficient) matrix. The elements of **GTC** depend only on system admittance matrix, and can be calculated for any given variation in admittance matrix:

$$\begin{pmatrix} \underline{E}_{th\,1} \\ \underline{E}_{th\,2} \\ \cdots \\ \underline{E}_{th\,i} \\ \cdots \\ \underline{E}_{th\,N} \end{pmatrix} = (\mathbf{GTC}) \cdot \begin{pmatrix} \underline{V}_{01} \\ \underline{V}_{02} \\ \cdots \\ \underline{V}_{0i} \\ \cdots \\ \underline{V}_{0N} \end{pmatrix}; \quad \mathrm{GTC}_{i,j} = k_{trij} \cdot e^{j\alpha_{ij}} \qquad (2)$$

Considering (1) and (2) one can notice that the remaining unknown variable for the estimation of the effect gained due to suggested countermeasure is $\underline{V}_{0i}$ (voltage at the point of constant steady state voltage magnitude). As the magnitude V_{0i} for the new steady stay will stay the same considering that excitation voltage and mechanical torque is constant, the focus is placed on the identification of the rotor angles corresponding to the new steady state. The purpose is to establish the method which is capable to assess the existence of the new steady state and the value of active power margin corresponding to the new operational conditions within a limited time. Conventional EMT analysis and power flow calculations might be not sufficiently fast. Especially for the case when system is approaching stability boundary after experiencing a disturbance and preventive countermeasure is required urgently in order to prevent instability emergence. The method described below reduces the computational burden comparing to conventional power flow and EMT simulations, allowing fast assessment. To illustrate the discourse the P-δ characteristic would be utilized (Fig. 1):

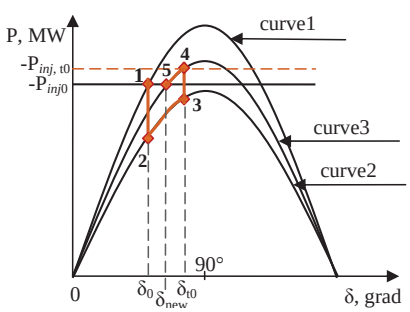

Figure 1. Simplified trajectories of the rotor angle δ over P-δ curves when initial steady state is afflicted by disturbance followed by countermeasure application.

Where: point 1-initial Steady state operational point, point 2-operational point immediately after disturbance, point 3-operational point in which decision about countermeasure application is taken, point 4-operational point immediately after application of countermeasure, point 5-Final equilibrium operational point corresponding to new steady state. P-δ curves are corresponding respectively to: 1-initial steady state operational conditions, 2-postdisturbance quasi-steady operation (system gradually is approaching ASSAS boundaries), 3-postcountermeasure new steady state operation.

In order to define if applied countermeasure would have sufficient impact preventing instability the dynamics of δ over P-δ curves corresponding to a given generator from point 3 to point 5 (Fig. 1) should be predicted for each generator in the grid. For the current study the assumption is made that the time slot between decision about countermeasure application and actual execution of it can be neglected, thus at the moment $t=t_0$ which corresponds to the point 3 the last actual measurements from PMU can be received, basing on this measurements the further dynamics of δ is to be predicted for the suggested countermeasure, which is expressed as variation of nodal admittance. At a moment t=t0 the countermeasure is applied, which changes the admittance matrix and transition to the new P-δ characteristic happens (curve 3). The trajectory of this process is described by section 3-4. As the change in rotor angles doesn't appear in step due to inertia it will stay the same immediately after countermeasure application $\delta_{i,t=t0+} = \delta_{i,t=t0-}$. Due to this immediate response to the applied variation in terms of injected power $P_{inj,t=t0+}$ can be defined according to (1) and (2), where the values of $\underline{V}_{0i}$ are assumed to be the same as in the latest measurements obtained from PMU corresponding to point 3, and the value of $\underline{Z}_{th}$ and **GTC** are updated accordingly to the suggested admittance variation.

$$P_{inj_{t=t_0+}} = \frac{E_{th\,t=t_0+} \cdot V_0}{Z_{th\,t=t_0+}} \cos(\gamma_{t=t_0+} + \phi_{th\,t=t_0+}) - \frac{V_0^{\,2}}{Z_{th\,t=t_0+}} \cdot \cos(\phi_{th\,t=t_0+}) =$$
$$= \frac{E_{th\,t=t_0+} \cdot V_0}{Z_{th\,t=t_0+}} \cos(\delta_{t=t_0-} - \theta_{th\,t=t_0+} + \phi_{th\,t=t_0+}) - \frac{V_0^{\,2}}{Z_{th\,t=t_0+}} \cdot \cos(\phi_{th\,t=t_0+}) \qquad (3)$$

Where $\theta_{t=t_0+}$ is the angle of corresponding Thevenin voltage.

Further trajectory of δ would be lying over the same P-δ, and would move towards equilibrium point. In order to define the first approximation for the rotor angle at point 5 another assumption is utilized- the magnitude of the Thevenin voltage is assumed to be the same as for the operational conditions corresponding to the point 4. Thus considering that active power output for generator at the new steady state operation should not change (reflecting the case of not available generators rescheduling) power injection for the new steady state is known and would be equal to the one at the initial steady state (point 1). Besides, one can notice that the second term in (3) would remain the same for the immediate post-contingency state and new steady state; furthermore it can be pre-calculated for suggested admittance matrix variation in advance. Thus first approximation of δ corresponding to new steady state can be found as it shown in (4):

$$\delta = \arccos\left[\left(\frac{E_{th\,t=t_0+} \cdot V_0}{Z_{th\,t=t_0+}} \cos(\gamma_{t=t_0+} + \phi_{th\,t=t_0+}) - P_{inj_{t=t_0+}} + P_{inj_0}\right) \frac{Z_{th\,t=t_0+}}{E_{th\,t=t_0+} \cdot V_0}\right] +$$
$$+ \theta_{th\,t=t_0+} - \phi_{th\,t=t_0+} \qquad (4)$$

This expression can be rewritten in matrix form for number of generators:

$$[\boldsymbol{\delta}] = \begin{pmatrix} \delta_1 \\ \cdots \\ \delta_i \\ \delta_N \end{pmatrix} \qquad (5)$$

When the first approximation for the rotor angles is obtained the value of the Thevenin voltage can be recalculated according to (2) and sequentially used for readjustment of the rotor angles. In order to facilitate this process the iterative approach, based on the Newton method [6], is initiated. The wish is to solve system of nonlinear equations (6) were the number of equations is the number of voltage sources minus one (slack bus is omitted from the solution as it's rotor angle is pre-defined):

$$\mathbf{y=f(x)} \tag{6}$$

where **x**,**y** and **f** vectors are defined as follows :

$$[\mathbf{x}]=[\boldsymbol{\delta}]=\begin{pmatrix}\delta_2\\ \dots\\ \delta_N\end{pmatrix};\quad [\mathbf{y}]=\left[\mathbf{P}_{gen}\right]=\begin{pmatrix}P_{gen2}\\ \dots\\ P_{genN}\end{pmatrix} \tag{7}$$

$$[\mathbf{f(x)}]=[\mathbf{P(\delta)}]=\begin{pmatrix}\dots\\ \frac{V_{0i}{}^2}{Z_{th_i}}\cdot\cos(\phi_{th_i})-\frac{E_{th_i}\cdot V_{0i}}{Z_{th_i}}\cos(\delta_i-\theta_i+\phi_{th_i})\\ \dots\end{pmatrix}$$

when (7) is defined (8) can be obtained:

$$\frac{\mathbf{dy}}{\mathbf{dx}}=\frac{\mathbf{df(x)}}{\mathbf{dx}}=\frac{\mathbf{dP(\delta)}}{\mathbf{d\delta}}=\mathbf{J(\delta)}; \tag{8}$$

where **J(δ)** is Jacobi matrix of **P(δ)** with respect to **δ**.

In order to define elements of Jacobi matrix the following derivatives are to be specified (9):

$$\mathbf{J(\delta)}=\frac{\mathbf{dP(\delta)}}{\mathbf{d\delta}};$$

$$\frac{\partial\left(\mathrm{P_i}(\delta)\right)}{\partial\delta_\mathrm{j}}=\frac{\partial\left(\mathrm{E}_{thi}\left(\delta_{j,j\neq i}\right)\cdot \mathrm{V}_{0i}/\mathrm{z}_{thi}\cdot cos(\delta_i-\theta_{thi}\left(\delta_{j,j\neq i}\right)+\phi_{thi})\right)}{\partial\delta_j}$$

for i = j

$$\frac{\partial\left(\mathrm{P_i}(\delta)\right)}{\partial\delta_\mathrm{i}}=\frac{\mathrm{V}_{0i}}{\mathrm{Z}_{thi}}\left[\frac{\partial\left(\mathrm{E}_{thi}\left(\delta_{j,j\neq i}\right)\right)}{\partial\delta_\mathrm{i}}\cdot cos(\delta_i-\theta_{thi}\left(\delta_{j,j\neq i}\right)+\phi_{thi})+\right. \tag{9}$$

$$\left.+\mathrm{E}_{thi}\left(\delta_{j,j\neq i}\right)\cdot\frac{\partial\left(cos(\delta_i-\theta_{thi}\left(\delta_{j,j\neq i}\right)+\phi_{thi})\right)}{\partial\delta_\mathrm{i}}\right]=$$

$$=-\sin(\delta_i-\theta\left(\delta_{j,j\neq i}\right)_{thi}+\phi_{thi})\cdot\mathrm{E}_{thi}\left(\delta_{j,j\neq i}\right)$$

for i ≠ j

$$\frac{\partial\left(\mathrm{P_i}(\delta)\right)}{\partial\delta_\mathrm{j}}=\frac{\mathrm{V}_{0i}}{\mathrm{Z}_{thi}}\left[\frac{\partial\left(\mathrm{E}_{thi}\left(\delta_{j,j\neq i}\right)\right)}{\partial\delta_\mathrm{j}}\cdot cos(\delta_i-\theta_{thi}\left(\delta_{j,j\neq i}\right)+\phi_{thi})+\right.$$

$$\left.+\mathrm{E}_{thi}\left(\delta_{j,j\neq i}\right)\cdot\frac{\partial\left(cos(\delta_i-\theta_{thi}\left(\delta_{j,j\neq i}\right)+\phi_{thi})\right)}{\partial\delta_\mathrm{j}}\right]$$

$$\frac{\partial\left(\mathrm{E}_{thi}\left(\delta_{j,j\neq i}\right)\right)}{\partial\delta_\mathrm{j}}=\frac{\mathrm{V}_{0j}\cdot k_{0trij}}{\mathrm{E}_{thi}}\cdot\left(\mathrm{Im}(\mathrm{E}_{thi})\cdot\cos(\delta_j+\alpha_{ij})-\mathrm{Re}(\mathrm{E}_{thi})\cdot\sin(\delta_j+\alpha_{ij})\right)$$

$$\frac{\partial\left(cos(\delta_i-\theta_{thi}\left(\delta_{j,j\neq i}\right)+\phi_{thi})\right)}{\partial\delta_\mathrm{j}}=-\sin(\delta_i-\theta_{thi}\left(\delta_{j,j\neq i}\right)+\phi_{thi})\cdot(-1)\cdot\frac{\mathrm{V}_{0j}\cdot k_{0trij}}{\mathrm{Im}(\mathrm{E}_{thi})}\cdot$$

$$\cdot\left[\frac{(\mathrm{Re}(\mathrm{E}_{thi}))^2\cdot\sin(\delta_j+\alpha_{ij})-\mathrm{Re}(\mathrm{E}_{thi})\cdot\mathrm{Im}(\mathrm{E}_{thi})\cdot\cos(\delta_j+\alpha_{ij})}{\mathrm{E}_{thi}{}^2}-\sin(\delta_j+\alpha_{ij})\right]$$

Wherever $\mathbf{J^{-1}}$ exists (8) can be rewritten:

$$\Delta\boldsymbol{\delta}=\mathbf{J}^{-1}\cdot\Delta\mathbf{P(\delta)}$$

for each iteration:

$$\begin{aligned}\Delta\mathbf{P}_k&=\mathbf{P}_{gen}-\mathbf{P}_k\\ \Delta\boldsymbol{\delta}_k&=\mathbf{J}^{-1}\cdot\Delta\mathbf{P}_k\\ \boldsymbol{\delta}_{k+1}&=\boldsymbol{\delta}_k+\Delta\boldsymbol{\delta}_k\end{aligned}$$

$$E_{th_{k+1}}=\boldsymbol{GTC}\cdot\begin{pmatrix}\mathrm{V}_{01}\cdot e^{j\delta_{1k+1}}\\ \mathrm{V}_{02}\cdot e^{j\delta_{2k+1}}\\ \dots\\ \mathrm{V}_{0i}\cdot e^{j\delta_{ik+1}}\\ \dots\\ \mathrm{V}_{0N}\cdot e^{j\delta_{Nk+1}}\end{pmatrix} \tag{10}$$

$$P_{k+1}(\delta)=\frac{V_{0i}{}^2}{Z_{th_i}}\cdot\cos(\phi_{th_i})-\frac{E_{th_i}\cdot V_{0i}}{Z_{th_i}}\cos(\delta_{i_{k+1}}-\theta_{i_{k+1}}+\phi_{th_i})$$

Where k is a number of iteration.

The iterative process continues until the sufficient accuracy $\Delta\delta_i<\varepsilon$ is achieved or the limit for number of iterations is exceeded indicating non convergence. The obtained results would be a solution for the new steady state operational conditions corresponding to point 5 (Fig1). In case of non-convergence of iterative process the conclusion that steady state could not be achieved for the given operational conditions can be made. Thus, basing on the suggested admittance matrix variation the assessment of new steady state existence and the value of active power margin can be carried out. Thus the sufficiency of the suggested preventive countermeasure expressed in terms of the variation of nodal admittances can be assessed in advance avoiding EMT simulation or running full scale load flow analysis. This approach enable close to real time decision support functionality for the operational personal in a control room.

The next section would demonstrate the validity of the suggested approach on the 8 bus test system and IEEE 30bus test system. Furthermore, the suggestions allowing speeding up the described algorithm would be proposed.

III. Results and Discussions

For the verification of the suggested approach two test systems are considered: 8 bus test system and IEEE 30 bus test system.

A. *Case I: Instability Prevention by applying control action with predicted resulting active power margins*

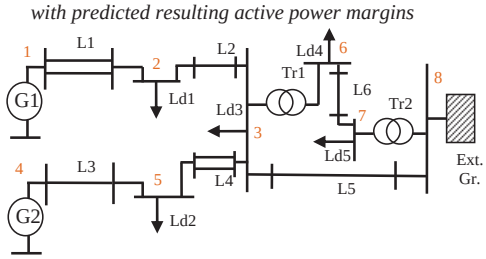

Figure 2. Single line diagram of 8 bus test system.

TABLE I. 8-BUS SYSTEM DATA:BRANCHES

Branch	L1	L2	L3	L4	L5	L6
X, Ohm	1.8	6	1.2	7.2	9.6	22.2

TABLE II. 8-BUS SYSTEM DATA:BUSES

Bus	Unom, kV	Pgen, MW	Qgen, MVar	Pload, MW	Qload, MVar
1	10	20	9.81	0	0
2	10	0	0	26	10
3	10	0	0	30	0
4	10	15	6.39	0	0
5	10	0	0	10	2
6	110	0	0	40	10
7	110	0	0	40	10
8	10	81.00	49.94	0	0

For the network shown in Fig. 2 the study case leading to loss of aperiodic small signal angular stability (ASSAS) is created, using Power Factory as a simulation tool. For the reference bus the bus of external grid connection (bus 8) is chosen. To initiate ASSAS problems in the test system the increase of the load Ld1 per 3% is initiated at t=5 seconds, which leads to visible instability at t=38.31 seconds (Fig. 3). At t=18.6 seconds early warning method [3] detects cross of ASSAS boundary.

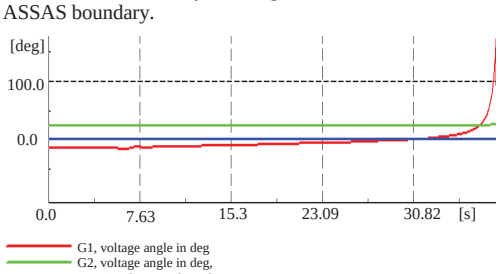

Figure 3. Instability caused by increase of the load Ld1 per 3%. Voltage angles at buses 1, 4 and 8.

The preventive countermeasure in form of injection of reactive power into the bus2, resulting in decrease of nodal admittance Y_{22} per 0.005j p.u. is suggested. The assessment of effectiveness of the suggested countermeasure is carried out following the method described in the Section2. The accuracy $\Delta\delta_i<10^{-5}$ is set a criterion for ending of iterative process. The following results are obtained:

TABLE III. PREDICTION OF PMARGIN

Gen	δpred	δactual	P marg-pred,%	P marg-act,%	Error, %	N iteration
G1	19.8072	19.8354	0.6310	0.6271	0.62	28
G2	50.1703	50.1985	0.6366	0.6319	0.74	

The elements of Jacobi matrix obtained during iterative process for the first 3 iterations appear as follows:

TABLE IV. ELEMENTS OF JACOBI MATRIX

Niter	$J_{1,1}$	$J_{1,2}$	$J_{2,1}$	$J_{2,2}$
1	0.0432	0.0141	0.0098	0.0772
2	0.0432	0.0140	0.0098	0.0772
3	0.0432	0.0141	0.0098	0.0772

It can be noticed that elements of Jacobi matrix are almost not varying from iteration to iteration, thus the recalculation of Jacobi matrix on each iteration is not needed. As inversion of matrix is computational heavy operation the conclusion made allows saving computational time considerably. Furthermore, as the diagonal elements are noticeably greater than off-diagonal elements assumption to eliminate off-diagonal elements from calculation is considered. Table V shows the results of preventive countermeasure assessment based on the proposed simplifications – calculation of Jacobi matrix only once at the beginning of iterative process where off-diagonal elements are accepted to be equal to zero.

TABLE V. PREDICTION OF PMARGIN

Gen	δpred	δactual	P marg-pred,%	P marg-act,%	Error, %	N iteration
G1	19.8079	19.8354	0.6309	0.6271	0.62	27
G2	50.1703	50.1985	0.6366	0.6319	0.74	

As one can see the introduced simplifications doesn't increase the error of assessment at the same time allowing great computational saving.

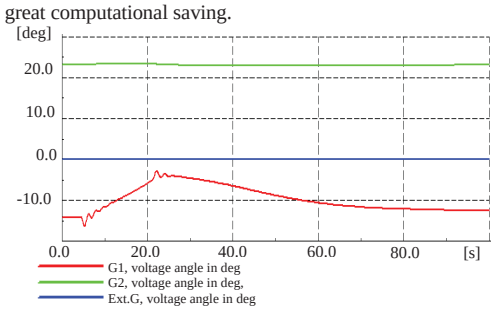

Figure 4. System response on application of the countermeasure

According to obtained prediction of resulting active power margin the suggested countermeasure should lead to stabilization of the system, even though with very low safety margin. Fig.3 shows the effect of the suggested countermeasure application which is in a good agreement with the predicted one

B. Case II: IEEE 30 bus test system

Fig. 5 shows IEEE 30-bus test system diagram. The system data are taken from power system test archive [7]. Few modifications were done to the system: synchronous compensators in the grid were replaced by generators, three-winding transformer was replaced respectively by two two-winding transformers. Generator G1 is representing external grid and chosen as a reference bus.

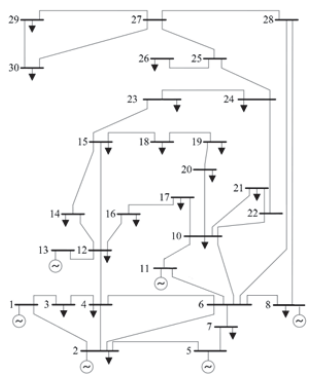

Figure 5. Single line diagram of IEEE 30 bus test system.

TABLE VI. GENERATOR DATA

Gen	G1	G2	G5	G8	G11	G13
P_{G},MW	108.75	40	40	40	30	30

TABLE VII. INITIAL PMARGIN

Gen	G1	G2	G5	G8	G11	G13
%ΔP_{inj}	80.04	53.04	60.47	63.65	41.21	27.42

The goal of current study is to determine whether after serious contingencies applied to the system the new steady state can be achieved and what would be the resulting stability margins. For this Purpose the following disturbances were applied to IEEE 30 bus test system at a time: Increase of load12 per 300%; trip of line3_4, line2_6 and line4_6. The contingencies are applied at t=5 seconds, immediately after this the assessment of the resulting steady state starts.

TABLE VIII. PMARGIN IMMEDIATELY AFTER DISTURBANCE APPLICATION

Gen	G1	G2	G5	G8	G11	G13
%ΔP_{inj}	99.01	44.03	55.25	57.26	19.13	17.59

Table IX demonstrates the elements of complete Jacobi matrix. For the calculations the simplification accepting off-diagonal elements being equal to zero was used instead.

TABLE IX. ELEMENTS OF JACOBI MATRIX

	$J_{i,1}$	$J_{i,2}$	$J_{i,3}$	$J_{i,4}$	$J_{i,5}$
$J_{1,j}$	0.8416	0.0146	0.0155	0.0064	0.0062
$J_{2,j}$	0.0162	0.8980	0.1901	0.0652	0.0288
$J_{3,j}$	0.0149	0.1695	0.8657	0.1392	0.0557
$J_{4,j}$	0.0062	0.0589	0.1255	0.4506	0.0223
$J_{5,j}$	0.0050	0.0198	0.0326	0.0160	0.3706

TABLE X. PREDICTION OF THE RESULTING PMARGIN

Gen	δpred	δactual	$P_{marg-pred,\%}$	$P_{marg-act,\%}$	Error, %	N iterations
G2	26.30	26.2372	52.73	52.62	0.21	11
G5	9.7873	9.7030	59.40	59.33	0.12	
G8	5.6775	5.5973	60.06	60.00	0.10	
G11	20.97	20.9237	38.54	38.44	0.25	
G13	34.64	34.64	23.03	23.89	0.59	

Results shown in the Table X demonstrate the correctness of the assessment method. The resulted new steady state was predicted with high accuracy.

IV. CONCLUSION

This paper considers the method allowing fast assessment of the effect which suggested variation of admittance matrix would have on the stability of the synchronous machines in the grid. The modification of Newton method applied to the system of nonlinear equations calculating the injection power for each of the synchronous generators when the remaining grid is represented as Thevenin equivalent is considered in this paper. Developed approach allows considerable save of computational time comparing to conventional EMT or load flow analysis when the post-disturbance new steady state should be assessed in advance within restricted time allowance.

REFERENCES

[1] A.G. Phadke, Hector Volskis, Rui Menezes de Moraes, Tianshu Bi, R.N. Nayak, Y.K. Sehgal, Subir Sen, Walter Sattinger, Enrique Martínez, Olof Samuelsson, Damir Novosel, Vahid Madani, and Yuri A. Kulikov, " The Wide World of Wide-area Measurement", Power and Energy Magazine, IEEE, vol. 6, pp.52-65 , 2008.

[2] M. Glavic and T. Van Cutsem, "Wide area detection of voltage instability from synchronized phasor measurements. Part I: Principle", IEEE Trans. Power Syst., vol. 24, pp.1408-1416 , 2009.

[3] H. Jóhannsson, R. Garcia-Valle, J. T. G. Weckesser, A. H. Nielsen and J. Østergaard, "Real-Time stability assessment based on synchrophasors", IEEE PES Trondheim PowerTech,2011

[4] H. Jóhannsson, J. Østergaard and A. H. Nielsen, "Identification of critical transmission limits in injection impedance plane", Int J Electr Power Energ Syst, 2012, http://dx.doi.org/10.1016/j.ijepes.2012.05.050

[5] E. Dmitrova, H. Jóhannsson and A.H. Nielsen, "Assessment of the Impact that Individual Voltage Source has on a Generator's Stability", International Power and Energy Conference IPEC, 2012.

[6] D. E. Whitney, "Comparative study of Various Minimization Techniques Used in Mathematical Programming", IEEE Transactions on Automatic Control, October 1969.

[7] Power System Test Archive, available online http://www.ee.washington.edu/research/pstca, Aug.1993

C

EARLY PREVENTION OF INSTABILITY-USE OF SELF PROPAGATING GRAPH FOR THE FAST SEARCH FOR OPTIMAL GRID NODES TO APPLY COUNTERMEASURES

This paper was published in the proceedings of the International Conference Power-Tech, June 2013, Grenoble

Early Prevention of Instability-Use of Self Propagating Graph for the Fast Search for Optimal Grid Nodes to Apply Countermeasures

Evgenia Dmitrova, Hjörtur Jóhannsson, Arne Hejde Nielsen
Elektro, Technical University of Denmark
Center for Electric Power and Energy
Kgs. Lyngby, Denmark
ed@elektro.dtu.dk, hj@elektro.dtu.dk, ahn@elektro.dtu.dk

***Abstract*—This paper presents a method for a fast determination of the grid nodes where countermeasures, in the form of changes in nodal admittance, would provide greatest impact on the stability margin for a specific generator that is facing the risk of instability. The sensitivity of the stability criteria for aperiodic small signal angular stability to the change in nodal admittance is used as a factor quantifying impact that the node has on the stability of a critical generator. In order to lower the number of nodes which are processed through sensitivity analysis, a self-propagating graph with discrete steps is applied. The suggested method is tested on the IEEE 30 bus test system and on the 1648 bus US west coast test system where the results show that the number of nodes processed through sensitivity analysis are well reduced compared to the full sensitivity analysis, illustrating the potential of the developed approach for the fast identification of the optimal nodes for countermeasure application.**

***Index Terms*- graph theory, power systems, sensitivity analysis, stability.**

I. INTRODUCTION

The gradual integration of phasor measurement units into real power systems opens up new possibilities for modern control methods, including adaptive preventive control [1-2]. The ability to keep hand on power system pulse is a great evolution in the field of situational awareness. Clear understanding of the actual operational conditions allows increasing efficiency of power systems, specifically in terms of transmission system loading. Conventionally, the limitation on power capacitance of a certain transfer pass was defined by stability boundaries, pre-defined on the basis of system statistical data and off-line simulations. Additionally, a certain safety margin was used as a buffer to ensure stable operation in case if actual operational conditions would be worse than pre-modeled ones. Thus, the worst case scenario has been considered as a benchmark for power transfer limits setting; however actual operational conditions might vary towards a "lighter" case compared to modeled ones. Knowing the actual stability boundaries would help improve the efficiency and at the same time reliability of power systems. Taking advantage of the phasor measurements, future perspectives are to obtain complete observability of a grid, which motivates research and development of new methods for the real-time systems stability monitoring. Among others, the method allowing detection of Aperiodic Small Signal Angular Stability (ASSAS) problems at the early stage of their emergence, utilizing wide area measurements, have been introduced in [3-4]. The method, which is based on the analytically derived expression for a stability boundary [3], gave inspiration for the development of the early prevention method. In this method, the warning message about approaching stability boundaries is used as a triggering signal for the search of appropriate countermeasures. The main functionality of the early prevention method is the fast identification of the optimal countermeasure, taking into account the actual allocation and availability of control reserves in the grid, which insures instability avoidance. In order to optimize the countermeasure, the nodes which have the highest potential to influence stability of the critical generator should be found. As a decision regarding the application of the countermeasure may be time restricted, the number of nodes which might be considered as control candidates should possibly be reduced, skipping those nodes in the analysis, which a priory cannot help much to improve a critical situation. The method for identification of the optimal nodes for countermeasure application was presented in [5] and utilizes sensitivity analysis for quantification of the impact which a node has on the stability of a critical generator. This paper is focused on the method allowing considerable reduction of the time needed for the search of the optimal node in the grid to which a countermeasure should be applied.

The paper is organized as follows: Section II contains the theoretical description of the proposed approach for a self-propagating graph; in Section III, illustration of the developed method applied to the IEEE30 bus test system and the 1648 bus US west coast test system is provided; Section IV contains the conclusion and perspectives for further research.

Notation: Uppercase bold letters refer to matrixes. Complex numbers are underlined, * - denotes complex conjugate.

II. METHODOLOGY

A. *Optimal node for the preventive countermeasure application*

For the search of the optimal node for which to apply a countermeasure when a given generator is facing the risk of ASSAS loss, the stability criterion derived in [4] is utilized. The criterion is formulated for the two bus system representation, where one bus is representing the critical generator under consideration and the rest of the system is reduced to the Thevenin equivalent (Fig.1).

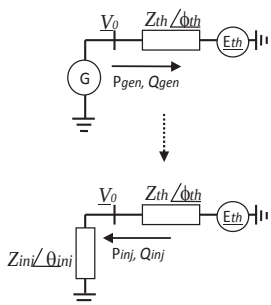

Figure 1. Equivalent system representation regarding critical generator.

The mathematical expression for the ASSAS criterion is shown in (1):

$$\begin{cases} Z_{inj} >= -Z_{th}\cdot \sin\theta_{inj}/\sin\phi_{th} & \text{–stable operation} \\ Z_{inj} < -Z_{th}\cdot \sin\theta_{inj}/\sin\phi_{th} & \text{–unstable operation} \end{cases} \quad (1)$$

Where Z_{inj} corresponds to the magnitude of the generators' injection impedance, measured at the node of constant steady state voltage magnitude V_0, Z_{th} is Thevenin equivalent of the system seen from the node of power injection. θ_{inj} and ϕ_{th} are the angles of $\underline{Z}_{inj}$ and $\underline{Z}_{th}$ respectively. The value of injection impedance is determined as follows:

$$\underline{Z}_{inj} = -\underline{V}_0^{\,2}/(P_{gen} + j\cdot Q_{gen})^* = \underline{V}_0^{\,2}/\underline{S}^*_{inj} \quad (2)$$

Where P_{gen}, Q_{gen} are an active and reactive power of a generator fed to a grid from the node of constant steady state voltage magnitude and $\underline{S}_{inj}$ is the corresponding injection power which is equal to $\underline{S}_{gen}$ with opposite sign.

It was shown in [5] that in order to identify the nodes, which have high effectiveness for countermeasure application, meaning that the variation of admittance in those nodes has considerable impact on the stability of a given generator, it is enough to find out which nodes are most influencing the Thevenin impedance seen by this generator. For this purpose the sensitivity of $K_{th} = Z_{th}/\sin\phi_{th}$ (1) to the variation of nodal admittance in each of the load nodes (nodes with neither generators nor constant voltage sources) should be calculated. For this study the rescheduling of the generators is assumed to be not available, which reflects the case of full loading operation; thus only load nodes are considered as a target for countermeasure application. To calculate the sensitivity of the Thevenin impedance, seen by a given generator, to the nodal admittance variation the same change in admittance ΔY is applied in each load node in sequence, which implicitly represents the application of the countermeasure. Thus, for the given generator *k* the following sensitivity is calculated (3) for each of the load nodes, forming the vector of sensitivities established in (4), where CEF stands for Control Efficiency Factor:

$$S_{Kth_{km}} = \left[\frac{\partial(Z_{th}/\sin(\varphi_{th}))_k}{\partial(\underline{Y}_{m,m})}\right] = \left[\frac{\partial(K_{th_k})}{\partial(\underline{Y}_{m,m})}\right] \quad (3)$$

Where m=1..M, M- number of load nodes in the grid

$$[CEF]_k = (S_{Kth_{k1}} \ldots S_{Kth_{km}} \ldots S_{Kth_{kM}}) \quad (4)$$

When normalized, the elements of the **CEF** matrix are representing the relative efficiency of a countermeasure application to the corresponding node.

The number of load nodes in the real system reaches thousands; calculation of sensitivities $S_{Kth_{km}}$ for all of them in order to define which would be the optimal one for countermeasure application would require large computational power, which is a crucial issue, especially if close to real-time sensitivity analysis (SA) is desired. At the same time the number of nodes, which actually have considerable impact on the stability of a certain generator, is noticeably lower than the number of load nodes in the grid; thus there is an interest in developing an algorithm allowing reduction of the number of nodes processed through SA, initially sorting out the nodes which a priori do not have high CEF.

B. *Self propagating graph utilisation for limiting the amount of nodes processed through sensitivity analysis*

In order to limit the number of nodes which are to be processed through SA, it is necessary to develop an approach enabling nodes assessment in a way that those nodes having very low impact on the stability of a given generator can be sorted out early on.

It was noticed that with the increase of topological distance between the considered node and the critical generator, the value of sensitivity $S_{Kth_{km}}$ tends to decrease. Depending on how meshed the grid is and what are the impedances of branches connecting the nodes the decrease of $S_{Kth_{km}}$ happens unevenly, and in fact is defined by equivalent transport admittance Y_{km} between the node and generator. However, in order to avoid the calculation of equivalent transfer admittance, the topological distance between the considered node and given generator was chosen as a reference criterion. As the main purpose of this study is to find the way allowing sorting out the nodes in which sensitivity $S_{Kth_{km}}$ is below certain minimum level, let us denote for

certainty the minimum acceptable sensitivity is $S_{Kth_{\min}}$. $S_{Kth_{\min}}$ is the criterion which would vary depending on topology of the grid. In meshed grids the sensitivity $S_{Kth_{km}}$ decreases faster, which means that the minimum acceptable value for $S_{Kth_{\min}}$ can be lowered in this case to ensure that a sufficient amount of load nodes capable of providing positive effect on generator's stability are considered. Furthermore, the sufficient number of nodes processed through SA, is dependent on the availability of the control reserves in the nodes with high sensitivity and generally might vary depending on the current control reserves allocation.

As there is a correlation between the increase of topological distance and the sensitivity decrease, the natural decision is to split nodes per sets with accordance to their topological distance to the critical generator. The topological distance in this context is the number of vertexes on the shortest path between the critical generator and given node, when the grid is represented as a graph; moreover, the edges in this graph are weightless. In order to organize the split of the nodes per sets, the concept of the self-propagating graph is used. The term "self-propagating graph" is reflecting the principle of discreet graphing where the nodes are added to the graph stepwise with respect to the length of the shortest path from the critical generator to the given node. On each step the set of equally topologically distant nodes is formed, each next set will contain the nodes which shortest path to the critical generator is one vertex more, comparing to the previous set. As soon as a new set of nodes is added to the graph, the sensitivity $S_{Kth_{km}}$ should be calculated for each of the nodes in the set. If the sensitivity in the node under consideration appears to be below the preset value $S_{Kth_{\min}}$, the node is marked as the dead-end node and further development of the graph through this node is blocked. Thus when the next set is formed, the path of the considered nodes cannot lay through the dead-end node.

In order to keep track of the visited nodes, which have been already included in the self-propagating graph, the nodes from the considered set are added to the list **L**, on each step of the propagation; before adding a node to the next set the check is carried out. Further efficiency improvement of the suggested algorithm can be achieved if the graphing can be organized in a way so that the resulting graph is a tree. By eliminating loops in the graph the double check of sensitivity at the same node can be avoided. Looping can take place in the created graph when a given node has more than one path with the same number of vertexes on the way to the beginning of the graph. This problem is avoided by utilizing first-in-first-out (FIFO) [6] queuing when forming the set. The check and update of the list **L** happens each time when the node is added to the queue. If the node is not listed in **L** it gets added to the self-propagating graph, at the same time **L** is updated by including this node to the list of visited nodes. This will allow keeping track of the visited nodes, not only when comparing a set of nodes to the previous set, but within a set as well. If those principles of graphing are followed, the resulting graph is a tree and all nodes added to the graph are visited only ones.

The propagation of the graph continues until either all load nodes in the grid were visited and sensitivity $S_{Kth_{km}}$ has been calculated for all of them, or further propagation of the graph is not possible as all the vertexes in the last added set were marked as a dead-end vertexes. Satisfying of the second condition for interruption of graph propagating means that the CEF for any other node, not included in the created graph, will be below $S_{Kth_{\min}}$ and those nodes should not be participating in SA. Thus the number of nodes which are included in the sensitivity analysis might be considerably reduced, which leads to noticeable improvement of computational time. The validity of the suggested approach was tested on the IEEE 30 bus test system and on the 1648 bus US west coast test system, and the results obtained are presented in the next section of this paper.

III. Results and Discussions

A. *Self-propagating graph method applied to the IEEE 30 bus test system*

Fig. 2 shows the IEEE 30-bus test system diagram, with the system data borrowed from the power system test archive [7]. Few modifications were done to the system: synchronous compensators in the grid were replaced by generators and three-winding transformers were replaced by two two-winding transformers. The terminal of generator G1 is chosen as a reference bus.

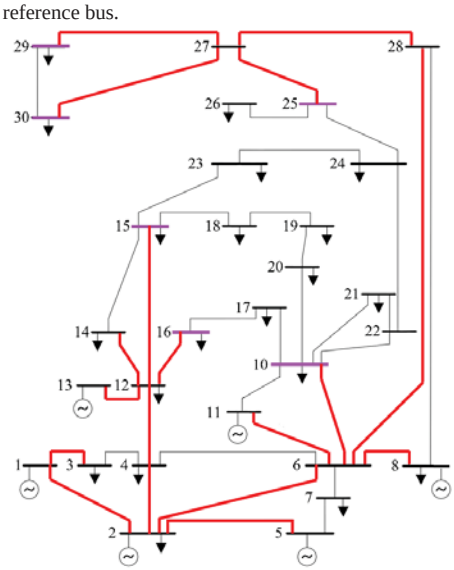

Figure 2. Single line diagram of IEEE 30 bus test system; red color is marking edges of resulting self-propagating graph, purple is marking dead-end vertexes.

For the demonstration of the method described in Section II of this paper generator G_1 was picked as a unit regarding which the SA is to be carried out. For the given study case the change in reactive component of shunt admittance equaled to $\Delta Y_{m,m}$=0.01p.u. was applied as a nodal admittance variation. The minimal sensitivity down to which the impact of the node to the stability of G_1 is considered noticeable was chosen to be equal to 0.3333, which is one third of the maximal sensitivity when **CEF** is normalized. Fig. 3 shows the list of sets formed according to the shortest topology distance to the source vertex, which is G_1 in this case.

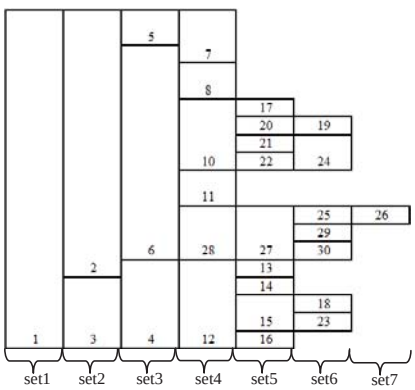

Figure 3. Formulation of the sets for the self-propagating graph beginning at the node corresponding to generator G_1

In Fig. 4 node sets are substituted by the corresponding value of the sensitivity $S_{Kth_{km}}$. The light green color marks the nodes noticeably influencing the stability of generator G1 (meaning that criterion $S_{Kth_{km}} > S_{Kth_{\min}}$ is satisfied), orange is for the first nodes on the path which are not matching the criterion of minimal sensitivity and marked as a dead-end vertexes. Calculation of sensitivities for the nodes lying further along the path is not processed and they are not included in the graph (they are marked with gray color).

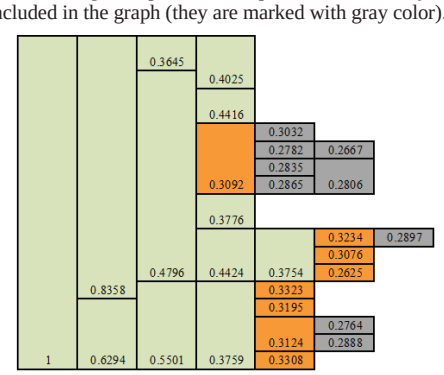

Figure 4. $S_{Kth_{1m}}$ in the corresponding nodes (Fig. 3) seen by generator G_1

As it can be noticed from Fig. 4, the value of sensitivity $S_{Kth_{km}}$ is lower for all the nodes which path from generator G_1 unavoidably passes through the node with sensitivity $S_{Kth_{km}} < S_{Kth_{\min}}$ and marked as a dead-end. Thus the part of the grid completely isolated from the generator under consideration by nodes marked as dead-end vertexes (Fig. 2) can be a priory excluded from SA as the value of sensitivity for the nodes in this area would invariably be below required minimal preset. This leads to the reduction of the nodes processed through SA from 29 to 20, improving considerably the computational time for the search of optimal countermeasure application nodes.

B. Test of the self-propagating graph method on the 1648 bus US west coast test system[1]

This Section is considering validation of the self-propagating graph method on the system containing 1648 nodes among which 313 are generators. For this study the assumption was made that all generators are controlled by Automatic Voltage Regulator (AVR), meaning that the point of constant steady state voltage magnitude V_0 is at the terminal of a generator. The admittance matrix, corresponding to the given system was obtained using MATPOWER network simulation packages [8]. According to the methodology described in the Section II the graph, containing nodes which have considerable impact to a given generator stability, should be created. That was done with respect to each generator in the grid, meaning that 313 self-propagating graphs were defined. Variation of admittance only in the load nodes was considered, reflecting the restriction on the re-dispatch of generators. In this study the focus was placed on illustrating the dependency of the self-propagating graph behavior on the value of the parameter $S_{Kth_{\min}}$. As mentioned in Section II, the value of minimal sensitivity is to be chosen depending on both the topology of the grid and the allocation of control reserves. As neither specific emergency scenario for the grid was considered, nor information about control reserves was available, the comparison analysis for three arbitrarily chosen values of $S_{Kth_{\min}}$ was carried out. Those values were picked in order to illustrate the "speed" of sensitivity decrease while increase of the topological distance between a given generator and considered load nodes. In this context the term "speed" defines how deep the self-propagating graph will spread into the grid before it stops due to minimal sensitivity limit. The following three values were considered in this study: $S_{Kth_{\min}} = [0.2\ 0.1\ 0.01] \cdot S_{Kth_{\max}}$, which equals to $S_{Kth_{\min}} = [0.2\ 0.1\ 0.01]$, as $S_{Kth_{\max}} = 1$ when being normalized. The step of admittance variation applied to each of the load nodes is equal to 0.001p.u. The number of nodes included in the self-propagating graph for each of the generators serves as the parameter reflecting the "speed" of the sensitivity $S_{Kth_{km}}$ decrease in the grid.

1 The 1648 bus US west coast test system provided in the PSSR E-30.06 is used, http://www.energy.siemens.com/us/en/services/power-transmission-distribution/power-technologies-international/software-solutions/pss-e.htm

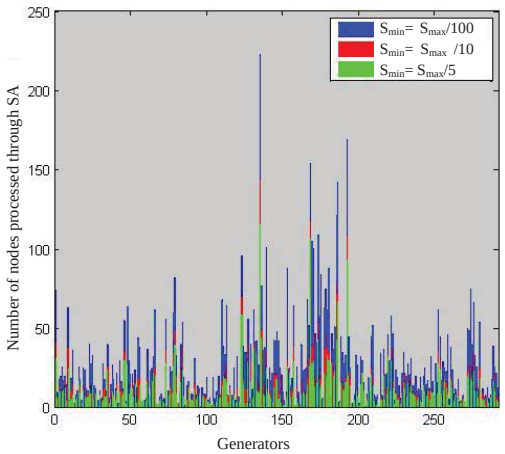

Figure 5. Number of nodes added to the self-propogating graph depending on the chosen value of $S_{Kth_{\min}}$

Fig. 5 demonstrates the joint bar diagram, where the number of nodes included in the self-propagating graph for each generator in the grid when applying different values of $S_{Kth_{\min}}$ is presented. The colors: red, green, blue correspond to the chosen values of minimal sensitivity $S_{Kth_{\min}}$ = [0.2 0.1 0.01]. Generators are represented over the x-axis, while the y-axis is showing the amount of the load nodes added to the self-propagating graph for the certain generator.

The obtained results demonstrate that even for a low value of minimal sensitivity, equal to 0.01, the maximum amount of nodes for which the SA should be processed for a given generator is 222, which is considerably less than total number of load nodes in the grid equal to 1325. It can be clearly seen that the extent of propagation of the graph inside the grid varies greatly for the different generators within similar value of $S_{Kth_{\min}}$, which is explained by the fact that the topology of the grid is not homogeneous with the regions of dominating either radial or meshed structure. In meshed topology sensitivity decreases faster this results in smaller number of nodes added to the self-propagating graph.

IV. Conclusion

The presented concept of the self-propagating graph allows considerable reduction of the number of nodes which should be processed through SA, when the search of the optimal node for application of the countermeasure is carried out. For the considered study case of the IEEE 30 bus test system, the initial number of nodes being subject to sensitivity analysis was 29, while applying the suggested approach this number is reduced to 20. The case of the 1648 bus US west coast test system has as well demonstrated great reduction in the number of nodes processed through SA – the largest amount of nodes added to the self-propagating graph was 222, while there are 1325 load nodes in the grid. Due to the reduction of the nodes which should be processed through SA, the saving in computational time is gained. Furthermore, it can be noticed that applying the developed method to the larger power systems results in a vast reduction of computational time needed for SA, as less than 20% of the load nodes are to be considered.

References

[1] M. Glavic and T. Van Cutsem, "Wide area detection of voltage instability from synchronized phasor measurements. Part I: Principle", IEEE Trans. Power Syst., vol. 24, pp.1408-1416 , 2009.

[2] M. Glavic and T. Van Cutsem, "Wide area detection of voltage instability from synchronized phasor measurements. Part II: Simulation Results", IEEE Trans. Power Syst., vol. 24, pp.1417-1425 , 2009.

[3] H. Jóhannsson, R. Garcia-Valle, J. T. G. Weckesser, A. H. Nielsen and J. Østergaard, "Real-Time stability assessment based on synchrophasors", IEEE PES Trondheim PowerTech, 2011

[4] H. Jóhannsson, J. Østergaard and A. H. Nielsen, "Identification of critical transmission limits in injection impedance plane", International Journal of Electrical Power & Energy Systems, vol. 43, no. 1, pp. 433-443, Dec. 2012, http://dx.doi.org/10.1016/j.ijepes.2012.05.050

[5] E. Dmitrova, H. Jóhannsson and A.H. Nielsen, "Early prevention of instability - search for optimal grid nodes for applying countermeasures", International Conference on Environment and Electrical Engineering EEEIC, Venice, 2012.

[6] Kruse, Robert L., "Data Structures & Program Design" (second edition). Englewood Cliffs, New Jersey 07632: Prentice-Hall, Inc. div. of Simon & Schuster, 1987. ISBN 0-13-195884-4.

[7] Power System Test Archive, available online http://www.ee.washington.edu/research/pstca, Aug.1993.

[8] R. D. Zimmerman, C. E. Murillo-Sánchez, and R. J. Thomas, "MATPOWER: Steady-State Operations, Planning and Analysis Tools for Power Systems Research and Education," Power Systems, IEEE Transactions on, vol. 26, no. 1, pp. 12-19, Feb. 2011.

D
ASSESSMENT OF THE IMPACT THAT INDIVIDUAL VOLTAGE SOURCE HAS ON A GENERATOR'S STABILITY

This paper was published in the proceedings of the 10th International Power and Energy Conference IPEC, December 2012, Ho Chi Minh

Assessment of the Impact that Individual Voltage Source has on a Generator's Stability

Evgeniya Dmitrova, Hjörtur Jóhannsson and Arne Hejde Nielsen
Elektro, Technical University of Denmark
Center for Electric Power and Energy
Kgs. Lyngby, Denmark
ed@elektro.dtu.dk, hj@elektro.dtu.dk, ahn@elektro.dtu.dk

***Abstract*—This paper presents an approach for splitting equivalent Thevenin voltage into components induced by each voltage source in the reduced grid. Thevenin equivalent representation of the system is sometimes used for stability assessment of a given generator, where the Thevenin voltage is one of the key variables affecting the stability conditions. Thevenin voltage is formed by components induced by each voltage source in the grid, while depending on topology and system parameters, the impact of these components on the equivalent Thevenin voltage $\underline{E}_{th}$ might vary considerably. This paper demonstrates how the impact of individual voltage source to $\underline{E}_{th}$ might be defined utilizing system admittance matrix. Knowledge about alternation of $\underline{E}_{th}$, while applying changes to either the admittance matrix or the generators' excitation and torque, gives a promising perspective for determination of effective countermeasures aimed at preventing instability. Suggested approach for $\underline{E}_{th}$ decomposition is applied to the IEEE 30 bus test system.**

Keywords-power systems; preventive countermeasure; stability; Thevenin equivalent

I. INTRODUCTION

Recent decades have seen great changes happen to the power systems: the integration of non-controllable renewable energy sources, decentralization of power production, introduction of energy markets, development leaps in computational technologies and the integration of WAMS. Current research focus includes topics such as electrical vehicle integration, energy storage, and controllable loads for system support. This development of power systems that is aimed at improving security of energy supply and reducing the impact on the environment, introduce challenges for the power system operation due to increased fluctuations of the system conditions. Flexibility, adaptiveness and smart control will become key features in reliable and safe operation of the future power system.

To meet these requirements and considering intensive development and integration of WAMS technology, new methods for real-time grid monitoring and analysis have begun to emerge, among others methods for stability assessment [1]-[4]. To simplify the stability assessment process, equivalent grid reduction is frequently used. For this purpose two circuit equivalents- Norton and Thevenin gained the most attention in power grid analysis [5]. Current work focuses on Thevenin equivalent and was inspired by Aperiodic Small Signal Angular Stability (ASSAS) assessment method introduced in [3-4]. Approach described therein allows real-time assessment of stability conditions for each generator in the grid. The ASSAS boundary is derived for the simplified two node system representation where the system, seen from a machine's terminal, is represented by a Thevenin voltage behind a Thevenin impedance. Both the Thevenin voltage and the Thevenin impedance are parameters having significant influence on the generator's stability.

This paper focuses on the improvement of the stability of the given generator. Considering that rescheduling of generator output might not always be possible during stressed conditions, Thevenin impedance and voltage alteration can be a good alternative for improving the system operation. Alteration of Thevenin impedance by applying changes to the load nodes was considered in [6], where the method for identification of the optimal load node, which has the highest potential for improving ASSAS of the given generator, was suggested. For that purpose, the sensitivity of the Thevenin impedance to variation of nodal admittances was examined. The next logical research step is to determine how the given change in the system admittance matrix will influence not only Thevenin impedance but also the Thevenin voltage seen by the generator in question. This Thevenin voltage is comprised of components induced by each voltage source in the grid. Thus, in order to analyze the dependency of Thevenin voltage on variations of the admittance matrix, it would be enough to identify the dependency of each voltage component. This paper presents methodology for identification of Thevenin voltage components brought on by each of the voltage sources in the system. The validity of the suggested concept was tested on the IEEE 30 bus test system.

The paper is organized as follows: Section II contains the theoretical description of the proposed approach for identifying the components of $\underline{E}_{th}$ induced by each voltage source in the network; in Section III, illustration of the developed method applied to the IEEE30 bus test systems is provided; Section IV contains conclusion and perspectives for the further research.

Notation: Uppercase bold letters refer to matrixes. Complex numbers are underlined, ^ - denotes complex conjugate.

II. DECOMPOSITION OF $\underline{E}_{TH}$ INTO COMPONENTS INDUCED BY EACH OF VOLTAGE SOURCES IN THE GRID

The derivation of the ASSAS boundary exploiting Thevenin equivalent system representation depicted in Fig. 1 is described in [3-4].

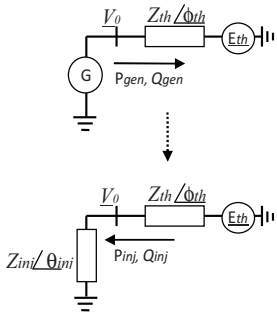

Figure 1. Equivalent system representation for a generator

The power injection from a given generator is represented at a node of constant steady-state voltage magnitude V0. The mathematical criterion for the aperiodic small signal angular stability given by [3]:

$$Z_{inj} \geq -Z_{th} \cdot \sin(\theta_{inj}) / \sin(\phi_{th}) \qquad (1)$$

Where Z_{inj} corresponds to the magnitude of the generators' injection impedance, measured at the node of constant steady state voltage magnitude V_0, Z_{th} is the Thevenin equivalent impedance of the system seen from the node of power injection. θ_{inj} and ϕ_{th} are the angles of $\underline{Z}_{inj}$ and $\underline{Z}_{th}$ respectively. The injection impedance is determined as:

$$\underline{Z}_{inj} = -\underline{V}_0^{\,2} / (P_{gen} + j \cdot Q_{gen})^{\wedge} = \underline{V}_0^{\,2} / \hat{\underline{S}}_{inj} \qquad (2)$$

Where P_{gen}, Q_{gen} are an active and reactive power of a generator fed to a grid from the node of constant steady state voltage magnitude and $\underline{S}_{inj}$ is corresponding injection power which equals to $\underline{S}_{gen}$ with opposite sign. For the system depicted at Fig. 1 the following expression can be written:

$$\hat{\underline{S}}_{inj} \cdot \underline{Z}_{th} = \underline{E}_{th} \cdot \hat{\underline{V}}_0 - \underline{V}_0^{\,2} \qquad (3)$$

Substituting S_{inj} from (3) to (2) we get:

$$\underline{Z}_{inj} = \underline{V}_0 \cdot \underline{Z}_{th} / (\underline{E}_{th} - \underline{V}_0) \qquad (4)$$

Considering (1) and (4) one may see that parameters determining the ASSAS boundary are $\underline{Z}_{th}$, $\underline{E}_{th}$ and $\underline{V}_0$. The method for defining of $\underline{Z}_{th}$ directly from the system admittance matrix is described in [3]. The current study is focused on identification of $\underline{E}_{th}$ directly from the admittance matrix. In order to estimate how the value of $\underline{E}_{th}$ will change when the changes to the admittance matrix are applied, the split of equivalent $\underline{E}_{th}$ per components induced by each of voltage sources contained in the grid is considered. The approach is based on the assumption that contribution from each voltage source in $\underline{E}_{th}$ is depending only on the topology of the grid and is not influenced by other voltage sources, which allows application of the superposition principle. That means the equivalent $\underline{E}_{th}$ for the system depicted in Fig. 1 will be equal to the sum of $\underline{E}_{th,i,}$ induced by each voltage source in the system (Fig. 2).

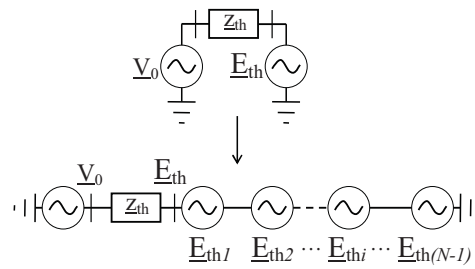

Figure 2. Expansion of Thevenin equalent for the system containing N voltage sources.

In its turn, the value of each $\underline{E}_{th,i}$ is defined by two factors: the value of the voltage measured at the point of constant steady state voltage magnitude and the topology of the grid. To illustrate this statement, the system depicted in Fig. 3 is used.

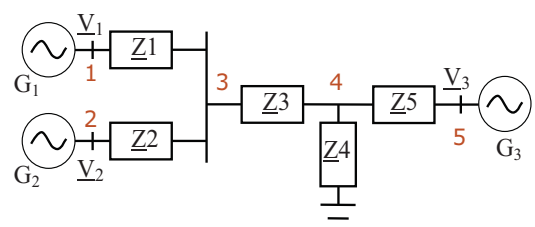

Figure 3. Single line diagram of 5 bus example system.

In this example, generator G_3 is chosen as the unit wherefrom the reduction of the grid and identification of the $\underline{E}_{th}$ components from generators G_1 and G_2 is carried out. Due to the assumptions taken, superposition can be applied, allowing the impact of generators G_1 and G_2 on $\underline{E}_{th}$ to be studied independently. Respectively, the system can be represented by two subsystems (Fig. 4).

The further procedure for identifying the $\underline{E}_{th,i}$ components from each subsystem should be as follows:

a) The generator which looks into the Thevenin equivalent should be open-circuited (G_3 in this case).

b) The voltage appearing at the node with the open-circuited generator (node 5 in this case) will be equal to the value of $\underline{E}_{th,i}$.

It should be noted that the voltage on the open end will be equal to the voltage at the nearest shunted node. While G_3 is open-circuited, the voltage at the bus 5 is equal to the voltage at the bus 4 (Fig. 3). Consequently, the Thevenin equivalent

voltage seen by generator G_3 can be determined as given in (5):

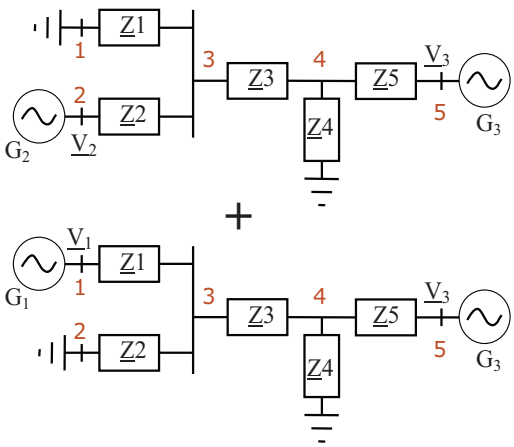

Figure 4. Single line diagram of subsystems.

$$\underline{E}_{th} = \left(\underline{V}_1 \cdot \frac{\underline{Z}_2}{\underline{Z}_1 + \underline{Z}_2} + \underline{V}_2 \cdot \frac{\underline{Z}_1}{\underline{Z}_1 + \underline{Z}_2} \right) \cdot \frac{\underline{Z}_4}{\frac{\underline{Z}_1 \cdot \underline{Z}_2}{\underline{Z}_1 + \underline{Z}_2} + \underline{Z}_3 + \underline{Z}_4} = \tag{5}$$

$$= \left(\underline{V}_1 \cdot \frac{\underline{Z}_2}{\underline{Z}_1 + \underline{Z}_2} \cdot \frac{\underline{Z}_4}{\frac{\underline{Z}_1 \cdot \underline{Z}_2}{\underline{Z}_1 + \underline{Z}_2} + \underline{Z}_3 + \underline{Z}_4} \right) + \left(\underline{V}_2 \cdot \frac{\underline{Z}_1}{\underline{Z}_1 + \underline{Z}_2} \cdot \frac{\underline{Z}_4}{\frac{\underline{Z}_1 \cdot \underline{Z}_2}{\underline{Z}_1 + \underline{Z}_2} + \underline{Z}_3 + \underline{Z}_4} \right) =$$

$$= \left(\underline{E}_{th1} + \underline{E}_{th2} \right)$$

As seen from (5), the components of $\underline{E}_{th.i}$ are represented as a product of the voltage measured at the point of constant steady state voltage magnitude and a coefficient, which is dependent on the structure of the grid. Let us denote this coefficient as the Grid Transformation Coefficient (GTC). Knowledge of $\underline{V}_1$, $\underline{V}_2$ as well as $\underline{Z}_i$ is assumed to be provided by PMU measurements. Relying on the availability of grid data mentioned above, a method for direct calculation of $\underline{E}_{th}$ can be suggested.

As noticed from (5), in order to identify $\underline{E}_{th}$ seen by a generator in an arbitrary system, an algorithm for determining a **GTC** matrix is needed, since the **GTC** matrix contains grid transformation coefficients for all voltage sources of the reduced part of the grid. Thus, a general methodology for identification of **GTC** on the basis of admittance matrix will be formulated. For certainty, let k denote the index of the generator's voltage magnitude controlled node in respect to which the reduction of the grid is taken. In order to define the component $\underline{E}_{th,i,}$ induced by generator i as seen from the node k, few manipulations are to be applied to the system admittance matrix. According to the superposition principle, the impact of each voltage source to $\underline{E}_{th}$ can be considered independently. Thus, to determine the Thevenin voltage component induced by generator i seen from the node k, all the remaining voltage sources in the system should be short-circuited. This operation is reflected in admittance matrix by removing the columns and rows corresponding to these nodes, which leads to the reduction of the admittance matrix size from {NxN} to {(N-N_{vs}+2)x(N-N_{vs}+2)}, where N_{vs}- and N- are number of voltage sources and the number of nodes in the original system, respectively.

Then node k should be open-circuited which is reflected in a structure of admittance matrix as a removal of the column and the row corresponding to this node as well as a removal of all elements which would have no power flow when the node k is open-circuited; this will lead to a further reduction of the admittance matrix. Depending on a grid topology the open-circuiting of the node k might cause cut off current for both branch elements and nodes. The $E_{th.i}$ seen from node k is equal to the voltage induced by generator i at the topologically nearest node q, which stays energized when the node k is open-circuited. The adjustment of admittance matrix to the open-circuiting of node k is realized by the algorithm analyzing system topology through {(N-N_{vs}+2)x(N-N_{vs}+2)} admittance matrix and removing elements which are not participating in the closed loops when the column and row corresponding to the node k are removed. Let us denote the final dimensionality of the reduced admittance matrix as {MxM}. After all the manipulations related to the reduction of the original admittance matrix are taken, the reordering of it should be done. The column and row corresponding to node i should respectively be placed as the last column and row of the final reduced admittance matrix as it shown at (6).

$$\left[\underline{Y}_{MM} \right] = \begin{pmatrix} \underline{Y}_{11} & \cdots & -\underline{Y}_{1M} \\ \cdots & \cdots & \cdots \\ -\underline{Y}_{M1} & \cdots & \underline{Y}_{MM} \end{pmatrix} = \begin{array}{|c|c|} \hline \underline{Y}_{n\_vc,\, n\_vc} & \underline{Y}_{n\_vc,\, vc} \\ \hline \underline{Y}_{vc,\, n\_vc} & \underline{Y}_{vc,\, vc} \\ \hline \end{array} \tag{6}$$

M-1 1

Where index *vc* stands for voltage magnitude controlled nodes, and *n_vc* for non-controlled.

The GTC between nodes i and q can be defined by utilizing the properly ordered final reduced admittance matrix when injecting current of 1A into the node i (7).

$$\begin{pmatrix} \underline{V}_1^{'} \\ \cdots \\ \underline{V}_q^{'} \\ \cdots \\ \underline{V}_M^{'} \end{pmatrix} = \begin{pmatrix} \underline{Y}_{11} & \cdots & -\underline{Y}_{1M} \\ \cdots & \cdots & \cdots \\ -\underline{Y}_{q1} & \cdots & -\underline{Y}_{qM} \\ \cdots & \cdots & \cdots \\ -\underline{Y}_{M1} & \cdots & \underline{Y}_{MM} \end{pmatrix}^{-1} \cdot \begin{pmatrix} \underline{I}_1 \\ \cdots \\ \underline{I}_q \\ \cdots \\ \underline{I}_M \end{pmatrix} = \begin{pmatrix} \underline{Y}_{11} & \cdots & -\underline{Y}_{1M} \\ \cdots & \cdots & \cdots \\ -\underline{Y}_{q1} & \cdots & -\underline{Y}_{qM} \\ \cdots & \cdots & \cdots \\ -\underline{Y}_{M1} & \cdots & \underline{Y}_{MM} \end{pmatrix}^{-1} \cdot \begin{pmatrix} 0 \\ \cdots \\ 0 \\ \cdots \\ 1 \end{pmatrix} \tag{7}$$

For convenience, let us introduce matrix [Z] which is the inverse of the admittance matrix $[Y_{MM}]^{-1} = [Z_{MM}]$. Thus the resulting voltage in the node i will be numerically equal to $\underline{V}_M^{'} = \underline{Z}_{M,M}^{'}$ while the voltage in node q equals to $\underline{V}_q^{'} = \underline{Z}_{q,M}^{'}$. Respectively, the following ratio can be written:

$$\underline{k}_{tr\_Mq} = \underline{V}_q^{'} / \underline{V}_M^{'} = \underline{Z}_{q,M} / \underline{Z}_{M,M} \tag{8}$$

This ratio is only dependant on system admittance matrix and is the desired voltage's GTC between nodes i and q. The

remaining (N-2) grid coefficients are defined following the same methodology forming **GTC** matrix (9).

$$GTC = \begin{pmatrix} 0 & \underline{k}_{tr21} & \dots & \underline{k}_{trN1} \\ \underline{k}_{tr12} & 0 & \dots & \underline{k}_{trN2} \\ \dots & \dots & \dots & \dots \\ \underline{k}_{tr1N} & \underline{k}_{tr2N} & \dots & 0 \end{pmatrix} \quad (9)$$

Where, the first digit of coefficients' index stands for the voltage source inducing the Thevenin voltage component $\underline{E}_{th,i,}$ and the second digit is referring to the generator seeing the Thevenin grid equivalent. Multiplication of the **GTC** matrix with the vector of voltages appearing at the point of constant steady state voltage magnitude gives the vector of equivalent Thevenin voltages seen by generators (10).

$$\begin{pmatrix} \underline{E}_{theqv\ 1} \\ \underline{E}_{theqv\ 2} \\ \dots \\ \underline{E}_{theqv\ M} \\ \dots \\ \underline{E}_{theqv\ N} \end{pmatrix} = (GTC) \cdot \begin{pmatrix} \underline{V}_1 \\ \underline{V}_2 \\ \dots \\ \underline{V}_M \\ \dots \\ \underline{V}_N \end{pmatrix} \quad (10)$$

For generator *i* the equivalent Thevenin voltage can be found according to the expression (11):

$$\underline{E}_{theqv\ i} = \underline{V}_1 \cdot \underline{k}_{tri1} + \underline{V}_2 \cdot \underline{k}_{tri2} + \dots + \underline{V}_M \cdot \underline{k}_{triM} + \dots + \underline{V}_{N-1} \cdot \underline{k}_{tri(N-1)} =$$
$$= \left(\underline{E}_{th1} + \underline{E}_{th2} + \dots + \underline{E}_{thM} + \dots + \underline{E}_{th(N-1)}\right) \quad (11)$$

Considering the system example (Fig. 3), the row of the **GTC** matrix corresponding to generator G_3 can be written as (12).

$$(GTC) = (\underline{k}_{tr13} \quad \underline{k}_{tr23} \quad 0) \quad (12)$$

The resulting Thevenin voltage seen by generator G_3 can then be represented as a sum of the components induced by the remaining voltage sources in the grid (13):

$$\underline{E}_{th3eqv} = (GTC) \cdot \begin{pmatrix} \underline{V}_1 \\ \underline{V}_2 \\ \underline{V}_3 \end{pmatrix} = \underline{V}_1 \cdot \underline{k}_{tr13} + \underline{V}_2 \cdot \underline{k}_{tr23} =$$
$$= \underline{V}_1 \cdot \frac{\underline{V}_4'}{\underline{V}_1'} + \underline{V}_2 \cdot \frac{\underline{V}_4'}{\underline{V}_2'} = \left(\underline{E}_{th1} + \underline{E}_{th2}\right) \quad (13)$$

Expression (13) can be rewritten in a way that shows more explicitly the transformation from original voltage vector to the Thevenin voltage component (14):

$$\underline{E}_{th3eqv} = \left(V_1 \cdot e^{j\delta 1}\right) \cdot \left(k_{tr13} \cdot e^{j\alpha 1}\right) + \left(V_2 \cdot e^{j\delta 2}\right) \cdot \left(k_{tr23} \cdot e^{j\alpha 2}\right) =$$
$$= \left(V_1 \cdot k_{tr13} \cdot e^{j(\delta 1 + \alpha 1)}\right) + \left(V_2 \cdot k_{tr23} \cdot e^{j(\delta 2 + \alpha 2)}\right) \quad (14)$$

Where α_i is the angle of $\underline{k}_{tri3}$, δ_i is the angle of the steady state constant voltage.

It can be noticed that the constant magnitude voltages seen by a given generator are experiencing both magnitude and angle transformation which is entirely dependent on the systems admittance matrix. Graphically this transformation is represented in the Fig. 5.

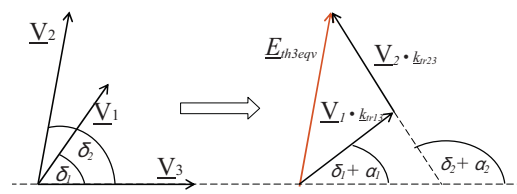

Figure 5. Application of superposition principle to the 5 bus test system .

In the general case, the formula for the definition of the equivalent Thevenin voltage seen by generator *k* can be written as follows (15):

$$\underline{E}_{th\ k\ eqv} = \sum_{\substack{i=1 \\ i \neq k}}^{Nvs} V_i \cdot k_{trik} = \sum_{\substack{i=1 \\ i \neq k}}^{Nvs} V_i \cdot \frac{V_k'}{V_i'} \quad (15)$$

The next section demonstrates the validity of the suggested approach considering the IEEE 30 bus test system.

III. Results and Discussions

A. IEEE30 bus test system: decomposition of Eth per components induced by each of voltage sources.

Fig. 6 shows the IEEE 30-bus test system diagram, with the system data borrowed from the power system test archive [7]. Few modifications were done to the system: synchronous compensators in the grid were replaced by generators, three-winding transformers were replaced by two two-winding transformers. The terminal of generator G_1 is chosen as a reference bus. The loading of the generators in the system as well as the voltages at the point of constant steady state voltage magnitude, are shown in Table I.

TABLE I. Generator Data

Gen	G_1	G_2	G_5	G_8	G_{11}	G_{13}
Pg,MW	108.81	40	40	40	30	30
Vo, p.u	1.679	1.722	2.513	2.383	2.214	1.875
Ang(Vo), grad	67.64	26.67	16.74	15.55	29.95	39.87

There are six synchronous generators in the test system. In order to find out how the rest of the generators in the grid are influencing stability conditions of the given generator, their influence on the Thevenin voltage seen by this generator should be studied. For this purpose the test system will sequentially be represented as Thevenin equivalent relatively each of generators in the grid. For each of the Thevenin equivalents the decomposition of the Thevenin voltage per

components corresponding to voltage sources will be represented.

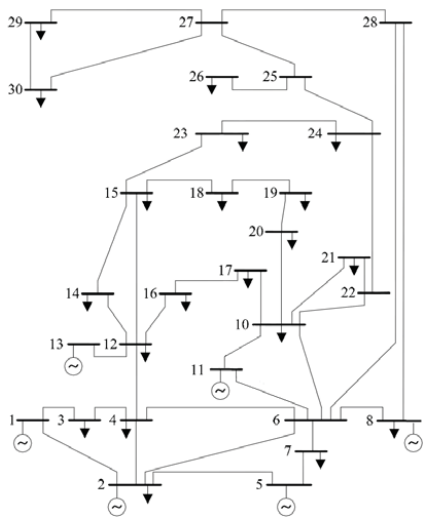

Figure 6. Single line diagram of IEEE 30 bus test system [8].

According to the methodology described in the section above, the reduced admittance matrix for each of the generators should be created to begin with. The reduced matrix is obtained by open-circuiting generator relatively which the system is reduced, and short-circuiting the remaining voltage sources, except for the voltage source which impact to $\underline{E}_{th}$ is to be defined. For each of generators the node in which the Thevenin voltage will be seen should be defined. Practically, it will be the node, topologically nearest to the considered generator, which remained energized while open-circuiting of this generator. For the IEEE 30 bus test system these nodes are mentioned in the Table II.

TABLE II. BUSES WHERE ETH APPEARS

Gen	G_1	G_2	G_5	G_8	G_{11}	G_{13}
Eth bus	1	2	5	8	11	12

For identification of the grid transformation coefficient (GTC) for each component of $\underline{E}_{th}$, seen by given generator, the current equal to 1A is sequentially injected into the remaining voltage source node in the reduced matrix. The number of reduced matrixes for the given generator utilized for identification of all components of $\underline{E}_{th}$ equals to N_{vs}-1. The same procedure is applied to all generators in the grid. The **GTC** matrix obtained for the IEEE30 bus test system is represented in the Table III.

TABLE III. ELEMENTS OF GTC MATRIX FOR IEEE 30 BUS TEST SYSTEM

G_1	G_2	G_5	G_8	G_{11}	G_{13}
0	|0.1322| ang -37.3466	|0.0895| ang -43.3246	|0.1102| ang -41.0637	|0.0541| ang -42.3022	|0.0526| ang -43.0729
|0.1762| ang -35.5036	0	|0.0866| ang -41.6280	|0.1056| ang -39.4651	|0.0518| ang -40.7694	|0.0501| ang -41.5195
|0.1471| ang -41.5268	|0.1067| ang -41.6202	0	|0.1007| ang -43.3910	|0.0491| ang -44.9176	|0.0463| ang -45.8760
| 0.1475| ang -39.4972	|0.1060| ang -39.7571	|0.0820| ang -43.6655	0	|0.0563| ang -40.4577	|0.0516| ang -41.8550
|0.1402| ang -38.5704	|0.1006| ang -38.8287	|0.0776| ang -42.9098	|0.1091| ang -38.2251	0	|0.0513| ang -38.4331
|0.1425| ang -39.3319	|0.1019| ang -39.6256	|0.0763| ang -43.9912	|0.1046| ang -39.6864	|0.0537| ang -38.4931	0

Substituting obtained GTC values into (10) the following results for $\underline{E}_{th}$ were carried out (Table IV):

TABLE IV. E_{TH} IDENTIFIED ON THE BASIS OF ADMITTANCE MATRIX

Gen / Eth	G_1	G_2	G_5	G_8	G_{11}	G_{13}
Eth1		|0.296| ang 32.14	|0.247| ang 26.10	|0.248| ang 28.13	|0.236| ang 29.07	|0.239| ang 28.31
Eth2	|0.228| ang -10.66		| 0.184| ang -14.94	|0.183| ang -13.09	|0.173| ang -12.16	|0.176| ang -12.97
Eth5	|0.225| ang -26.61	|0.218| ang -24.85		|0.206| ang -26.92	|0.195| ang -26.13	|0.192| ang -27.27
Eth8	|0.263| ang -25.53	|0.252| ang -23.94	|0.240| ang -27.87		||0.260| ang -22.69	|0.249| ang -24.12
Eth11	|0.119| ang -12.41	|0.115| ang -10.84	|0.109| ang -14.90	|0.123| ang -10.52		|0.119| ang -8.57
Eth13	|0.099| ang -3.17	|0.094| ang -1.64	|0.087| ang -6.03	|0.097| ang -1.94	|0.096| ang 1.44	
Eth, sum	|0.923| ang -18.13	|0.886| ang -3.90	|0.807| ang -6.25	|0.800| ang -3.14	|0.893| ang -6.81	|0.907| ang -8.45

In order to assure the applicability of the suggested approach, the results demonstrated in Table IV are compared with values of $\underline{E}_{th}$ obtained by solving circuit equations for the system depicted in Fig. 6 (Table V).

TABLE V. E_{TH} IDENTIFIED ON THE BASIS OF CIRQUIT EQUATIONS

Gen / Eth	G_1	G_2	G_5	G_8	G_{11}	G_{13}
Eth	|0.923| ang -18.13	|0.886| ang -3.90	|0.807| ang -6.25	|0.800| ang -3.14	|0.893| ang -6.81	|0.907| ang -8.45

As can be noticed from Table IV and Table V, $\underline{E}_{th}$ obtained by applying the two different methodologies yields the same results proving the validity of the suggested approach.

B. Application of the $\underline{E}_{th}$ decomposition for the improvement of generators stability.

In this section an example of $\underline{E}_{th}$ decomposition application will be considered. For the assessment of the generators' stability, the maximum injectable active power margin, $\%\Delta P_{inj}$ defined in [3], is utilized (16).

$$P_{inj} = \frac{E_{th} \cdot V_0}{Z_{th}} \cos(\gamma + \phi_{th}) - \frac{V_0^2}{Z_{th}} \cdot \cos(\phi_{th}) ,$$

$$\therefore \quad P_{inj,\max} = -\frac{E_{th} \cdot V_0}{Z_{th}} - \frac{V_0^2}{Z_{th}} \cdot \cos(\phi_{th}) , \qquad (16)$$

$$\%\Delta P_{inj} = \frac{P_{inj,\max} - P_{inj}}{P_{inj,\max}} \cdot 100\%$$

Where (see equivalent system in Fig. 2) E_{th} and Z_{th} stand for magnitudes of Thevenin voltage and impedance, φth is the angle of the Thevenin impedance, V_0 corresponds to constant steady state voltage magnitude and γ is the angle between $\underline{V}_0$ and $\underline{E}_{th}$.

Initial stability margins of the generators are shown in TableVI:

TABLE VI. STABILITY MARGIN, INITIAL CONDITIONS

Gen	G_1	G_2	G_5	G_8	G_{11}	G_{13}
$\%\Delta P_{inj}$	1.27	48.67	55.54	61.62	39.58	25.80

To illustrate the application of $\underline{E}_{th}$ decomposition, improvement of stability conditions for the generator G_1 is considered. The assumption is made that the rescheduling of generator G_1 is not possible. As a measure aimed at improving stability, an increase of torque, equal to 0.03 p.u., is subsequently applied to each of the remaining generators of the IEEE 30 bus test system, leading to an increase of corresponding δ. As can be seen from the **GTC** matrix in Table III, the highest magnitude transformation coefficient for $\underline{E}_{th,i}$ seen by G_1 belongs to generator G_2. This means that considering a similar rate of change applied to the vector of voltages, the impact of this change to the resulting Thevenin equivalent will be than higher than larger is magnitude of GTC corresponding to given voltage source. The GTC angle has less influence on the resulting $\underline{E}_{th,i}$ appearing as the added angle α_i for the initial voltage angle δ_i (14). In order to improve stability conditions both the magnitude of $\underline{E}_{th}$, seen by the generator, as well as the angle between the generators' constant steady state voltage and $\underline{E}_{th}$ should be maximized. Thus, the greatest effect of stability improvement considering the **GTC** matrix is expected when the torque of G_2 is increased. Table VII shows the resulting stability margin for the G_1 after additional torque has been applied to the remaining generators in the grid.

TABLE VII. STABILITY MARGIN OF G1 UNDER CONDITION OF ADDITIONAL TORQUE APPLIED IN SECUENT TO THE REMAINING GENERATORS

Gen	G_2	G_5	G_8	G_{11}	G_{13}
G_1, $\%\Delta$Pinj	1.5532	1.4895	1.5395	1.4783	1.5085

As it was suggested on the basis of the **GTC** matrix analysis the increase of G_2 torque yields the greatest improvement to stability margin. Thus, one of the possible applications of the **GTC** matrix is the identification of optimal generators in the grid for improvement of stability conditions for the given generator.

IV. SECTION IV. CONCLUSION

This paper presented an approach for splitting equivalent Thevenin voltage $\underline{E}_{th}$ seen by a given generator, into components induced by each voltage source in the grid. By representing $\underline{E}_{th}$ in terms of such components, it provides an understanding of how much impact a given voltage source (generator) can have on the aperiodic rotor angle stability of a given generator. Furthermore, the **GTC** matrix allows the analysis of how certain variations in the admittance matrix will result in change of impact which voltage sources have on the stability of the given generator. This knowledge can be used for the assessment of the efficiency of suggested preventive countermeasures that aim at improving stability by influencing elements in the system admittance matrix. Further research work will be focused on quantification of preventive countermeasures needed to provide a certain active power stability margin for all generators in the system.

REFERENCES

[1] M. Glavic and T. Van Cutsem, "Wide area detection of voltage instability from synchronized phasor measurements. Part I: Principle", IEEE Trans. Power Syst., vol. 24, pp.1408-1416 , 2009.

[2] M. Glavic and T. Van Cutsem, "Wide area detection of voltage instability from synchronized phasor measurements. Part II: Simulation Results", IEEE Trans. Power Syst., vol. 24, pp.1417-1425 , 2009.

[3] H. Jóhannsson, R. Garcia-Valle, J. T. G. Weckesser, A. H. Nielsen and J. Østergaard, "Real-Time stability assessment based on synchrophasors", IEEE PES Trondheim PowerTech,2011

[4] H. Jóhannsson, J. Østergaard and A. H. Nielsen, "Identification of critical transmission limits in injection impedance plane", Int J Electr Power Energ Syst, 2012, http://dx.doi.org/10.1016/j.ijepes.2012.05.050

[5] J.M. Nilsson and S.A. Riedel, "Electric circuits", 9th edition, Pearson Prentice Hall, 2011

[6] E. Dmitrova, H. Jóhannsson and A.H. Nielsen, "Early prevention of instability - search for optimal grid nodes for applying countermeasures", International Conference on Environment and Electrical Engineering EEEIC, 2012.

[7] Power System Test Archive, available online http://www.ee.washington.edu/research/pstca, Aug.1993.

[8] Single line diagram of IEEE 30 bus test system, available online http://een.iust.ac.ir/profs/jadid/SCPM.pdf

E
EARLY PREVENTION OF INSTABILITY - SEARCH FOR OPTIMAL GRID NODES FOR APPLYING COUNTERMEASURES

This paper was published in the proceedings of the 11th International Conference on Environment and Electrical Engineering EEEIC, May, 2012, Venice

Early Prevention of Instability - Search for Optimal Grid Nodes for Applying Countermeasures

Evgeniya Dmitrova, Hjörtur Jóhannsson, Arne Hejde Nielsen
Elektro, Technical University of Denmark
Centre for Electric Technology
Kgs. Lyngby, Denmark
ed@elektro.dtu.dk, hj@elektro.dtu.dk, ahn@elektro.dtu.dk

Abstract— **This paper proposes a method for automatically determining which nodes in a given grid would have the largest contribution to an improvement of stability margins when wide-area control actions, in form of load changes, are applied to the nodes. The assessment of the influence each node in the grid has on the stability of the given generator is based on sensitivity analysis. The sensitivity of the stability criteria for aperiodic small signal angular stability to the corresponding change in the nodal admittances used to generate a prioritized candidate list over possible nodes for preventive counter measures application. The suggested method is tested on an 8 bus test system and IEEE 30 bus test system; the obtained results show that the proposed approach identifies the system nodes having the highest potential for improvement of critical stability margins.**

Keywords; power systems; stability; sensitivity analysis; preventive countermeasures;

I. INTRODUCTION

Development of the phasor measurement technology [1], and further intensive implementation of phasor measurement units (PMU) to the real power systems [2], accompanied with development of computational facilities, offers new opportunities for the wide area monitoring and control in real time. Considering perspectives of complete observability of the power systems based on the synchronized wide area measurements new methods for the real time stability assessment have started to emerge [3]-[5]. Considered methods provide detection of the instability on the early stage of its occurrence insuring awareness of the critical operational conditions prior to actual system collapse. Availability of such methods directly leads to the question: what countermeasures might be taken in order to bring system to the stable operation? Accordingly, the challenge of the development of real-time early prevention methods is to be taken as a next step. In [5,6], the concept of element-wise assessment of a particular mechanism of stability is presented as a promising approach for the development of methods giving early warning for an emerging stability problem. Naturally, such early warning methods are capable of only monitoring a certain type of instability, as instability detection algorithm is tailored to the physical processes staying behind the instability phenomena. Respectively, the preventive algorithms based on early warning methods are to be aimed on the contrariety to the certain instability mechanism. However, an early warning information for an emerging instability is required but not sufficient for the successful withstanding it. Having information regarding the type of instability mechanism and knowing the type of countermeasures opposing it, it is vital to determine the necessary rate of the control action and the optimal location in the grid for its application in order to effectively improve the stability. On the receipt of warning message regarding upcoming instability it is necessary to define quickly which nodes in the grid are having greater impact on stability of the critical unit in order to apply control actions leading to the most considerable improvement of the operational situation.

This paper describes an approach for defining a list of the optimal nodes in the system, at which countermeasures should be carried out for the prevention of aperiodic small signal angular instability. The Early warning method for the detection of that type of instability is described in [5, 6].

The paper is organized as follows: in Section II, the theoretical description of the proposed approach for the search of the optimal node in a grid for preventive countermeasure application is considered; in Section III illustration of the developed method applied to the simple test systems is provided; Section IV contains conclusion and perspectives for the further research.

Notation: Uppercase bold letters refer to matrixes. Complex numbers are underlined, *- denotes complex conjugate.

II. METHODOLOGY

A. Optimal node for the preventive countermeasure application

A method for enabling early warning for aperiodic small signal angular instability is described in [5, 6]. The method utilizes analytical expression for the actual stability boundary for each generator in the system. The stability boundary is expressed in terms of equivalent system parameters, where the system is represented by Thevenin equivalent (Fig. 1) from a node of active power injection. The power injection from a given generator is represented at a node of constant steady-state voltage magnitude. The mathematical expression for the aperiodic small signal angular stability boundary is given by [5]:

$$Z_{inj} = -Z_{th} \cdot \sin\theta_{inj} / \sin\varphi_{th} \qquad (1)$$

978-1-4577-1829-8/12/$26.00 ©2012 IEEE

$$\begin{cases} Z_{inj} >= -Z_{th} \cdot \sin\theta_{inj} / \sin\varphi_{th} & \text{–stable operation area} \\ Z_{inj} < -Z_{th} \cdot \sin\theta_{inj} / \sin\varphi_{th} & \text{–instable operation area} \end{cases}$$

Where Z_{inj} corresponds to the magnitude of the generators' injection impedance, measured at the node of constant steady state voltage magnitude V_0, Z_{th} is the magnitude of Thevenin equivalent impedance of the system seen from the node of power injection. θ_{inj} and φ_{th} are the angles of $\underline{Z_{inj}}$ and $\underline{Z_{th}}$ respectively. The injection impedance is determined as:

$$\underline{Z_{inj}} = -V_0^2 / (P_{gen} + j \cdot Q_{gen})^* \qquad (2)$$

Where P_{gen}, Q_{gen} are respectively active and reactive power of a generator fed to a grid from the node of constant steady state voltage magnitude.

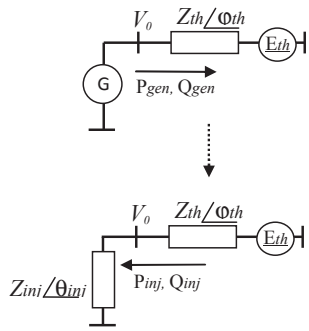

Figure 1. Equivalent system representation for a generator.

The main benefit of monitoring, in real-time the stability boundary for each generator, is that it provides information about where in the system severe stability problems are emerging. This useful knowledge makes it possible to apply countermeasures pointed to the exact unit in the grid in case if it is about to cross boundaries for unstable operation.

This paper focuses on using load nodes (nodes with neither generators nor constant voltage sources) in the grid as candidates for taking countermeasures to avoid an emerging instability. It is assumed in following that a rescheduling of the generation is not possible, which reflects the case of full loading operation. Considering the expression for the stability boundary (1) one may see four degrees of freedom Z_{inj}, Z_{th}, θ_{inj}, φ_{th}. In order to ensure a stable operation of the given generator, any of these parameters can be influenced. In order to vary Z_{th} and φ_{th} changes to admittances of the grid have to be applied. To define which of the load nodes in the grid are the most influential on the stability of the given generator, it is enough to find out which of them has greater impact on the corresponding values of Z_{th} and φ_{th}.

It is shown in [5] how $\underline{Z_{th}}$ can be determined using admittance matrix of the system, ordered in a certain way. The same matrix is to be utilized for finding out which nodes in the grid have greater impact on the Thevenin impedance seen from the node of constant steady state voltage magnitude of the given generator. Properly ordered admittance matrix for N nodes system, containing V nodes of constant voltage is presented as:

$$\left[\underline{Y}_{NN}\right] = \begin{pmatrix} \underline{Y}_{11} & \cdots & -\underline{Y}_{1N} \\ \vdots & \ddots & \vdots \\ -\underline{Y}_{N1} & \cdots & \underline{Y}_{NN} \end{pmatrix} = \begin{array}{|c|c|} \hline \underline{Y}_{n\_vc,\, n\_vc} & \underline{Y}_{n\_vc,\, vc} \\ \hline \underline{Y}_{vc,\, n\_vc} & \underline{Y}_{vc,\, vc} \\ \hline \end{array} \quad \begin{matrix} \\ \\ \text{N-V} \end{matrix} \quad \begin{matrix} \\ \\ \text{V} \end{matrix} \qquad (3)$$

Where index *vc* stands for voltage controlled nodes, and *n_vc* for non-voltage controlled.

Diagonal elements of admittance matrix Y_{ii} are containing the sum of admittances connected to the node *i*, while off diagonal elements Y_{ij} contain negative value of the admittance between node *i* and *j*. Current paper considers only variation of the diagonal elements of admittance matrix assuming off diagonal elements being unchangeable, meaning that branch elements of the grid - such as lines and transformers are taken to have constant admittance, while nodal shunt elements are the subjects to variations. The diagonal elements of $\underline{\mathbf{Y}}_{vc,vc}$ are constant and the only altering part of (3) are diagonal elements of $\underline{\mathbf{Y}}_{n\_vc,n\_vc}$, namely the nodal shunts. The value of the composite nodal shunt equals to (4):

$$\underline{Y}_{n\_vc\ sh,\, m} = \sum_{j=1}^{N} \underline{Y}_{j,\, m} \qquad (4)$$

Where m=1…(N-V).

(N-V) load nodes in the grid are forming a set of potential candidates for applying countermeasure. To define which of those nodes are the most influencing on each of the k Thevenin impedance ($Z_{th\,k}$) seen from node of constant steady state voltage magnitude of the *k* generators, sensitivity analysis is used. Referring to the formula defining the stability boundary (1) the sensitivity of ($Z_{th}/\sin\varphi_{th}$) ratio to variation of nodal composite shunt admittances is considered. For the further usage lets denote $Z_{th}/\sin\varphi_{th} = K_{th}$.

The sensitivity of K_{th} to active and reactive component of composite nodal shunt admittance is considered separately (5). This is done for having the possibility of independent control of reactive and active power consumption in the load nodes.

$$\begin{aligned} S_{Kth\,P} &= \left[\frac{\partial(Z_{th} / \sin(\varphi_{th}))_j}{\partial(real(\underline{Y}sh_{m,m}))}\right] = \left[\frac{\partial(K_{th_j})}{\partial(real(\underline{Y}sh_{m,m}))}\right] \\ S_{Kth\,Q} &= \left[\frac{\partial(Z_{th} / \sin(\varphi_{th}))_j}{\partial(imag(\underline{Y}sh_{m,m}))}\right] = \left[\frac{\partial(K_{th_j})}{\partial(imag(\underline{Y}sh_{m,m}))}\right] \end{aligned} \qquad (5)$$

Where j=1...k, m=1…(N-V)

The idea is to define relative efficiency of countermeasure application among the (N-V) candidate nodes. To do this the same variation of composite shunt admittance $\Delta Ysh_{m,m}$ is applied sequentially to each of (N-V) nodes. As a result two sensitivity matrixes sized {k}x{N-V} are created, denoting these matrixes as CEF (control efficiency factor) (6) .

$$[CEF]_Q = \begin{pmatrix} S_{Kth_1 Q_1} & \cdots & S_{Kth_1 Q_{(N-V)}} \\ \vdots & \ddots & \vdots \\ S_{Kth_k Q_1} & \cdots & S_{Kth_k Q_{(N-V)}} \end{pmatrix} \quad [CEF]_P = \begin{pmatrix} S_{Kth_1 P_1} & \cdots & S_{Kth_1 P_{(N-V)}} \\ \vdots & \ddots & \vdots \\ S_{Kth_k P_1} & \cdots & S_{Kth_k P_{(N-V)}} \end{pmatrix} \quad (6)$$

As further operations on these matrixes are uniform only operations on **CEF***Q* are considered, all the obtained conclusions may refer equally to **CEF***P*. Elements of **CEF** reflect relative efficiency of the control action applied to the load node *m* in respect to stability of generator *k*.

However, generally, control reserves are not available in each load node of the grid; furthermore allocation of reserves in the grid is not fixed: it varies with the operational conditions and depends on the maintenance plan. To adapt the countermeasure candidate search to the actual available control reserves in the grid, the commitment matrix, listing the nodes actually capable of provision control reserve, is created. Control participant matrix **C** sized {N-V}x{N-V} is diagonal matrix where the diagonal element $C_{m,m}$ equals either 1 indicating that node *m* is offering control service or 0 if there is no control reserves allocated in node *m*. To obtain the relative control efficiency of the nodes adjusted to reserve availability **CEF** matrix should me multiplied with control participation matrix **C**. Resulted matrix being normalized with respect to rows would provide prioritized list of control application nodes for each of generators (7).

$$[CEF]_Q = \begin{pmatrix} S_{Kth_1 Q_1} & \cdots & S_{Kth_1 Q_{(N-V)}} \\ \vdots & \ddots & \vdots \\ S_{Kth_k Q_1} & \cdots & S_{Kth_k Q_{(N-V)}} \end{pmatrix} \quad [C] = \begin{pmatrix} C_{11} & 0 & & 0 \\ 0 & C_{nm} & & 0 \\ \cdots & \cdots & & \cdots \\ 0 & 0 & \cdots & C_{(N-V)(N-V)} \end{pmatrix}$$

$$[CEF2]_Q = [CEF]_Q \cdot [C] = \begin{pmatrix} CEF2_{11} & \cdots & CEF2_{1(N-V)} \\ \vdots & \ddots & \vdots \\ CEF2_{k1} & \cdots & CEF2_{k(N-V)} \end{pmatrix} \quad (7)$$

Necessary to mention, that topology structure has drastic impact on $\underline{Z}_{th}$ and correspondingly the list of nodes having the greatest impact on the K_{th} might change considerably if grid reconfiguration takes place. For this reason **CEF2** is expected to be redefined on a mandatory basis each time when the grid topology changes or when there are changes in the **C** matrix.

B. Group control realization

In case of post-contingency or extremely loaded operation of a power system it may happen that several generators are operating close to their stability boundaries. Under such conditions it might be desirable to improve stability of several generators simultaneously initiating minimum control actions. In order to define the node in the grid, optimal for simultaneous stability maintenance for the number of given generators some additional operations on **CEF2** should be taken.

The number of critical units are forming the group control set k_{gr}. According to the defined set the nodes having simultaneous significant impact on the stability of each element of the set should be determined. In order to do this rows of **CEF2** corresponding to the generators from the k_{gr} are summarized element wise (8). The elements of the resulting vector **GrC** (group control vector) are representing integral control efficiency factor (ICEF) for each of (N-V) load nodes in the grid.

$$for\ k_{gr} = \{k_{gr1}, k_{gr2}, k_{gr3} \ldots k_{grn}\} \subseteq \mathrm{k},$$

$$[GrC] = \left[\sum_{i=k_{gr1}}^{k_{grn}} CEF2_{i,1} \quad \sum_{i=k_{gr1}}^{k_{grn}} CEF2_{i,2} \quad \ldots \quad \sum_{i=k_{gr1}}^{k_{grn}} CEF2_{i,(N-V)} \right] \quad (8)$$

To ensure that participation of each $CEF2_{k,m}$ in the $GrC_{1,m}$ is considerable, which means that given load node *m* has influence on the stability of all the generators from the control group, filtering should be applied. The filter is based on setting the low limit for the weight coefficients *wc* of $CEF2_{k,m}$ (9):

$$wc_{k_{grn},m} = CEF2_{k_{grn},m} \,/\, GrC_{1,m} \quad , \quad \forall wc_{k_{grn},m} \geq \frac{1}{2N_{k_{gr}}} \quad (9)$$

Where N_{kgr} is number of generators included in the control group.

If there are nodes meeting the conditions of (9) they are stored to the candidate list for group control, where the optimal node for the countermeasure application is defined by the maximum value of the integral control efficiency factor (10).

$$OptC = \max[GrC] \quad (10)$$

In case condition (9) is not met by any node the critical generators should be controlled separately which would require more changes in the grid comparing to group control, however provide better efficiency for each of the troubled units.

III. Results and Discussions

For the verification of the suggested approach two test systems are considered: 8 bus test system and IEEE 30 bus test system.

A. Instability Prevention by applying control action to the defined optimal node

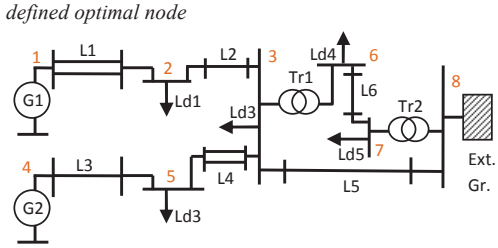

Figure 2. Single line diagram of 8 bus test system.

TABLE I. 8-BUS SYSTEM DATA:BRANCHES

Branch	**L1**	**L2**	**L3**	**L4**	**L5**	**L6**	**L7**	**L8**
X, Ohm	0.6	3	0.78	1.62	40	18.5	12.3	12.3

TABLE II. 8-BUS SYSTEM DATA:BUSES

Bus	Unom, kV	Pgen, MW	Qgen, MVar	Pload, MW	Qload, MVar
1	10	20	13.68	0	0
2	10	0	0	19	10
3	10	0	0	17	0
4	10	18	14.50	0	0
5	10	0	0	10	11
6	110	0	0	40	10
7	110	0	0	10	40
8	10	58.25	63.65	0	0

For the network shown in Fig. 2 the study case leading to loss of aperiodic small signal angular stability (ASSAS) is created, using Power Factory as a simulation tool. For the reference bus the bus of external grid connection (bus 8) is chosen. To initiate ASSAS problems in the test system the trip of the line L1 at t=5 seconds is applied, which results in generator G1 goes out of step at t=19.77 seconds (Fig. 3). The early warning detected cross of ASSAS boundary at t=11 seconds.

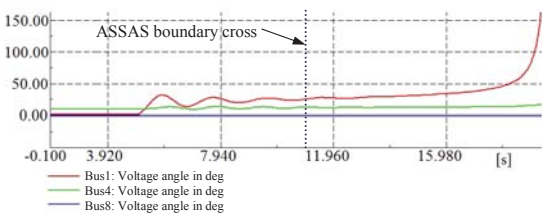

Figure 3. Trip of the line L1. Voltage angles at buses 1, 4 and 8.

The rate of shunt admittance variation $\Delta Ysh_{m,m}$ used for sensitivity definition equals to 0.01 *S* for active or reactive component respectively. For the post-contingency topology sensitivity matrixes **CEF***Q* and **CEF***P* are obtained:

TABLE III. ELMENTS OF MATRIXES CEF2_Q, C, CEF2_Q

Bus	SKth_Q G1	SKth_Q G2	diag([C])	CEF2_Q G1	CEF2_Q G2
1	0.001155	7.31E-07	0	0	0
2	0.000384	1.04E-06	1	1	0.002081
3	2.02E-06	9.88E-06	1	0.005273	0.01976
4	3.68E-07	0.001201	0	0	0
5	5.13E-07	0.0005	1	0.001337	1
6	9.88E-07	5.10E-06	1	0.002575	0.010191
7	1.14E-07	6.04E-07	1	0.000298	0.001207
8	0	0	0	0	0

According to **CEF2** elements (Tables III, IV) the node, most influencing stability conditions of G1, both with respect to variation of active and reactive component of nodal shunt admittance is bus 2. Correspondingly suggested countermeasure aimed on prevention of stability loss is to be applied to bus 2. For the given study case the change in reactive component of shunt admittance equaled to $\Delta Ysh_{2,2}$=0.01 S was applied as a countermeasure.

TABLE IV. ELMENTS OF MATRIXES CEF2_P, C, CEF2_P

Bus	SKth_P G1	SKth_P G2	diag([C])	CEF2_P G1	CEF2_P G2
1	0.000514	2.14E-06	0	0	0
2	0.00037	3.07E-06	1	1	0.018503
3	3.29E-06	6.21E-06	1	0.008899	0.0374
4	1.08E-06	0.000225	0	0	0
5	1.50E-06	0.000166	1	0.004067	1
6	1.81E-06	3.58E-06	1	0.004892	0.021547
7	2.20E-07	4.42E-07	1	0.000595	0.002664
8	0	0	0	0	0

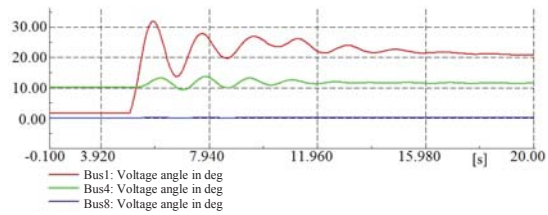

Figure 4. Countermeasure applied to bus 2 after L1 trip. Voltage angles at buses 1, 4 and 8.

The control action applied to the defined optimal node led to successful prevention of instability. The same counteraction being applied to the other buses in the test system hasn't resulted in stabilization of the G1.

B. IEEE 30 bus test system: group control realization

Fig. 5 shows IEEE 30-bus test system diagram. The system data are taken from power system test archive [7]. Few modifications were done to the system: synchronous compensators in the grid were replaced by generators, three-winding transformer was replaced respectively by two two-winding transformer. Generator G1 is representing external grid and chosen as a reference bus.

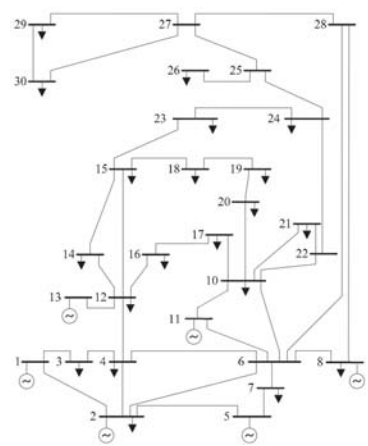

Figure 5. Single line diagram of IEEE 30 bus test system [8].

TABLE V. GENERATOR DATA

Gen	G1	G2	G5	G8	G11	G13
P_G,MW	108.98	40	40	40	30	30

The goal is to define which nodes in the meshed grid are the most influencing on the stability of generators and find out if there is a potential for the group control.

For the comparison of the generators' operational conditions in terms of stability, maximum injectable active power margin $\%\Delta P_{inj}$ defined in [5] is utilized (11).

$$P_{inj} = -\frac{E_{th}\cdot V_0}{Z_{th}}\cos(\delta+\varphi_{th}) - \frac{V_0^2}{Z_{th}}\cdot\cos(\varphi_{th}),$$

$$\therefore \quad P_{inj,\max} = -\frac{E_{th}\cdot V_0}{Z_{th}} - \frac{V_0^2}{Z_{th}}\cdot\cos(\varphi_{th}), \qquad (11)$$

$$\%\Delta P_{inj} = \frac{P_{inj,\max} - P_{inj}}{P_{inj,\max}}\cdot 100\%$$

Where ($\Rightarrow$ equivalent system (Fig. 2)) E_{th}, Z_{th} stand for magnitudes of Thevenin voltage and impedance respectively, φ_{th} is angle of Thevenin impedance, V_0 corresponds to magnitude of constant steady state voltage and δ is angle between $\underline{V_0}$ and $\underline{E_{th}}$.

At the initial conditions generators have the following margins:

TABLE VI. STABILITY MARGIN, INITIAL CONDITIONS

Gen	G1	G2	G5	G8	G11	G13
$\%\Delta P_{inj}$	98.98	43.65	55.02	57.21	39.89	30.98

To demonstrate the group control effect, other changes were applied to the original system aiming on worsening of operational conditions. Two branch elements were put out of service: line L1-2 and transformer Tr4-12. Additionally, series of contingencies are initiated: at t=10 seconds two transformers Tr6-11 and Tr6-10 are tripped; at t=60 seconds 30 MW load is connected to bus 17 (Fig. 6). Taken action resulted in serious decrease in stability margins of generators G11 and G13 (Table VII). Taking as a benchmark for the sufficient stability margin traditional 20% security margin [9], countermeasures aimed on improvement of G11 and G13 stability are to be applied. The potential of group control for k_{gr}={G11, G13} is examined.

In order to determine proper nodes in the grid for the group control, the matrixes **CEF2** are obtained. For the given case matrix **CEF2**$_Q$ is considered.

TABLE VII. STABILITY MARGIN, POST-CONTINGENCY CONDITIONS

Gen	G1	G2	G5	G8	G11	G13
$\%\Delta P_{inj}$	99.01	44.03	55.25	57.26	19.13	17.59

TABLE VIII. ELEMENTS IN CEF2Q FOR IEEE 30-BUS TEST SYSTEM

Bus	CEF2_Q G2	CEF2_Q G5	CEF2_Q G8	CEF2_Q G11	CEF2_Q G13
1	0	0	0	0	0
2	0	0	0	0	0
3	0.583393	0.278675	0.579039	0.001755	0.001076
4	0.91435	0.43706	0.907493	0.002643	0.00164
5	0	0	0	0	0
6	0	0	0	0	0
7	1	1	1	0.010908	0.005251
8	0	0	0	0	0
10	0.02387	0.041246	0.005461	1	0.101487
11	0	0	0	0	0
12	0.025482	0.039925	0.010325	0.215648	1
13	0	0	0	0	0
14	0.028537	0.042739	0.013723	0.11707	0.676101
15	0.024207	0.040916	0.006537	0.180503	0.571329
16	0.033027	0.045261	0.020483	0.275853	0.464686
17	0.038233	0.049354	0.027041	0.415394	0.083085
18	0.030672	0.044862	0.015926	0.304691	0.278338
19	0.032234	0.045855	0.018149	0.444423	0.152935
20	0.029989	0.044639	0.014721	0.606168	0.129757
21	0.016712	0.038211	0.006393	0.758073	0.0808
22	0	0	0	0	0
23	0.001163	0.030743	0.031185	0.253387	0.33216
24	0.039666	0.010905	0.096037	0.405637	0.144398
25	0	0	0	0	0
26	0.268973	0.108153	0.451901	0.215908	0.081769
27	0	0	0	0	0
28	0	0	0	0	0
29	0.50896	0.235	0.821882	0.128465	0.051589
30	0.452197	0.197718	0.742339	0.11031	0.043958

Basing on the **CEF2** the list of the nodes capable to influence simultaneously on the stability of G11 and G13 can be defined. As it is seen from Table VIII, three nodes having the highest CEF for G11 and G13 are buses 10, 21, 20 and 12, 14, 15 respectively. However, considering realization of group control, it is required that node, chosen for the control application should have commensurable CEF for all generators from the control group k_{gr} (9). Therefore, the buses 10, 12, 14, 20 and 21 are not included in the control action candidate list as influencing mostly the stability of only one generator from the group. Thus, the nodes matching the condition (9) comprise the list of candidates for the control application, prioritized according to the value of the ICEF (8). Below, three nodes having the largest ICEF for the k_{gr}={G11, G13} and two having the smallest are listed:

TABLE IX. ELEMENTS OF GRC

Bus	15	16	19	4	3
$GrC_{1,j}$	0.751	0.740	0.597	0.004	0.002

To compare the effect of group control the same countermeasure – reduction of the reactive power consumption in the node per 10 MVar is applied sequentially to each of the nodes from Table IX. The simulation of series of contingencies and application of countermeasure at t=150 seconds to the bus 12 is depicted at Fig. 6.

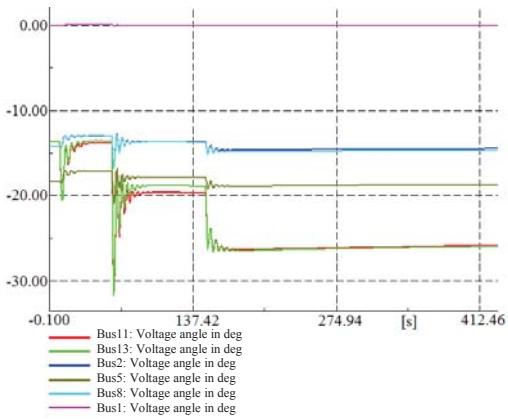

Figure 6. Voltage angles at generator buses 1, 2, 5, 8, 11 and 13.

Fig. 6 clearly indicates that applied countermeasure is mostly influencing exactly the generators from the k_{gr}={G11,G13} ,that is confirming the possibility of group control realization for the given set of units.

TABLE X. STABILITY MARGIN, GROUP CONTROL REALIZATION

Gen	G1	G2	G5	G8	G11	G13
$\%\Delta P_{inj}$ bus 15	98.97	43.21	54.68	56.73	21.09	20.34
$\%\Delta P_{inj}$ bus 16	98.97	43.19	54.67	56.72	21.25	20.23
$\%\Delta P_{inj}$ bus 19	98.97	43.24	54.70	56.75	21.38	19.75
$\%\Delta P_{inj}$ bus 4	98.99	44.24	55.44	57.47	19.25	17.70
$\%\Delta P_{inj}$ bus 3	98.98	44.18	55.41	57.44	19.16	17.60

Table X presents the comparison of the relative countermeasure efficiency. The nodes having large integral control efficiency factor $GrC_{1,j}$ proved to be the most optimal for improving stability of the given group of generators. The target of 20% stability margin was reached when control action is applied to the busses 15 and 16. While introducing the same countermeasure to the bus 19 results in improvement of stability but less than desired 20% margin. Nodes with small $GrC_{1,j}$ showed very low influence on the stability of chosen group of generators. At the same time the stability of the generators not belonging to the control set is varying insignificantly. Therefore, the obtained results demonstrate validity of the suggested methodology for detection of the optimal node for the group control realization.

IV. CONCLUSION

The paper describes the method for identification of the optimal node in the grid for control action application in order to improve stability of the critical generator or group of generators. The proposed approach allows adaptability of the method to the arbitrary grid topology, taking into account allocation of the control reserves. The sensitivities of Thevenin impedance to the variation of nodal admittances are considered. It is shown that these sensitivities can be used for the identification of countermeasure relative efficiency when applied to the corresponding nodes. According to the value of relative countermeasure efficiency the prioritized list of nodes for control action application is created. Consequently, the method enables efficient contrariety to emerging instability initiating control actions at the node of highest control efficiency potential. Generalization of the suggested methodology for the prevention of other types of instability (e.g. transient instability) may be promising, providing that corresponding analytically derived stability boundary is available; however additional studies in this field are needed. The further research work will be aimed on the definition of the minimal control action amount, needed for successful instability prevention, when being applied to the detected optimal nodes.

REFERENCES

[1] A. G. Phadke, J. S. Thorp, and M. G. A. Adamiak, “New measurement technique for tracking voltage phasors, local system frequency, and rate of change of frequency,” IEEE Trans. Power App. Syst., vol. PAS-102, no. 5, pp. 1025–1038, May 1983.

[2] W. Sattinger,”Application of PMU Measurements in Europe TSO Approach and Experienc”, Trondheim PowerTech, 2011.

[3] M. Glavic and T. Van Cutsem, "Wide area detection of voltage instability from synchronized phasor measurements. Part I: Principle", IEEE Trans. Power Syst., vol. 24, pp.1408-1416 , 2009.

[4] M. Glavic and T. Van Cutsem, "Wide area detection of voltage instability from synchronized phasor measurements. Part II: Simulation Results", IEEE Trans. Power Syst., vol. 24, pp.1417-1425 , 2009.

[5] Hjörtur Jóhannsson “Development of Early Warning Methods for Electric Power Systems”, PhD thesis, Denmark University of Technology, 2010.

[6] Hjörtur Jóhannsson, Garcia-Valle, Rodrigo, WeckesserJohannes Tilman Gabriel,Nielsen, Arne Hejde and Jacob Østergaard Jacob, “Real-Time Stability Assessment based on Synchrophasors”, IEEE PES Trondheim PowerTech,2011

[7] Power System Test Archive, available online http://www.ee.washington.edu/research/pstca, Aug.1993.

[8] Single line diagram of IEEE 30 bus test system, available online http://een.iust.ac.ir/profs/jadid/SCPM.pdf

[9] Savu Crivat Savulescu, “Real-time stability assessment in modern power system control centres”, Piscataway, NJ : IEEE Press [u.a.], 2009.